Amorphous and Glassy Semiconducting Chalcogenides ☆

M Frumar, University of Pardubice, Pardubice, Czech Republic
B Frumarova, Institute of Macromolecular Chemistry, Academy of Sciences of the Czech Republic, Prague, Czech Republic
T Wagner, University of Pardubice, Pardubice, Czech Republic
GK Sujan, University of Malaya, Kuala Lumpur, Malaysia

1 Introduction

Amorphous and glassy chalcogenides (AGCs) form a large group of noncrystalline compounds and alloys. They contain sulfur, and/or selenium and/or tellurium, and one or more of other elements (As, Sb, Ge, Si, Al, Ga, In, Ag, Cu, etc.) that form compounds or solid solutions. Chalcogenides usually also include elemental chalcogens, pure or doped sulfur, selenium and tellurium, and their alloys. The AGCs can be stoichiometric or nonstoichiometric with relatively broad ranges of composition, in which they form homogeneous glasses and amorphous films (Tsiulyanu and Ciobanu, 2016; Hassanien and Akl, 2015; Golovchak *et al.*, 2015; Sharma *et al.*, 2015).

AGCs rarely include oxides; however, many properties of oxides are different from other chalcogenides and the oxides are not discussed in this chapter. Crystalline chalcogenides are also not discussed, even though many AGCs can form crystalline compounds. These chalcogenides have been known and applied for centuries, as pigments (e.g., HgS), later as luminophors (CdS, ZnS, etc.), detectors (CdS, CdSe, CdTe, HgTe, PbS, PbSe, PbTe, etc.), thermoelectric generators (Bi_2Te_3, Sb_2Te_3, etc.), lubricants (MoS_2), etc.

Amorphous selenium has been applied industrially for its semiconducting properties in solid photocells due to its high photoconductivity ($\Delta\sigma_{foto} \geq 10^3\,\Omega^{-1}\,cm^{-1}$) and photovoltaic effect. Glassy sulfur has been known for centuries

☆*Change History*: October 2015. G.K. Sujan provided an abstract, nine keywords, and five most recent references within the text.

 doi:10.1016/B978-0-12-803581-8.09804-0

as a product of quick cooling of liquid sulfur (sulfur melt is poured into cold water). The glassy sulfur is plastic and crystallizes easily.

Large research and industrial interest in AGC started with the effort to develop infrared (IR) optical elements and devices for night vision and sensors, for example, for defense and other applications. The oxide glasses are not transparent in IR region of spectrum, while the sulfides are transparent in the region $\approx$0.5–11 μm, selenides $\approx$1–15 μm, and tellurides $\approx$1.3–20 μm (Tauc, 1974). The glassy chalcogenides (GCs) are relatively easy to prepare in large sizes and machined into lenses and other elements, whose manufacture with single crystals would be more difficult and much more expensive. The composition regions of AGCs are much broader than in crystals and, therefore, their properties can be changed (tuned) in much broader regions. They can be easily doped as well.

The interest in AGC abruptly increased in the 1950s when surprising semiconducting properties in some AGCs were discovered. Up to that time it was believed that the semiconducting properties were inherent only to crystalline solids and that the band structure of electronic states was a consequence of long-range order in crystals. Obviously, the long-range order cannot be found in melts, in glassy or amorphous chalcogenides. The discovery of semiconducting properties of AGC triggered intensive research and opened up new possibilities for their applications. In a short time, the high dark resistance of amorphous Se and its large decrease with illumination was applied in copying machines of Xerox type and later in laser printers (Mort, 1989), which changed fundamentally the office work and nowadays represent a yearly multibillion market. The discovery of large changes of resistivity of AGC in high electrical fields (threshold and memory switches) started a further boom of interest in AGC, promising construction of fast electrical switches and electrical nonvolatile memories with high density, high capacity, low switching voltage, and low price (Fritzsche, 1973).

The AGCs doped with Ag^+ ions have also important applications (Srivastava and Mehta, in press). They have an increased index of refraction, decreased solubility in inorganic etchants, and high ionic conductivity. They can be applied in high-resolution photoresists, optical IR gratings, optical waveguides, as ionic sensors, in solid and thin film batteries, and in electrochemical nonvolatile memory elements. The last boom of interest in amorphous chalcogenides (ACs) is connected with their fast phase changes and with their application for optical data storage that resulted in optical data disks (originally compact disk (CD), nowadays digital versatile disk (DVD), and Blue-ray). A further application in high-density nonvolatile phase-change and multilevel electrical memories that supposedly will replace the so popular flash-type memories in the near future is currently being developed. These memories based on phase-change materials will be characterized by lower energy consumption, higher data density, and smaller size (Bez, 2009).

In addition to semiconducting behavior, the AGCs possess many other interesting features that are connected with their amorphous state and with their metastability. Thermodynamically, all glasses and amorphous materials in equilibrium conditions should tend to crystallize and lower their Gibbs energy. In metastable (glassy or amorphous) state they have usually lower density and larger free volume than the corresponding crystals (Zallen, 1983). This property enables faster movement and diffusion of atoms and ions within the amorphous matrix. It has been applied in ionic conductors and solid-state batteries (Bychkov *et al.*, 2004). Larger free volume of AGC enables also easy doping and fast changes of the state (e.g., crystallization).

The possibility to produce chalcogenide fibers and thin films that are transparent in IR region and applicable in light amplifiers, lasers, and sensors for different chemical and physical properties of materials is also important. The AGC sensors can be applied in different ranges of the electromagnetic spectrum, including IR and X-ray regions, in environmental monitoring, as chemical and ionic sensors, as biomedical-, pollutant-, X-ray, and diagnostical sensors, as surgical knives, and eye safe radars (Kasap and Rowlands, 2000). High index of refraction, high optical nonlinearity, and low ultrasound losses make the AGC attractive for applications in optics and opto-electronics.

High-intensity luminescence of AGC doped by rare-earth (RE) elements, especially in the near- and mid-IR region of spectrum, is suitable for construction of light sources, light generators, and amplifiers. Further, the luminescence of AGC can be applied, together with high nonlinear index of refraction, in optical signal processing (up-conversion, signal couplers, frequency mixing, light amplifiers, lasers, etc.).

The AGCs can crystallize, some of them very quickly and easily, others form stable glasses that crystallize with difficulties. The crystalline state possesses often different optical and electrical properties than amorphous one. This discovery led to a deep interest in AC for data storage. The large effort given to the study of this effect resulted in commercial production of optical memory disks that are cheap and light, removable, nonvolatile, and with very large storage capacity (originally CD, now DVD, and Blue-ray, up to 100 GB in triple layer recordings, or even more in laboratory prototypes). The crystallization and amorphization of AC can be produced also by very short electrical pulses, which resulted in the fabrication of electrical nonvolatile memories. Their size can be scaled down, below the values of today's flash memories (Bez, 2009). They can be also used for construction of memory arrays and multi-level memories (Raoux and Wuttig, 2009) that should further increase the data-storage density. Furthermore, multi-level recording could be closer to the work of the brains of animals (humans) and could also change the computer philosophy that is nowadays based on the binary code but can eventually be changed to ternary or multinary codes.

Many other changes of structure and properties of AGC can be induced by illumination with an intense light of energy equal or larger than their band gap (E_g); in some cases, even with the light of sub-band-gap energy.

Nearly mature for commercial use are memories based on holographic recording in thin AC films, again with capacities of several orders higher than those of today's DVDs.

The optically induced changes also include the changes of refractive index and other effects that are used, or can be used, in construction of optical waveguides, planar optical circuits, and gratings.

2 Glassy State – AGCs

Amorphous and glassy state of any material can be characterized by the absence of both long-range order and translational symmetry that result from randomness in their structure. Consequently, contrary to crystals, they exhibit no sharp X-ray diffraction peaks (**Figure 1**; Prikryl, 2009).

The glasses are materials usually frozen from their melts at cooling rates so high that nucleation and crystal growth are impeded. The glasses are then undercooled polymerized liquids. Melts, as well as glasses, have higher Gibbs energy than corresponding crystals; the AGCs are thermodynamically metastable. Glass formation is not a rare phenomenon. Many chalcogenide materials can form glasses in relatively large masses (e.g., $m > 1$ g, technologically even $m > 1$ kg).

The glass-forming ability and stability can be evaluated by several semi-empirical criteria, for example, by the Hruby criterion (Hruby, 1972):

$$H_r = (T_c - T_g)/(T_m - T_c) \quad [1]$$

where T_c, T_g, and T_m are temperatures of crystallization, glass transition, and of melting, respectively. This criterion is based on the idea that the high difference between T_c and T_g provides a wide range for processing of the glass without crystallization, and high T_c (small T_m–T_c) prevents the crystallization at elevated temperatures.

Some chalcogenides are bad glass formers. In order to produce glasses from their melts, the cooling rates must be high, for example, for several-nanometer thin films of Ge–Sb–Te system materials, the necessary cooling rate is $\geq 10^9$–10^{11} K s^{-1} (Raoux and Wuttig, 2009). Such materials cannot be prepared as bulk glasses of larger volume at all. Melts of some chalcogenides are polymeric and viscous and they can be cooled slowly without any crystallization as the transport of atoms or molecules necessary for crystallization is slow. Such glasses can be prepared from their melts (**Figure 2**) and the corresponding glasses can be annealed for a long time below their glass-transition temperature, $T < T_g$, without any crystallization. The systems As–S, As–Se, As–Ge–S, As–Ge–Se, Ge–Sb–S, and Ge–Sb–Se are typical examples of such glasses. The tendency to form glasses of the systems of As–S and As–Se is so high that their crystals can be prepared from their melts only with large difficulties. The crystallization of such glasses needs a special thermal treatment. Some other AGCs are also very stable and do not crystallize easily (e.g., GeS_x and $GeSe_x$, where $x \geq 2$). The general problems of glass formation, of formation of glasses in individual systems and of glass transition, are broadly discussed.

The term amorphous state or amorphous solid is usually applied for thin noncrystalline films, prepared by deposition of vapors on a substrate and subsequent quick cooling. It is also used for strongly damaged crystals (e.g., produced by long milling of powdered crystals or by ion or neutron bombardment). It is also used for solids quickly precipitated from solutions and for gel materials prepared by sol–gel method. Amorphous solids can be even more disordered than glasses. Their structure, energy, and disorder can become close to those of annealed glasses after their annealing at temperatures near glass-transition temperatures, T_g.

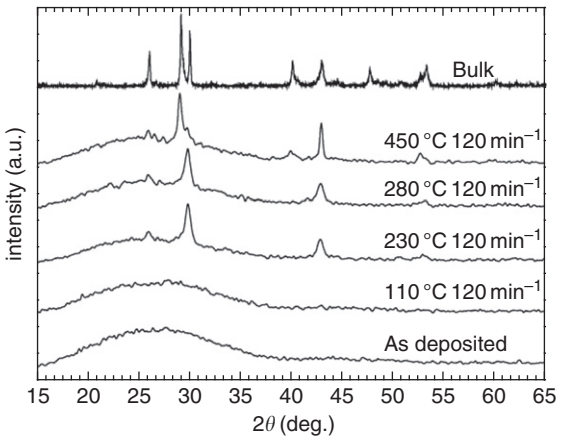

Figure 1 X-ray diffractograms of $Ge_2Sb_2Te_5$ thin films. As-deposited films and films heated up to 110 °C are amorphous. Crystallization to cubic fcc crystal modification starts at 230 °C, hexagonal modification of $Ge_2Sb_2Te_5$ appears from 450 °C. Bulk samples are crystalline and contain both fcc and hcp modifications (Prikryl, 2009).

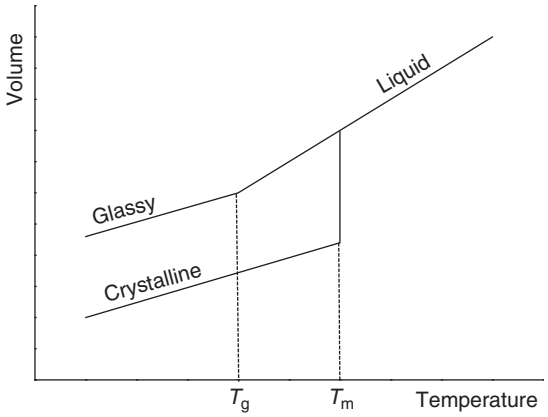

Figure 2 Temperature dependence of the volume of a liquid that can crystallize when cooled slowly, or to form a glass when cooled quickly. T_g is glass-transition temperature; below it the viscosity of the melt is so high that the glass behaves like a solid. T_m is the melting temperature.

3 Composition and Preparation of AGCs

The AGCs are formed by chalcogens and one or more of other elements such as P, As, Sb, Bi, Si, Ge, Al, Ga, In, Ag, Cu, and lanthanides. They can contain many other elements and/or compounds as dopants or additives. It should be noted that the size of glass-forming regions depends not only on the composition but also on cooling rate and starting temperature of the melt. The glass-forming regions are enlarged with increasing cooling rate. The glass-forming ability and stability can be evaluated by the Hruby empirical criterion discussed in the previous section (eqn [1]). Other empirical or semi-empirical criteria can also be applied.

The melts of many chalcogenides can dissolve, contrarily to corresponding crystals, much larger amounts of their own components, of different compounds and elements, or of other additives. They can easily become nonstoichiometric with different composition. As a result, the glasses with a wide range of properties can be prepared from such melts.

The glass-forming regions of some chalcogenides, for example, of Ag-doped chalcogenides are not generally very large (Popescu, 2000), when they are prepared from the melt. In spite of that, large amount of Ag can be dissolved in many AGCs by photo-doping without any crystallization or phase separation (e.g., up to 57 at.% in GeS_3 films; Kawasaki *et al.*, 1999). It occurs not only for glasses with overstoichiometry of chalcogen but also for glasses formed from stoichiometric compounds. This may occur thanks to the structure of a-chalcogenides (higher disorder than the bulk glasses, high free volume, and flexible structure) and to the special character of Ag chemical bond (see Section 4).

The composition of glassy chalcogenides (GC) for optical fiber production should be chosen from the glass-forming regions that give glasses stable enough without any danger of spontaneous or induced crystallization, because even traces of heterogeneous inclusions can scatter the light and lower their transmittivity substantially. The composition areas of glasses for good fibers are then much smaller than the glass-forming regions for thinner optical elements made from AGCs, such as lenses, prisms, plates, and thin films.

3.1 Bulk Glass Preparation

The GC with good glass-forming abilities can be prepared directly from their melts. The chemical synthesis of the glass or of precursors of the glass can proceed from pure elements or compounds, very often in evacuated and sealed silica ampoules or closed containers in order to avoid losses of volatile S or Se and to prevent oxidation. In some cases, the quenching is necessary, for example, by cooling of the container with the melt in air, cold water, or in liquid nitrogen. The glasses obtained by quick cooling are stressed because of different cooling rates near the container (ampoule) walls. They should be annealed at least for a short time at temperatures close to glass-transition temperature T_g but below it, in order to relax the glass and remove the stress.

The large free volume of AGC enables their easy doping by many elements or ions and it supports the increase of mobility of doped ions, significant for thin solid electrolytes (e.g., AGC doped by Ag^+, Li^+ ions). Such group of glasses can be prepared by doping of AGC by metals, or their compounds, such as AgX (X = Cl, Br, I), Ag_2Ch (Ch = S, Se, Te), $RECl_3$, RE_2Ch_3 (RE is for rare-earth element), or by other elements or compounds. In all cases, either homogeneous or phase-separated glasses (composites or glasses containing nanoparticles) are obtained. The Ag-doped AC can also be prepared by silver ion exchange from solutions or melts (Paje *et al.*, 2000). Thick films of AC can be prepared using sol–gel method and spin-coating technique, for example, from *n*-butylamin solutions of the starting glass (Wagner *et al.*, 2003). In such a case, the prepared films might contain excess solvent, which can be removed by heating the film under vacuum.

The RE-doped glasses can be prepared by classical melting process from RE elements or corresponding compounds (RE_2Ch_3 or REX_3), where Ch and X represent chalcogen and halogen, respectively.

3.2 Preparation of Thin Films

The thin films of amorphous chalcogenides can be prepared by quick cooling of their vapors during their deposition on cold or heated substrates. Evaporation and deposition can proceed by physical methods, such as physical vapor deposition (PVD), sputtering, classical vacuum evaporation, flash evaporation, and pulsed laser deposition (PLD), or by chemical reactions from gaseous precursors, such as chemical vapor deposition (CVD).

During PVD processes, the material is evaporated by heating the starting feedstock or by electronic or ionic bombardment of the material (target) surface, mostly in vacuum, at lower pressure, or in inert gas atmosphere. High-energy laser pulses (PLD) can also be used for evaporation. Separated evaporation boats or targets of different composition may be employed for the preparation of thin films of complex composition materials.

The temperature of the surface of evaporated material and the temperature of vapors during the evaporation is often relatively high (e.g., for pulsed laser evaporation up to $\leq 10^4$ K; Frumar, 2005) and the vapors can dissociate into molecular fragments or into atoms or ions with lower molecular mass. An example of particles found in pulsed-laser-evaporated $Ge_2Sb_2Te_5$ and GeTe is given in Wagner *et al.* (2007). After condensation of such vapors on a substrate, nonhomogeneous films are obtained. The synthetic chemical reactions among fragments, which should give rise to the desired material, are generally slow at lower temperatures. Nano-regions of different composition distributed in the volume, or gradient of composition, can thus be found. Many as-evaporated films are therefore inhomogeneous and far from thermodynamic equilibrium. Their composition, homogeneity, and structure are strongly influenced by the preparation conditions (deposition temperature and rate, direction of deposition, temperature of substrate, atmosphere and pressure in the deposition chamber, etc.).

Glasses of the As–S system can serve as another example of the vapor dissociation. They dissociate, according to following simplified reaction (Frumar *et al.*, 1997):

$$2(As_2S_3)_n \leftrightarrow n\, As_4S_4 + n\, S_2 \qquad [2]$$

with $n \gg 1$. Other reactions also take place in the vapors, because As_4, S_8, As_4S_3, and As_2S_6 particles were found in the vapors. Some of such fragments were identified even in the Raman spectra of deposited films.

Annealing of as-evaporated films at temperatures close to glass transition, where the atoms and molecules start to be more mobile and reactive, considerably lowers the content of such fragments and the material becomes much more homogeneous. The structure and properties of the film are then close to those of annealed bulk glasses.

The fractional evaporation of materials containing more- and less-volatile components can also take place during classical vacuum evaporation. More-volatile fragments are evaporated at first, followed by lower volatile parts of a sample. After condensation of vapors on a substrate, films of changed stoichiometry or films with gradient of composition are obtained (Nemec *et al.*, 2005).

Thin Ag-doped amorphous films can also be prepared by electrochemical deposition of Ag^+ ions from solutions or by photo-doping of chalcogenides, when each bilayer (Ag or Ag compound/chalcogenide) is illuminated by light or exposed to electronic (e)-beam (Wagner and Frumar, 2003). The silver is dissolved in chalcogenide, forming, for example, Ag–As–S, Ag_2S–GeS–GeS_2, Ag_2S–GeS_2, Ag_2Se–Ga_2Se_3–$GeSe_2$, Ag–As–Te, Ag–B–Si–S, Ag–Se–Te, Ag–$GeSe_x$, Ag–Ge–Sb–Se, and AgI–As_2Se_3 system films. The process is discussed later (Section 6.3).

Ag-doped AC films can be prepared also by the so-called chemical plating, when the chalcogenide film, for example, $GeSe_4$, is treated by a Ag^+ salt, for example, by $AgNO_3$ or $[Ag(CN)_2]^-$ solutions. The thin Ag_2Se (Ag_2S) layer is then formed on the surface of AGC by chemical reaction, with thickness growing up with the dipping time. The following exposure of such sample to light or to an e-beam causes dissolution and photo-doping of Ag into AGC (Wagner *et al.*, 2001).

Using the so-called step-by-step solid-state reaction, the composition of the doped films can be tailored, and the required content of Ag may be introduced. Single-phase samples of AC containing up to 27 at.% Ag and thickness up to 2.5 μm were obtained by such a method in the Ag–$Ag_{30}S_{70}$ system.

3.2.1 Physical vapor deposition

There are many different methods which generically come under the PVD category. In the following, we present those which are often applied for the preparation of AGC layers. Classical thermal vacuum evaporation and vapor deposition is well known and commercial equipments are broadly available. Preparation of thin films, of complex chalcogenide systems (binary, ternary, or multinary), by classical thermal evaporation of samples in high vacuum is also largely applied. The fractional evaporation of components of the glass with different volatility can be realized, making the obtainment of nonhomogeneous and non-stoichiometric films possible. Flash evaporation and PLD are also possible solutions and very often give films with composition close to source material.

During flash evaporation, the finely powdered GC is slowly poured onto a hot boat so that the individual powder particles are immediately evaporated and the vapor is deposited on the substrate. The inhomogeneity and nonstoichiometry of the prepared films are much lower in this case and a further annealing contributes to remove microvolumes of material of locally changed composition.

In the case of sputtering and co-sputtering, the evaporation is due to bombardment of a material target by ions in plasma discharge (direct current (DC) or alternating current (AC)) at low gas pressure. The ions can be concentrated on the target by magnetic field. Sputtering can proceed from one or more independent targets.

In the case of PLD, the evaporation of the target material proceeds under the effect of short laser pulses (from femtoseconds to tens of nanoseconds) of high intensity and high energy (e.g., pulses of some excimer laser emitting in ultraviolet (UV) region, energy ≥ 5 eV, intensity $\sim 10^8$–10^9 W cm^{-2}) directed to the surface of the target. Every pulse evaporates, due to its high energy, all components simultaneously, independently on their volatility. The stoichiometry of the resulting film is often preserved (Frumar, 2005). The kinetic energy (temperature) of particles (atoms, ions, fragments, and atomic clusters) evaporated by these intense laser pulses is of the order of $\sim$keV and the reactions among the particles or fragments during condensation are much quicker as compared with thermally evaporated films. The structure of films prepared by PLD method can be closer to the structure of target glass – again as compared with films prepared by classical thermal vacuum evaporation. As an example, we mention the amorphous PLD As–Se films. The PLD films contain less wrong As–As and Se–Se bonds and lower content of As_4Se_4, As_4Se_3, Se_8, or Se_n particles, in comparison with thermally evaporated films or even with bulk glasses (Frumar *et al.*, 2006; Nemec *et al.*, 2005).

The PLD method is also suitable for the preparation of thin films of RE-doped chalcogenides (Frumar, 2005). The classical vacuum evaporation gives low content of RE elements in the film, because the formed RE chalcogenides have very low volatility.

The films prepared by P are more homogeneous. Their spectra are nearly without narrow sharp features, the material contains only small amounts of molecular species such as As_4Se_4, As_4Se_3, and low concentration of As–As bonds. On the contrary, these molecular entities are present in the bulk glass that is not fully homogeneous in the nanoscale region. Raman spectra of bulk $As_{57.14}Se_{42.86}$ (As_3Se_2) glass (full line); as-deposited (dashed line) and exposed (dotted line) PLD As_3Se_2 thin films. The Raman bands of molecular entities are more pronounced in bulk glass because the content of As is higher. The thin films prepared by PLD are more homogeneous (Frumar *et al.*, 2006), adapted.

3.2.2 Chemical vapor deposition

The deposition of material (thin films) on a substrate surface proceeds by chemical reaction from vapors of precursors (e.g., from $(GeCl_4)_g + x(H_2S)_g$ or from $(GeCl_4)_g + (x/2)(S_2)_g$, in which process germanium chalcogenides (GeS_x) are formed). The number of precursors and of possible chemical reactions is large and the composition of prepared material can be very complex. In order to obtain very pure glasses or films, organochalcogen and organometallic compounds are applied. Such compounds can be obtained in high purity with extremely low content of contaminants.

3.2.3 Deposition from solutions

Thin films of AC can be also prepared by sol–gel method from the solution of some chalcogenides in proper solvents, for example, in derivates of alkyl amines by dip- or spin-coating method. Choice of the proper solvent is the main problem, especially for selenides and tellurides containing transition metals or RE elements that are not soluble in most solvents without degradation. In spite of this, the spin-coating method has been successfully applied even for the preparation of films of Ge–Se–Te system (Kohoutek *et al.*, 2007). The original chalcogenide could be received back from the solution obtained by evaporation of excess of solvent.

Chemical reaction also proceeds during Ag photo-doping, Ag electrochemical depositions, chemical plating, or during step-by-step reactions.

3.3 Chemical Reactivity of AGC

The AGC can be attacked by oxygen and humidity that cause the oxidation or hydrolysis of the surface. They can be also attacked by many reactive gases and alkaline or oxidizing solutions (Vlcek *et al.*, 1991). Sulfide and selenide glasses with sulfur or selenium excess are also attacked by CS_2 or aromatic hydrocarbons (benzene, toluene, etc.) that can remove eventually an over-stoichiometric (excess) chalcogen.

The solubility of arsenic-based sulfides can also be changed by sorption or chemisorption of tetraalkylammonium ions, in which at least one alkyl is long enough. The exposure, doping, and photo-doping can strongly influence the solubility of AGC in different solvents, including reactive solvents. Part of this problem is also discussed in Section 6.

Due to the relatively high reactivity of AC, their surface must be protected if they operate in atmospheric conditions, otherwise they have to be kept in vacuum or in inert atmosphere.

4 Structure, Crystallization, and Microliquation of AGC

4.1 Structure of AGC

The structure of AGC depends on the chemical nature of the components, on their content, the energy of atomic interactions, and on the temperature. The short-range order and the size and quality of the first coordination sphere depend generally on the energy and character of individual chemical bonds. The short-range order of amorphous As_2S_3 and As_2Se_3 is similar to this one in these crystals (Grigorovici, 1974). The arsenic atoms usually have the coordination number (CN) = 3; the CN of sulfur is usually 2. The As–As and S–S bonds and the molecules of As_4S_4, As_4Se_4, As_4S_3, and As_4Se_3 are usually present in amorphous arsenic sulfides and selenides, as well.

The structure of glassy chalcogenides prepared at different temperatures can be different, as well. Generally, the state and structure of AGC also depend on the pressure and presence of low-intensity electrical and magnetic fields during their preparation, although their influence is rather negligible.

The structure of the GC is similar to their melts at temperatures near their glass-transition temperatures, where the viscosity of the melt is so high that it practically prevents further atomic movement.

The structure of some AGC and their X-ray radial distribution function can be described by several simplified models, for example, by the perturbed crystal approach – amorphous solids are considered as high-temperature crystal forms, which contain a high number of inherent structural defects (Gutzow and Schmelzer, 1995).

The microcrystal or cluster approach supposes that the a-solid consists of crystallites that are small enough to be detectable by X-ray diffraction and the crystallites are randomly oriented.

The continuous network model, which is applied most frequently, supposes that the AGCs are formed by infinite, non-periodical network of three-dimensional (3D) arrays of atoms distributed randomly, partly-, or fully-chemically ordered. The rules of crystalline state are not valid, but the short-range order (at least the first coordination sphere of individual atoms) is often preserved in many covalent AGCs. It does, however, mean that, for example, atoms A of the A–B system are preferably surrounded by atoms B not only in crystals, but also in liquids and glasses. When the melt of the glass-forming material is cooled below glass-transition temperature, T_g, the clusters of atoms (macromolecules) become large and practically immobile. The coordination numbers of individual atoms and the lengths of chemical bonds cannot be further changed easily. The glass could be still inhomogeneous at atomic scale and can contain small volumes of different composition, even small nanocrystals or small regions of unmixed glass.

The microstructure of AGC can have many possible arrangements, depending on the conditions for their preparation and treatment (e.g., annealing temperature and annealing time); the structure has also different corresponding energy states. The structure of AGC can be changed between these states by outer conditions, which provide many possible configurations for AGC. According to S. R. Ovshinsky "The amorphous and glassy state have much more freedom in its composition and structure, while the crystal at given conditions has only one possible state."

The presence of nonbonding (lone) electron pairs on chalcogen and on pnictide atoms (As, Sb, and P) plays also important role in the formation of the structure of AGC. Nonbonding electrons band that is overlapping with valence band and forms its upper part (Fritzsche, 1974) can be excited and creates a third chalcogen bond, or they can be changed to bonding electrons, while the former bonding electrons become nonbonding. The bonding angles, coordination, and structure of AGC can be thus easily changed (Adler *et al.*, 1985). Such changes do not need a large energy because the nonbonding electron states and bonding electron states are overlapping in the valence band of the covalent AGC.

The melt of many chalcogenides can be dissociated at higher temperature and the dissociated state can be preserved in chalcogenide glass. For the simplified A–B system with not very large differences among the energies of the forming bonds A–B, A–A, and B–B, the equilibrium constant K, and the number of X–Y bonds can be expressed by:

$$K = \frac{[\mathrm{A}-\mathrm{B}][\mathrm{B}-\mathrm{A}]}{[\mathrm{A}-\mathrm{A}][\mathrm{B}-\mathrm{B}]} \cong Ce^{-\varepsilon/kT} \qquad [3]$$

where [X–Y] is the concentration of chemical bonds between atoms X and Y and $\varepsilon = 2\varepsilon_{AB} - \varepsilon_{AA} - \varepsilon_{BB}$. The ε_{AB}, ε_{AA}, and ε_{BB} are energies of A–B, A–A, and B–B chemical bonds, respectively. When the value of $|\varepsilon/kT|$ is small, the structure of the system resembles the continuous random network model (see Section 4) with statistical positions of atoms A and B. Such system contains a large concentration of the so-called wrong bonds between atoms A–A and B–B. When the (ε/kT) is larger, the system becomes chemically well-ordered and the number of heterobonds (X–Y) is much higher than the number of homopolar (wrong) bonds (X–X or Y–Y). It is to be noted that the disorder of a given system also depends on temperature according to eqn [3], and can be frozen down by quick cooling.

The fact that the AGC can dissolve very large amounts of different elements, for example, of metals such as Ag (up to 57 at.%, see above), is enabled by the structure and the large free volume of AGC and by the character of chemical bonding of Ag and of AGC. The Ag is introduced into AGC as an Ag^+ ion and its charge is compensated by C_1^- defects (negatively charged onefold coordinated chalcogen). The Ag^+ ion is bonded by two, three, or four coordination bonds between free Ag d-orbitals and lone

pairs of chalcogens (Fritzsche, 2000). Such bonds can be converted back to the original state when Ag^+ ion moves to a new position. Then new coordination bonds with new chalcogen lone pairs and with unoccupied d-orbitals of Ag^+ are formed, which may be repeated many times. As a result, the Ag^+ ions in AGC can move easily. The Ag^+-doped glasses are good ionic conductors. The activation energy of Ag^+ diffusion decreases with increasing Ag concentration (Ribes *et al.*, 2001).

Experimentally found value of CN of Ag^+ in sulfides and selenides is between 3 and 3.5, while in tellurides CN $\sim$4. The structure of Ag-photo-doped As–S films is similar to the structure of Ag–As–S glasses; the Ag is threefold coordinated by sulfur, whereas the arsenic atoms remain threefold coordinated by chalcogens. The lower coordination number of Ag in AC can be explained by lack of accessible chalcogens in the vicinity of Ag^+ ions, especially when the Ag content is high. In some cases, the introduction of Ag into chalcogenides of As, Sb, or Ge also causes the formation of As–As, Sb–Sb, or Ge–Ge bonds. The Ag–Ag, Ge–S, Ag–S, Ag–Ge, and Ge–Ge interactions were found in GeS_2–Ag_2S in Ag_2S–As_2S_3 glasses by neutron diffraction (Bychkov and Price, 2000). The CN of Ag becomes higher than four in Ag–As–Te glasses for higher content of Ag. The X-ray analysis of $(Ag_2Te)_x(AsTe)_{1-x}$ glasses with $x=0$–3 revealed that As atoms are three times coordinated, and Ag atoms are roughly fourfold coordinated with Te atoms. The coordination of Te atoms increases from 1.93 to 3.60 with increasing Ag content (Usuki *et al.*, 2001).

4.2 Crystallization of AC

The ACs are thermodynamically metastable, in equilibrium state they crystallize. The crystallization rate for any given system depends on the temperature, as can be illustrated by the so-called T–T–T curves. Only when the melt is cooled very fast, the interval of crystallization temperatures can be exceeded and glasses can be prepared. This is important especially for thin films of phase-change memory (PCM) materials. After melting of such thin films by very short optical or electrical pulses ($\tau >$ fs, mostly $\tau >$ ns), their cooling rate can be as high as 10^{11} K s^{-1} (Yamada, 2009). With such a cooling rate, glassy films can be prepared from nearly any material, including strongly nonstoichiometric PCM. Upon crystallization, formation of different phases may occur as the composition regions of glasses are much broader than those in crystals. The crystallization process (the formation of crystal nuclei and their growth) is often slow, especially when it requires the atomic transport for the formation of different phases. The overall crystallization rate is then limited.

The crystallization of AC can proceed starting from homogeneous nucleation, when the crystal nuclei are formed randomly in the whole volume of the glass due to decrease of Gibbs energy due to crystallization. In such a case, change of Gibbs energy, ΔG, of nucleation barrier is given by:

$$\Delta G(r^*) = \frac{16\pi\sigma^3}{3(g_2 - g_1)^2} = \frac{16\pi\sigma^3}{3}\frac{V^2 T_K^2}{\Delta H_T^2 \Theta^2} \quad [4]$$

where σ is surface energy of the interface of nucleus-melt (or glass), T_K is temperature of phase transformation, ΔH is enthalpy of phase transition, Θ is undercooling in K, V is atomic volume, g_i is the Gibbs energy of individual atoms, and r^* is the critical size of nucleus. Intensity of nucleation is given by:

$$I = K_V \exp\left[-\frac{(\Delta G + \Delta G_a)}{kT}\right] \quad [5]$$

where,

$$\Delta G = \frac{16\pi\sigma^3}{3(\Delta G_v)^2}$$

is the thermodynamic barrier of nucleation, and ΔG_a is the kinetic barrier of transport of mass over the interface crystal-melt (glass). ΔG_v is the change of Gibbs energy per unit volume. While ΔG is very low at lower temperatures, ΔG_a increases exponentially with decreasing temperature and is a governing factor at lower transition temperatures.

If some crystallization centers are present in AGC (heterogeneous inclusions, surface, small crystals, not fully melted crystals, surface of substrate, and interface with other layers or walls of the tube or of container), the crystallization can proceed according to the so-called heterogeneous crystallization. In such a case, the nucleation barrier is much lower (eqn [6]), since the variation of Gibbs energy connected to a single nucleous is smaller and crystallization is much quicker:

$$\Delta G(r^*) = \frac{16\pi}{3}\frac{\sigma^3}{(g_2 - g_1)^2}F \quad [6]$$

The first part of the right-hand side of eqn [6] is identical to the case of homogeneous crystallization (eqn [4]), the function F has very low value for the beginning of heterogeneous nucleation ($F \ll 1$, Gutzow and Schmelzer, 1995, p. 285).

Both homogeneous and heterogeneous mechanisms are very important for the whole processes of crystallization, especially for PCM materials, where fast crystallization (several nanoseconds or maximally several tens of nanoseconds) is necessary. Partly crystallized glasses can have lower thermal expansion coefficient and better mechanical properties (hardness, toughness, …). If the size of formed crystallites is lower than the wavelength of the light, such materials are well transparent and can be applied in different optical elements.

4.3 Microliquation

The melts of chalcogenides can usually dissolve relatively large excess of components of the glass or of other elements or compounds. The homogeneity regions of the melt or of the glass are lowered at lower temperatures. As a result, not only crystallization but also some unmixing effect could be observed, when two or more nonmiscible liquids or nonmiscible glasses are formed from a formerly homogeneous matrix. The size, amount, and composition of separated liquids, and consequently glassy phases depend on temperature, thermal history, and on composition of original melt. The size of separated phases can be very low and the separation is invisible for $d < \lambda$. When the size of separated phases is larger ($d \geq \lambda$), the scattering of the light is observed. (Vogel, 1979). Small crystals in phase-separated glasses can be considered as macrodefects.

5 Defects in AGC

The defects play an important role in crystalline solids, since they may control many of their physical and structural properties (electrical conductivity, type of conductivity, mobility of free carriers, optical absorption, luminescence, etc.). The definition of defect is relatively clear and simple: the defects are represented by changes in local or extended order of the crystal.

In amorphous solids, the situation is not so clear as the atoms in amorphous and glassy solids are not confined in exact positions; there are many fluctuations in bond lengths, bond angles, CNs, and local composition. It is difficult to discriminate between small position fluctuations and high fluctuations that they should be considered as defects or not. The border between small deviation of structure and structural defect is not sharp. The concentration of irregularities in the AGC can be as high as 10^{21} cm^{-3}. Disturbance of the local order results in the formation of localized states in the forbidden energy gap of AGC. They are formed often near the band edges (in the band tails, the effect of disturbances is small). High density of such defect states in the gap pins the Fermi level near the middle of energy gap (**Figure 3**).

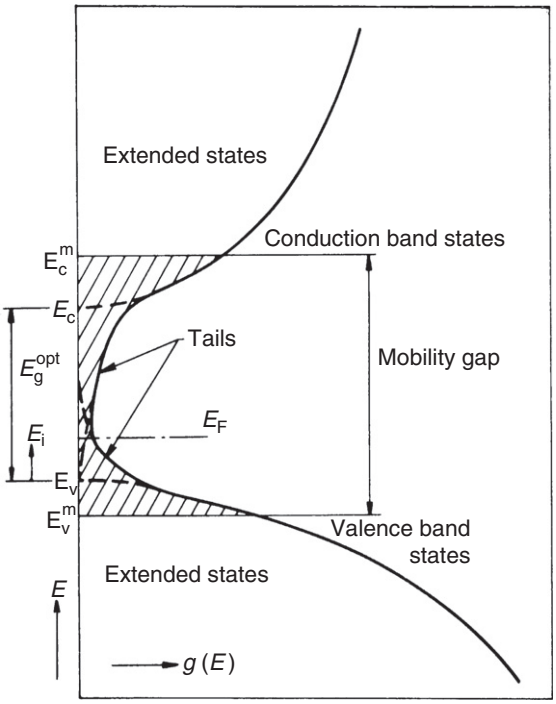

Figure 3 Density of electron states $g(E)$ as function of energy E in amorphous semiconductors, according to the Mott–Cohen–Fritzsche–Ovshinsky model. E_g^{opt} is determined by extrapolation of delocalized states. E_v^m and E_c^m are mobility edges (Tauc, 1974, p. 177). With kind permission of Springer Science and Business Media.

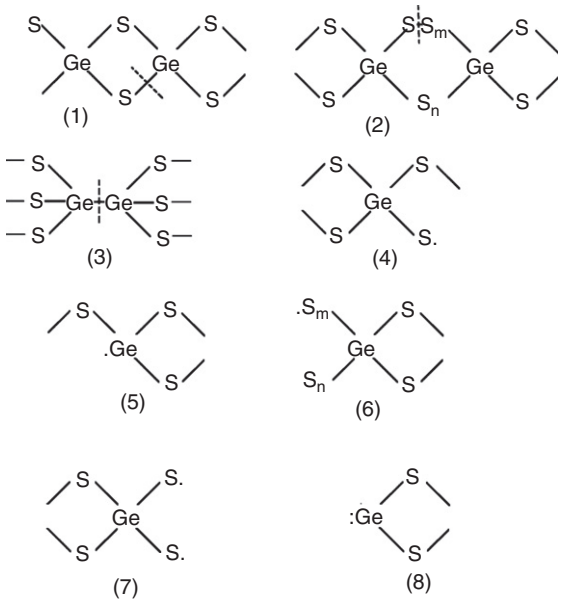

Figure 4 Structural units and proposed defect centers in Ge–S system glasses. Expected breaking of chemical bonds is described by dashed lines. Different paramagnetic defects are formed and their spectra are different due to their different symmetry. The unpaired electron on sulfur atoms is pictured by a dot; *m* and *n* are integers, $m \geq 1$; $n \geq 1$. The electron paramagnetic resonance (ESR) spectra were simulated on the base of molecular orbital (MO) model. The computed spectra were in good agreement with experimental results (Cerny *et al.*, 1979). With kind permission of Springer Science and Business Media.

In fresh-evaporated films, the presence of products of dissociation of evaporated materials can be also found. During deposition on a cold substrate, these products were not able to react with other dissociated particles in order to form the original targeted material.

Some defects can be charged, for example, $-S^-$, $-Se^-$, C_1^-, C_3^+, Ag^+, Li^+, and RE^{3+}, and some can have unpaired electrons (dangling bonds, e.g., in Ge–S system glasses; **Figure 4**; Cerny and Frumar, 1979). Charged defects are very common in chalcogenide glasses, especially in sulfides and selenides, due to the breaking of many chemical bonds caused by fluctuations of composition and structure. As the electronegativity of S (2.5), Se (2.4), and Te (2.1) is higher than the one of Si (1.8), Ge (1.7), As (2.0), and Sb (1.8) (Wells, 1975), both electrons of covalent chemical bond between chalcogen and element of lower electronegativity can be captured (after bond breaking) by more electronegative chalcogen. The reaction $M{-}C = M^+ + C^-$, is likely to take place, where M^+ is for more positive element with lower electronegativity and C^- is for negatively charged chalcogen, and M–C represents the covalent bond between M and C.

The changes in CNs of chalcogen and other atoms lead to the formation of over-coordinated and under-coordinated atoms (e.g., C_3^+ and C_1^- for chalcogen) that can be also charged. The subscript is here for the CN, the superscript is for the charge. The formation of such defects costs a relatively low energy (Kastner *et al.*, 1976). The concentration of intrinsic defects in AGC can be high (up to 10^{21} cm^{-3}). The Fermi level is effectively pinned near the middle of energy gap due to gap levels introduced by intrinsic defects.

The extrinsic defects in AGC are formed by atoms, molecules, or additives that do not belong to the original AGC matrix. It is often difficult to determine whether some additives are forming the glassy matrix (glass formers or glass modifiers) or behaving like extrinsic defects. The extrinsic additives can be added to the melt, introduced by co-evaporation, diffusion, doping, photo- or electrically-enhanced diffusion, reactions of AGC with environment, ion implantation, etc. The extrinsic defects can also be included into glass by contamination of the melt or precursor materials by crucible (ampoule) walls, and from impurities in starting materials.

Interaction of the surface of AGC or their precursors with air or water vapors can cause creation of –OH, =O, $-S^-$, –SH, $-Se^-$, –SeH groups on the surface of material. These groups also form extrinsic defects. The presence of such defects is not desirable, especially in chalcogenide fibers where they substantially lower their transparency; they are absorbing in IR region of spectrum. This problem is discussed in Section 6.2.

The dopants and alloying elements in AGC have, contrary to crystals, much smaller influence on Fermi-level position because the concentration of extrinsic dopants is often lower than the concentration of intrinsic defects. Most of the atoms in the AGC melt can satisfy their CNs (8-N rule; Mott and Davis, 1991), so the impurity atoms are not confined to matrix coordinations such as P or B in crystalline silicon. Their influence on semiconducting properties of AGC is then much lower.

The amorphous Se is an exception in doping of AGC. Even (10^{-3}–10^{-4}) at % of oxygen or chlorine can change the electrical conductivity of a-Se by several orders (Kasap and Rowlands, 2000). There are also other exceptions but not so sensitive; some

dopants can change not only the density but also the sign of prevailing free carriers. The Bi doping of AGC (Frumar and Tichy, 1987) can convert the usual p-type conductivity of most chalcogenides to n-type. However, even in this case, the concentration of Bi shall be relatively high, $c \geq 10$ at.% Bi. The n-type conductivity of crystalline Bi_2S_3 and Bi_2Se_3 is ascribed to vacancies in chalcogen sublattice; some Bi atoms are undercoordinated, which can occur in amorphous chalcogenides as well (Frumar and Tichy, 1987). The n-type electrical conductivity was also found in amorphous In_2S_3 and In_2Se_3 films (Marsillac *et al.*, 1996), possibly again due to sub-stoichiometry of chalcogens.

Similar effect as for Bi can be seen in Li- and Cd- or Ni- doped AGC. Their concentration can be, however, lower, for example, for Ni in Ge–As Se–Te $\approx$0.3–1 at.% (see e.g., Hamakawa, 1982, p. 218).

Some dopants are mainly electrically active (Cd, Ni, Bi, Li, Ag, Cu; and O or Cl in a-Se), while most of transition metals, or RE ions in AGC are mainly active optically (absorption and luminescence). In RE-doped AGC, the RE ions enforce their own coordination and their electronic states are localized. In these glasses, the light absorption and luminescence proceed between inner f–f electron levels of RE ions, so both levels are discrete and do not influence the electrical properties of the material.

The extended defects that are created by nucleation embrya, small crystals, or small nonmiscible glassy inclusions can be also found in many AGCs. Fluctuations of density, index of refraction, and chemical composition can be considered also as the extended defect or macrodefects of AGC. They influence optical transmission by photon scattering so that a very low concentration is necessary, especially in fibers, where the optical thickness is large and equals to fiber length. The extended defects can scatter the light and effectively reduce the optical transmission. Their content can be partly lowered by annealing of the AGC near the glass-transition temperature when the glass structure relaxes and fluctuation of density, composition, and index of refraction is lowered. The fluctuations of chemical composition in films are reduced by chemical reactions or diffusion among different composition entities in AGC. The relaxed glass becomes more homogeneous and closer to thermodynamic equilibrium.

The surface of any AGC can be also considered as an extended defect. The AGCs are generally sensitive to oxidation or hydrolysis, so they shall be prepared and treated in vacuum or in an inert atmosphere. Fibers, lenses, and other elements working in atmospheric conditions shall be covered by protective layers, otherwise the absorption by S–H, Se–H, O–H, and =O groups can considerably lower their optical transmittance (see Section 7).

6 Properties of AGC

Hardness (h) of AGC is generally lower than the one of oxide glasses. The hardness in the As–S system glasses spans from $h = 15$ kg mm^{-2} for AsS_{10} to $h = 109$ kg mm^{-2} for $AsS_{1.25}$. The hardness in the As–Se system glasses increases from $h = 66$ kg mm^{-2} for $AsSe_{0.8}$ to $h = 150$ kg mm^{-2} for As_2Se_3, then it drops to $h = 52$ kg mm^{-2} for $AsSe_{20}$. The glassy Se has the hardness $h = 42$ kg mm^{-2}. The hardness of Ge–Se system glasses spans from $h = 68$ kg mm^{-2} for $GeSe_{24}$ to $h = 223$ kg mm^{-2} for Ge_2Se_3. In the Ge–Sb–Se system, it spans from $h = 71$ kg mm^{-2} for $GeSbSe_{18}$ to $h = 43$ kg mm^{-2} for Ge_6SbSe_{13} (Borisova, 1981).

Thermal properties of AGC are typical for glasses. Temperatures of glass transition, T_g, glass crystallization, T_c, and melting of crystallized glass, T_m, are mostly lower than those of oxide glasses. Some AGCs, especially those containing halides, can be liquid at room temperature or even below it. Such glasses can be used as immersion layers or adhesive layers between lenses or more complex optical elements.

Thermal conductivity of most chalcogenides is low.

Heat capacity of AGC follows the Neumann–Kopp rule. It means that the specific heat (c_p, c_v) of AGC equals to the sum of specific heats of constituting elements. The heat capacity c_p of Ge–Se system glasses drops from Se ($c_p = 23$ J g at^{-1} K^{-1}) to $GeSe_2$ (21.8 J g at^{-1} K^{-1}) and increases again to GeSe (Borisova, 1981). The coefficient of thermal expansion of AGC is often higher than the one for oxide glasses. The coefficient of thermal expansion of As–Se system glasses linearly decreases with composition from 47×10^{-6} K^{-1} for Se to 20×10^{-6} K^{-1} for As_2Se_3 (all at 0 °C) and then steeply increases again.

Detailed information on thermal properties, hardness, densities, and glass-transition temperatures, T_g, of many glasses can be found in Popescu (2000).

6.1 Electrical Properties, Electronic and Ionic conductivity, Solid Electrolytes

The electrical conductivity of most undoped AGC is of p-type, the holes are the prevailing charge carriers. The reason is not fully clear. It could be explained by the higher electronegativity of chalcogen atoms that can capture more easily an electron forming C_1^- defect rather than capturing a hole. The values of electrical conductivity spans in a broad region from $10^{-16}\,\Omega^{-1}$ cm^{-1} for sulfur-rich As–S glasses to $10^{-3}\,\Omega^{-1}$ cm^{-1} for some telluride glasses. The detailed information on electrical conductivity and optical properties of many AGC can be found in Borisova (1981), Mott and Davis (1991), Popescu (2000), Kasap and Rowlands (2000), Tauc (1974), Adler *et al.* (1985), Mort (1989), Zallen (1983), Boetger (1985), and Elliott (1995). The ionic conductivity of Ag-doped glasses can be also high ($10^{-5}\,\Omega^{-1}$ cm^{-1}).

The energy bands do have not sharp edges and some electronic states are extended to the forbidden gap and localized because of fluctuation of bond lengths, bond angles, and CNs (see above). The mobility of free carriers in these localized states is much lower than in extended ones and a mobility gap is formed (Fritzsche, 1974). The extended electron states in the conduction band

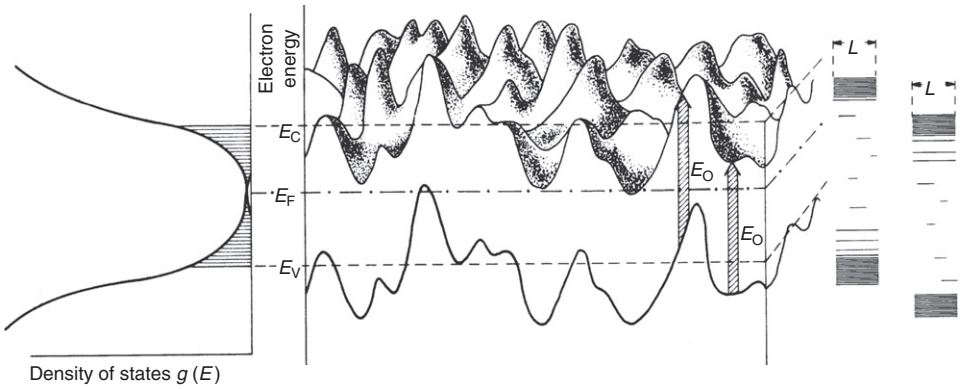

Figure 5 Sketch of the symmetric part of long-wavelength potential fluctuations. The E_0 corresponds to an average optical gap. E_c and E_v are the percolation thresholds or mobility edges. The left-hand side shows the density of states. The distribution of localized gap states between E_c and E_v is not necessarily smooth and monotonic. On the right-hand side, the states in two volume elements of size L^3 are sketched. The length of the horizontal bars illustrates schematically whether the states are localized or extended within L^3 (Fritzsche, 1974).

are above the hills; the extended states of holes are below the valence band minima (**Figure 5**). At lower temperatures, the electronic transport is controlled at low electric fields by hopping of free carriers within the localized tail states, at higher temperatures the transport is governed by electron transitions from localized states to the extended states and vice versa, and eventually between the extended states in the bands. The DC conductivity σ is not activated for variable-range-hopping when the Fermi level lies inside a wide band of localized states. The σ is given by:

$$\sigma = \sigma_{\mathrm{VRH}} \exp\left(-T_0/T^{1/4}\right) \qquad [7]$$

In some amorphous semiconductors, the DC conductivity is activated down to the lowest temperatures and is given by:

$$\sigma = \sigma_0 \exp(-\beta(E - E_{\mathrm{F}})) = \sigma_0 \exp(-\Delta E/kT) \qquad [8]$$

where $\beta = 1/kT$, E the transport energy, and E_{F} is the Fermi energy. σ_0 is often 10^3–$10^4\ \Omega^{-1}\,\mathrm{cm}^{-1}$, but values as high as $10^8\ \Omega^{-1}\,\mathrm{cm}^{-1}$ and as low as $10^{-5}\ \Omega^{-1}\,\mathrm{cm}^{-1}$ were also reported. For a comprehensive review of hopping theory, the reader may refer to Boetger (1985).

The n- and p-type conductivity in AGC was shortly mentioned in part devoted to defects, (Section 5). The electrical conductivity of AGC in high electrical fields abruptly increases, charge carriers are excited to energies above the mobility gap, and the conductivity proceeds via extended states. Details are discussed later in connection with memory and threshold switching (Section 7).

The thermoelectric power S of p-type AGC can be expressed (Mott and Davis, 1991) for $\mathrm{E} > \mathrm{E_c}$ by:

$$S = -\frac{k}{e}\left[\frac{E_{\mathrm{c}} - E_{\mathrm{F}}}{kT} + A_{\mathrm{c}}\right] \quad \text{for } E < E_{\mathrm{v}} \qquad [9]$$

$$S = \frac{k}{e}\left[\frac{E_{\mathrm{F}} - E_{\mathrm{V}}}{kT} + A_{\mathrm{v}}\right] \qquad [10]$$

$$A_{\mathrm{C}} = \frac{\int_0^{\infty} \frac{\varepsilon}{kT}\delta(\varepsilon)\mathrm{d}\varepsilon}{\int_0^{\infty} \delta(\varepsilon)\mathrm{d}\varepsilon} \quad \text{for } \varepsilon = E - E_c \qquad [11]$$

$$A_{\mathrm{V}} = \frac{\int_{-\infty}^{0} \frac{\varepsilon}{kT}\delta(\varepsilon)\mathrm{d}\varepsilon}{\int_{-\infty}^{0} \delta(\varepsilon)\mathrm{d}\varepsilon} \quad \text{for } \varepsilon = E_v - E \qquad [12]$$

Most of AGC has relatively high electrical resistivity and thermoelectrical power measurements are difficult.

6.1.1 The Hall effect

The experimentally found values of the Hall coefficient were always negative and not dependent on the sign of Seebeck coefficient. Due to very low mobilitities of free carries, the Hall effect was exceedingly difficult to be measured.

6.1.2 Ionic conductivity

Pure AGCs are electronic conductors and the prevailing charge carriers are holes. The AGC doped by Li^+, (or other alkaline ions), or doped by Ag^+ or Cu^+ ions can be good ionic conductors when the concentration of Ag or Li is higher than ≈ 5 at.%. The glasses with Ag content above 30 at.% can be considered as ionic superconductors (Frumar and Wagner, 2003); the conductivity of $AgAsS_2$ glass is, for example, $\sigma = 10^{-5}\,\Omega^{-1}\,cm^{-1}$. The addition of Ag to chalcogenide glasses (up to 57.1 at.% for GeS_3 glasses) increases the electrical conductivity due to ionic conductivity of Ag^+ ions for up to 11 orders of magnitude (for 30 at.% of Ag, Kawasaki *et al.*, 1999).

In glasses of the Ag_2S–As_2S_3 system three regions of ionic conductivity and of silver transport numbers t_{Ag} were found (Frumar and Wagner, 2003). The first one, with $x_{Ag} < 30$ ppm and small silver transport number, $t_{Ag} \approx 0.1$; the second region (30 ppm $< x_{Ag} <$ 1–3 at.%, $t_{Ag} \approx 0.8$–1), which is considered as critical percolation domain, and then the so-called modifier controlled domain, $x_{Ag} >$ 10–15 at.% Ag, $t_{Ag} \approx 1$.

6.2 Optical Properties, Photo-Induced Effects, Luminescence, and Nonlinear Optical Effects

6.2.1 Optical transmittivity

The sharp structure of optical spectra observed in crystalline solids is not to be found in AGC. The fluctuations of bond lengths, bond angles, index of refraction, and of density that are caused by lack of long-range order in atomic structure broaden the absorption bands and absorption edges. The optical transparency of AGC is limited by short-wavelength absorption edge near the energy gap, E_g, and by lattice vibrations (multi-phonon absorption) in the long-wavelengths part of the spectrum. Typical loss spectra of some chalcogenide glass fibers are given in (Sanghera and Aggarwal, 1998).

The AGCs are well transparent in the IR part of spectrum, (sulfides 0.5–11 μm, selenides 0.8–15 μm, and tellurides 1.3–20 μm). The transparency depends on composition, wavelength, and thickness. Some AGCs are also transparent in the visible part of the spectrum (e.g., Ge–S and As–S system glasses, especially those with excess of sulfur). Most of AGCs (sulfides and selenides, pure and with excess of metallic component, e.g., As, Ge, Ga) are not transparent in the visible part of spectrum; most of telluride glasses possess good IR transmittivity and metallic-like reflectivity in the visible part of spectrum.

The minimal absorption coefficient in optical windows of transparency of AGC is higher than in silica glasses and fibers. The minimal absorption coefficient of AGC can be lowered by their annealing, further purification of starting elements, and distillation or purification of products. The content of intrinsic defects, for example, those formed by wrong bonds depends on AGC, on chemical bond energies among elements of the glassy matrix, and on temperature. These energies are in AGC lower than in oxides and the densities of intrinsic defects should be higher. The defects decrease the optical transmittivity, which is crucial in optical fibers. The chalcogenide fibers will not be, therefore, well applicable for the long-distance optical transmissions; they can be fully acceptable for shorter distance light or signal delivery, as for surgical knives, sensors, etc. They can be also excellent materials for waveguides and planar optical circuits (Section 7).

The short-wavelength absorption edge that corresponds to the transition from the valence or nonbonding band to the conduction band, and partly to the transitions from localized electron states in the band gap to the band, is not as sharp as in crystals. It is a result of fluctuations of bond angles and bond lengths. The absorption edge in AGC can be generally divided into several parts (e.g., according to the Tauc to A, B, and C, Tauc, 1974). The part A of high absorption ($\alpha > 10^4\ cm^{-1}$) is connected with band–band electronic transitions and can be linearized by the formula $(\alpha h\nu)^{1/n} = (h\nu - E_g^{opt})$ and can be used for determination of E_g^{opt} (**Figure 6**); α is the absorption coefficient, $n \approx 2$ for many glassy chalcogenides (Tauc, 1974).

The part B is the so-called absorption or Urbach tail. It covers several orders of α and can be found between $\alpha \approx 0.1$ and $\alpha \approx (10^3$–$10^4)\ cm^{-1}$. The dependence of log α versus $h\nu$ is linear in this region (Tauc, 1974; Ticha and Frumar, 1974).

The weak absorption tail (part C) with absorption coefficient $\alpha \leq$ 1–10 cm^{-1} is caused by absorption of impurities and by scattering of light on inhomogeneities and microvolumes with different index of refraction. The fluctuation of density and composition causes the scattering of light and also lowers the transition of AGC in this region (Tauc, 1974). The value of α also depends on thermal history of the material. The detailed discussion of optical properties of AGC is given, for example, in Tikhomirov and Elliott (1995).

6.2.2 Absorption by impurities and doping elements

The short-wavelength absorption edge of Ag-containing AGC is red-shifted; the index of refraction is higher when compared with undoped glasses. Their optical transmittivity, reflectivity, and E_g^{opt} are changed by Ag doping; the coefficient of the optical nonlinearity, χ^3, is increased (Frumar and Wagner, 2003; Frumar *et al.*, 2003a,b). The optical gap E_g^{opt} of $Ag_x(As_{0.33}S_{0.67})_{100-x}$ photo-doped films decreased with increasing content of Ag from 2.45 eV ($x = 0$) to 1.9 eV ($x = 0.41$), while the index of refraction increased from 2.38 to 2.8 (Wagner *et al.*, 1994). The doping by RE elements or by transition metals raises the selective absorption in discrete parts of the spectrum (see, e.g., **Figure 7**; Sourkova *et al.*, 2009).

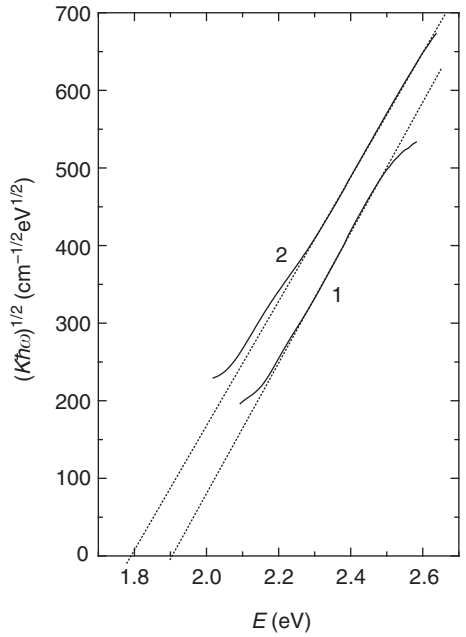

Figure 6 Spectral dependence of $(k\hbar\omega)^{1/2}$ of thin films (1, solid) fresh-evaporated Sb_2S_3, (2, solid) fresh-evaporated $Sb_2S_3 + Sm^{3+}$. Dotted lines are for extrapolation to zero value of $k\hbar\omega$ that corresponds to Tauc optical energy gap E_g^{opt}. The k is for absorption coefficient (Frumarova *et al.*, 2003).

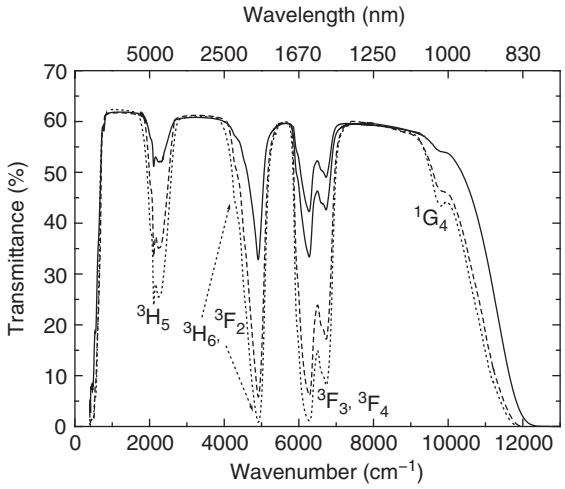

Figure 7 Transmission spectra of $(Ga_5Ge_{25}Sb_{10}Se_{60})_{100-x}(Pr_2Se_3)_x$ glasses: $x=0.1$ (thinner solid line), $x=0.2$ (thicker solid line), $x=0.5$ (dashed line), $x=0.6$ (dotted line). The thicknesses of all the samples are comparable. The absorption bands correspond to electron transitions from the $^3H_4$ ground level to higher energy levels given in the figure (Sourkova *et al.*, 2009).

The optical transmission in IR window of AGC is often reduced due to the presence of contaminations (e.g., metallic and nonmetallic impurities, O, OH, S–H, Me–O, Se–H, Se=O, and S=O bonds; that influence the minimal achievable absorption coefficient. The latter impurities can be removed only with large difficulties, while the metallic impurities can be removed more easily.

Many doping elements and also nonstoichiometric content of glass-building elements (such as excess of sulfur or excess of As in As_2S_3-based glasses) do not create new absorption bands in forbidden gap when their content is low, but broaden the electronic states near valence and conductivity bands and change the value of energy gap. It is probably due to the fact that most of the elements in the melt, and, consequently in the glass, can satisfy their valence and coordination demands, forming some structural or molecular units or forming also homonuclear bonds, for example, As–As, or S–S in As–S system. Such units form solid solution with the glass. If the concentration of such species is higher, they change the value of energy gap (**Figure 8**; Frumar *et al.*, 2003a,b).

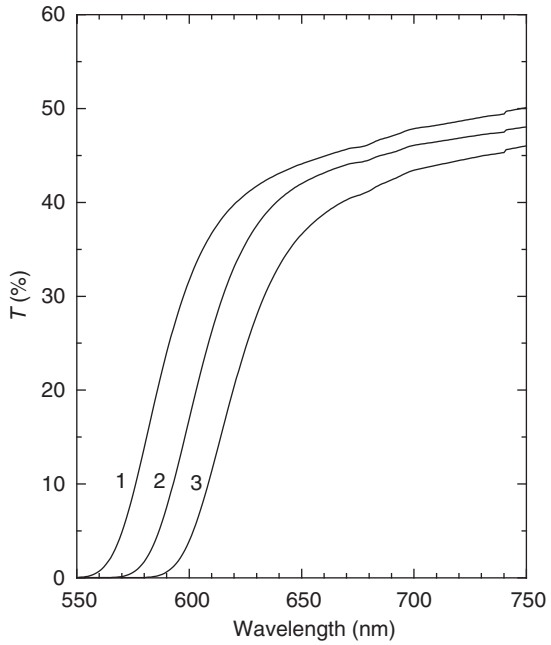

Figure 8 Optical transmittance of bulk glasses of As–S system. 1: $As_{38}S_{62}$; 2: $As_{40}S_{60}$; 3: $As_{42}S_{58}$. Thickness of the sample $d=2.45$ mm (Frumar *et al.*, 2001b). With kind permission of INOE Bucharest.

The individual absorption bands inside the optical window of AGC can be seen distinctly in chalcogenide glasses doped by RE elements (**Figure 7**; Sourkova *et al.*, 2009). Such absorption bands are connected with inner f–f electron transitions inside the RE ions. The excited state can relax after absorption with light emission often in near- and mid-IR spectral region (see Section 6.2).

In contrast to many oxides, the AGCs contain heavier elements, so the vibration frequencies are lower and are shifted further to the IR part of the spectrum. The short-wavelength edge is also shifted toward lower energies because of lower energy gaps of AGC containing heavy elements. Due to this fact, sulfides, selenides, tellurides, and their solid solutions have been used as optical materials well transparent in the IR region (Section 6).

The sulfur and selenium in AGC are usually twofold coordinated and the valence angles between two covalent bonds of sulfur or selenium are between 90 and 109 ° (bonds are formed preferentially by atomic p-orbitals). Such structure is flexible and the angle between two bonds can be easily deformed. Vibrations of structural units interconnected via such chalcogen atoms are practically independent (strongly localized, weakly coupled structural units, for example, AsS_3 pyramids in As_2S_3, or GeS_4 or $GeSe_4$ tetrahedra in germanium-containing AGCs). Their vibrations can be interpreted as vibrations of nearly free oscillators. Such an approach is very reasonable and in good agreement with experimental results and is broadly used for the interpretation of IR and Raman spectra.

Index of refraction, n, of chalcogenide glasses is considerably higher than in oxides. The polarizability of heavier atoms is higher and the index of refraction therefore increases from sulfides to tellurides (e.g., n(a-As_2S_3)=2.4, n(a-GeS)=2.3, n(a-As_2Se_3)=3.5, and n(a-GeTe)=3.8). The polarizability of atoms is proportional to the real part of dielectric constant $\varepsilon_1=n^2-k^2$, where n is the index of refraction and k is index of absorption. For small values of k (transparent region of the spectrum), the $n=\sqrt{\varepsilon_1}$.

The values of index of refraction of crystalline chalcogenides are even higher than those of glassy or amorphous forms of the same material (e.g., n(c-As_2S_3=2.98), n(c-GeS)=3.5, and n(c-GeTe=6), which has been applied in PCMs because the reflectivity strongly depends on the index of refraction n. The index of refraction depends on the wavelength; an example of spectral dependence of n of several Sb–Te thin films is given in **Figure 9** (see also Section 7). Due to higher values of index of refraction and of higher reflectivity of most of AGC, the optical IR elements should have anti-reflection coatings for reducing the reflection losses.

The index of refraction of many chalcogenide systems can be changed (tuned) in broad ranges by change of AGC composition. The Ag-doped AGCs have higher index of refraction when compared with undoped glasses. The index of refraction of GeSe films increases due to Ag doping from 2.38 to 2.8 (Wagner *et al.*, 1994). Even a higher index of refraction (up to 3.3) was found in telluride glasses of Ag–Se–Te system. They can contain up to 20 at.% Ag (e.g., in $Ag_{20}Se_{70}Te_{10}$), forming homogeneous glasses. The AC films, in which the index of refraction can be tuned by composition, have been used as anti-reflection layers for many semiconductors and optical elements. For such films it is seen that:

$$n_1 \approx (n)^{1/2} \qquad [13]$$

where n_1 is index of refraction of anti-reflection layer, n is index of refraction of the substrate (of given material). Multilayered chalcogenides can be used as the very selective filters or reflectors (**Figures 10(a)** and **10(b)**; Kohoutek *et al.*, 2009).

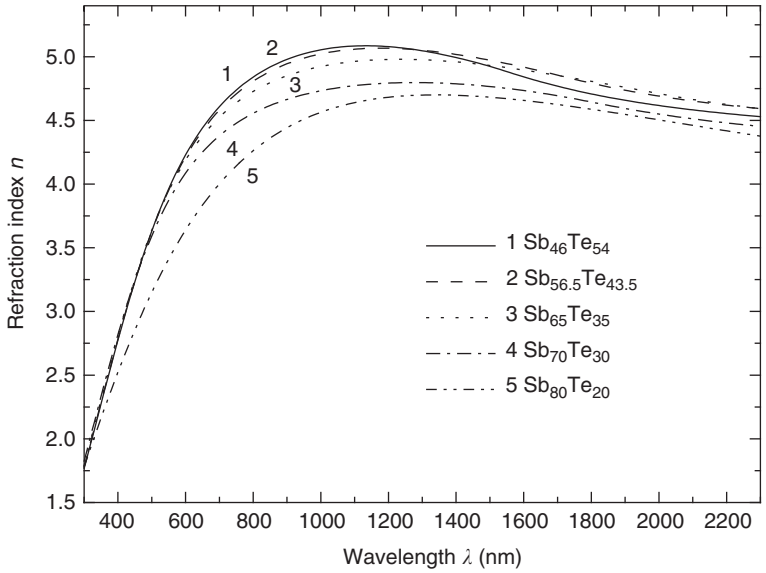

Figure 9 Spectral dependence of refractive index n of as-deposited amorphous thin films of Sb–Te system prepared by pulsed laser deposition.

The index of refraction of thin films depends on many factors (thermal prehistory, on evaporation method, and conditions of evaporation (thermal, flash, sputtering, temperature T, atmosphere, and pressure of evaporation); for films obtained by laser ablation energy of light pulses is important as well. The values of n of thin films are then much more scattered. This is especially true for fresh-evaporated films that can be chemically nonhomogeneous. The a-films annealed near glass-transition temperature are relaxed and their properties are often close to the properties of bulk glasses.

The spectral dependence of the index of refraction of amorphous chalcogenide films can be described using the Wemple–DiDomenico relationship for a single oscillator (**Figure 11**):

$$n^2(\omega) - 1 = \frac{E_0 E_d}{E_0^2 - (\hbar\omega)^2} \qquad [14]$$

where $\hbar\omega$ is the photon energy, E_0 is the single oscillator energy, and E_d is the dispersion energy.

The dispersion of index of refraction can be modeled (described) by the Tauc–Lorentz formula, which is also applicable in the area of higher absorption (Jellison and Modine, 1996). In the part of the spectrum at longer wavelengths (with low absorption), the Cauchy dispersion formula can be applied (Tompkins and McGahan, 1999).

The reflectivity of the material at normal incidence in nonabsorbing region ($k \to 0$) is given by:

$$R = \frac{(n - n_0)^2}{(n + n_0)^2} \qquad [15]$$

where n_0 is the index of refraction of incident medium (e.g., air) and n is index of refraction of given material.

6.2.3 Luminescence

Intrinsic luminescence of AGC is relatively weak (Cernoskova *et al.*, 1995). Contrary to this, the extrinsic luminescence of RE-doped AGC is strong and can be found in visible, near- and mid-IR spectral regions. Compared with other glass hosts, the AGCs are unique. They are well transparent in the IR region of the spectrum; they have higher index of refraction and lower phonon energy. As a result, they possess large stimulated emission cross section and because of their low phonon energy ($\approx$300–400 cm^{-1}), the nonradiative electron transitions between f–f levels of RE ions are of low intensity (eqn [16]). The luminescence of RE-doped AGC is then very intensive even in the IR region of spectra, where the emissive transitions of electrons in other hosts are effectively quenched.

The nonradiative decay rate, ω_p, due to multi-phonon relaxation, depends on the energy gap, ΔE between electron f–f energy levels, and phonon energy, $\hbar\omega$. It can be expressed by Miyakawa–Dexter equations (Brocklesby and Pearson, 1994):

$$\omega_p = \omega_0 \exp\left(\frac{-\alpha \Delta E}{\hbar\omega}\right) \qquad [16]$$

where ω_0 is a host-dependent constant, $\alpha = \ln(p/g) - 1$, $p = \hbar\omega$, and g is the electron–phonon coupling strength.

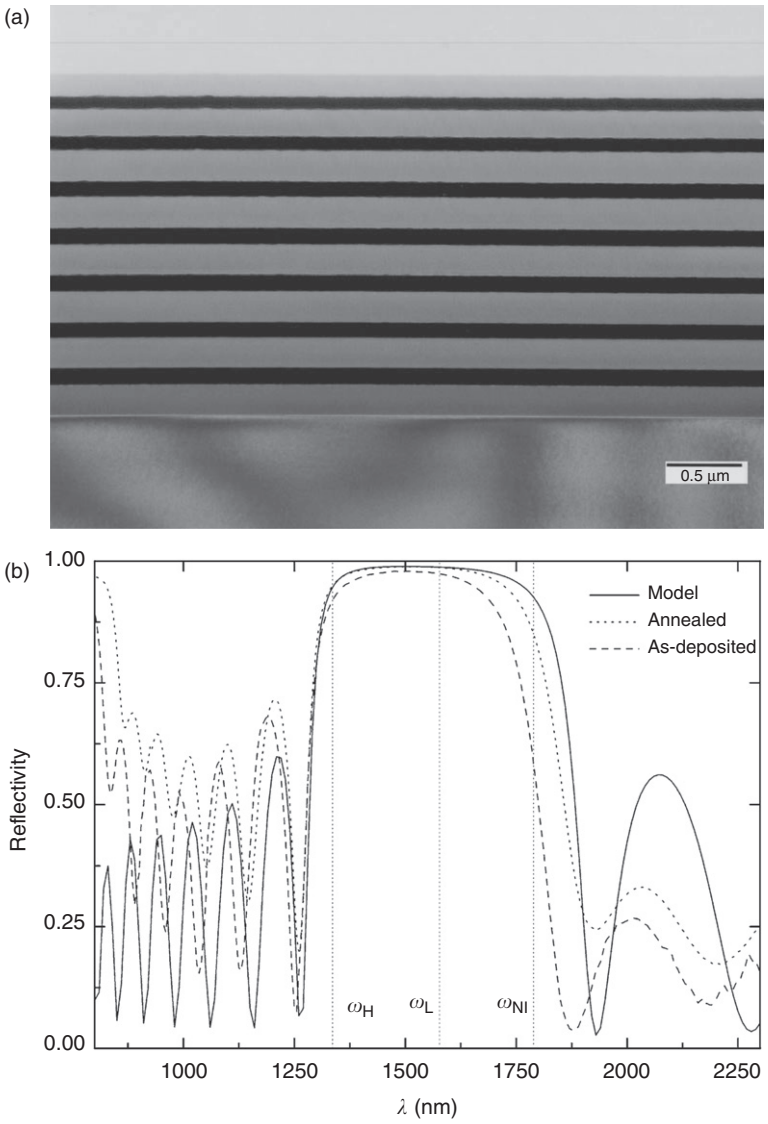

Figure 10 (a) The cross-sectional transmission electron microscope (TEM) image depicts periodic alternation of $Ge_{25}S_{75}$ (brighter) and $Sb_{40}Se_{60}$ films in the all-chalcogenide near-infrared reflector. (b) A normal incidence reflectivity spectra of the chalcogenide reflector (see above) are shown for as-deposited, annealed (T=165 °C for 10 h) reflectors in comparison with theoretical spectrum of annealed multilayer (Kohoutek *et al.*, 2009).

Sulfides and selenides of RE elements are not good glass formers themselves; they can be dissolved in many AGCs and form relatively stable glasses. The introduction of lanthanoides into AGCs generally decreases their glass-forming abilities. Besides, some AGCs can contain relatively large quantities of RE (Ga_2S_3–La_2S_3 – up to 15–50 mol.% of La_2S_3; GeS_2 up to 40% of La_2S_3, where La is for lanthanoide. The glasses containing Ga_2S_3, or In_2S_3, or corresponding selenides possess also increased ability to dissolve larger amounts of RE compounds, when compared with As_2S_3- or GeS_2-based glasses. Among the most investigated are the glasses of the systems Ga–La–S (e.g., $(Ga_2S_3)_{70}(La_2S_3)_{30}$), Ga–Na–S (e.g., $(Ga_2S_3)_{66}(Na_2S)_{34}$), Ge–Ga–Sb–S (e.g., $Ge_{20}Ga_5Sb_{10}S_{65}$), Ba–In–Ga–Ge-S and Ge–Ga–Se (e.g., $Ge_{30}Ga_5Se_{65}$), and many others, such as Ga_2S_3–La_2S_3–CsI, Ga_2S_3–CsCl, Ge–Sb–S system glasses. The solubility of RE is also relatively high (up 15%) in the systems Ga_2S_3–Nd_2S_3–GeS_2, Ga_2S_3–GeS_2–Er_2S_3 (Tveryanovich, 2004). The T_g of the last mentioned glasses depends on the composition of the glass (Adam, 2002); for many of them, T_g is from the region of 360–536 °C, which secure them good thermal stability.

In some cases, the solubility of RE compounds is lower and homogeneous glasses could be obtained very often only for RE elements content $\approx$100 ppm. Such small solubility is high enough for many applications.

The addition of alkaline halides increases the solubility of RE in AGCs; it increases the E_g and the transparency in visible part of spectrum and stabilizes the glasses against crystallization. The halide ions can be added to AGCs before glass melting in the form of CsI, GaI_3, SbI_3, PbX_2, or REX_3, where X is halogen. The phonon energy in chalcohalide glasses is higher than in AGCs that lower the luminescence intensity in IR region when the content of halide ions is high. The introduction of heavy elements or their halides

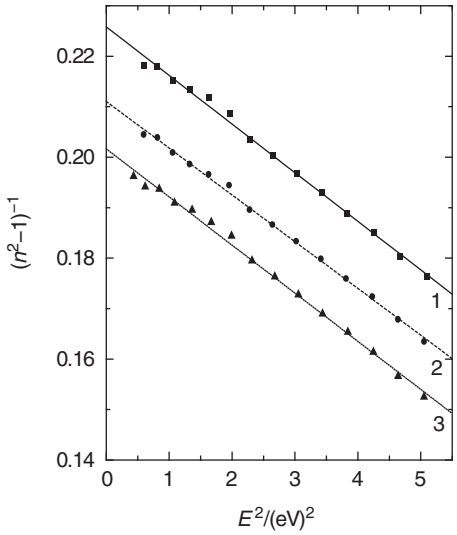

Figure 11 Plot of refractive index factor $(n^2-1)^{-1}$ vs. E^2 of $As_{38}S_{62}$ films. The n is refractive index and E is energy of the light. 1: fresh-evaporated film, 2: exposed film, 3: annealed film. Standard deviation of $(n^2-1)^{-1} \sim 1 \times 10^{-3}$ (Frumar *et al.*, 1999).

(e.g., $PbCl_2$, $PbBr_2$, and PbI_2) into AGC increases the solubility of RE compounds in chalcogenide matrix, too. The index of refraction is then increased (Frumarova *et al.*, 2009). The PbS in GeS_2–Ga_2S_3 glasses can increase the index of refraction, too, because of higher polarizability of heavy and large Pb ions (Aitken and Quimby, 1997).

The coordination number of RE^{3+} ions in AGC is often ~ 6 and such coordination number is probably valid also for chalcohalide glasses. The RE^{3+} ions are surrounded by S or Se in sulfide and selenide glasses. The RE^{3+} ions in chalcohalide glasses prefer the surrounding by halide atoms (Adam, 2002).

During crystallization of RE-doped AGC, the RE chalcogenides crystallize mostly at first. Microvolumes with higher concentration of RE chalcogenides can be formed even in the melt or in the glass when concentration of RE is high. This fact can lower the luminescence intensity due to concentration quenching (Tveryanovich, 2004).

For evaluation of electron transition probabilities, radiative lifetimes, branching ratios, and quantum efficiency of emission transitions among f–f electron levels of RE in AC, the phenomenological approach of Judd–Offelt is often used:

$$f_{\text{exp}}((S,L)\mathcal{J},(S',L')\mathcal{J}') = f_{\text{calc}}((S,L)\mathcal{J},(S',L')\mathcal{J}')$$

$$= \frac{8\pi^2 m\nu}{3h(2\mathcal{J}+1)} \times \left[\frac{(n^2+2)^2}{9n} \sum_{t=2,4,6} \Omega_t \left|\langle (S,L)\mathcal{J}||U^{(t)}||(S',L')\mathcal{J}'\rangle\right|^2\right] \quad [17]$$

where f_{exp} and f_{calc} are experimental and calculated oscillator strengths, h is Planck's constant, m is electron mass, t is a mean wave number of the absorption band, $\mathcal{J}$ is the ground-state total angular momentum of RE^{3+} ion (for Pr^{3+}, $\mathcal{J}=4$), n is the refractive index of the material, Ω_t ($t=2$, 4, 6) are the phenomenological Judd–Ofelt intensity parameters, and the $\langle (S,L)\mathcal{J}||U^{(t)}||(S',L')\mathcal{J}'\rangle$ are the reduced matrix elements of the tensor operator, $U^{(t)}$ of rank t. The reduced matrix elements, $U^{(t)}$, are only slightly sensitive to the glassy host and, some are given by Weber (1968).

The calculated values of the Judd–Ofelt intensity parameters obtained, for example, for Pr^{3+} ions in Ge–Ga–Se glasses, were $\Omega_2 = 6.0 \times 10^{-20}$ cm^2, $\Omega_4 = 16.8 \times 10^{-20}$ cm^2, $\Omega_6 = 5.0 \times 10^{-20}$ cm^2. Root-mean-square deviation, which represents the quality of the fit, was equal to 10^{-6}.

From the Judd–Ofelt parameters, spontaneous transition probabilities A^{ed} of electric dipole transitions can be determined by:

$$A^{\text{ed}}[(S,L)\mathcal{J};(S',L')\mathcal{J}'] = \frac{64\pi^4 e^2 n}{3h(2\mathcal{J}+1)\bar{\lambda}^3}\left[\frac{(n^2+2)^2}{9}\right]$$

$$\times \sum_{t=2,4,6} \Omega_t \left|\langle (S,L)\mathcal{J}||U^{(t)}||(S',L')\mathcal{J}'\rangle\right|^2 \quad [18]$$

where e is the electron charge and λ is the average wavelength of the transition. Neglecting the values of the contributions of magnetic dipole transitions, which are generally low, it can be assumed that the total spontaneous emission probability A of a transition is given by the value of A^{ed}.

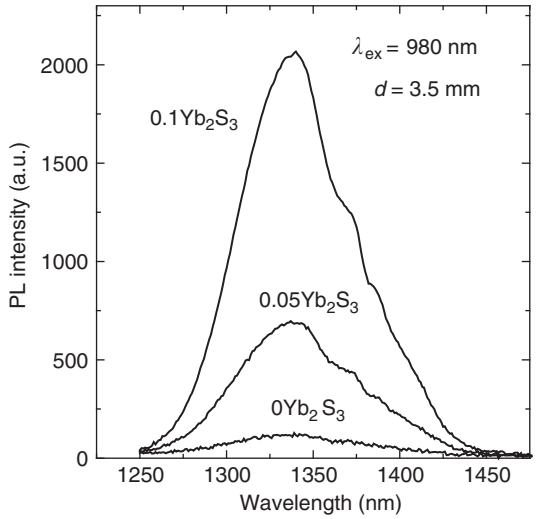

Figure 12 Luminescence spectra of Pr^{3+} and Yb^{3+} co-doped GeS_2–Sb_2S_3–PbI_2 glasses under excitation 980 nm (Frumarova *et al.*, 2009). The intensity of luminescence band corresponding of electron transition from $^1G_4$ to $^3H_4$ level of Pr^{3+} ions is increased by increasing content of Yb^{3+} ions. The energy scheme is given in **Figure 13**.

The fluorescence branching ratio β of electron transitions from an initial manifold $|(S,L)\mathcal{F}\rangle$ to lower levels $|(S',L')\mathcal{J}'\rangle$ is given by (Wei *et al.*, 1994):

$$\beta[(S,L)\mathcal{J};(S',L')\mathcal{J}'] = \frac{A[(S,L)\mathcal{J};(S',L')\mathcal{J}']}{\sum_{S',L',\mathcal{J}'} A[(S,L)\mathcal{J};(S',L')\mathcal{J}']} \quad [19]$$

In Sm-doped Ge–Ga–Se glasses (Nemec *et al.*, 1999), which can serve as an example, the analysis of oscillator strenthgs was given, the probable radiative electron transitions in Sm^{3+} ions, spontaneous emission probabilities and branching ratios of individual electron transitions and the calculated values were compared with experimental data.

Pr-doped GeS_2–Sb_2S_3–$PbCl_2(PbI_2)$ systems (Frumarova *et al.*, 2009) offer another example of RE luminescence in AGCs. Here the room temperature luminescence in near and mid-IR parts of spectrum (bands with maxima near 1.3, 1.6, 2.2, 2.4, and 4 μm) was clearly observed. The intensity of the luminescence in this system can be increased by co-doping with Yb_2S_3 (**Figure 12**). The probable electron transitions are given in **Figure 13**.

Some RE-doped chalcogenide glasses are very stable and good glass formers, which make them potentially applicable also as optical amplifier and oscillator materials. Optical losses in RE-doped AC fibers are higher than those in silica glasses (e.g., 1 db m^{-1} at 4 μm for Ga–La–S sulfide glass fiber 2-m long due to OH, S–H, and Se–H groups absorption. It seems that up to now, the RE-doped fibers can be used for short or medium distance applications or for application in planar optical circuits. The RE-doped chalcogenide glasses have been studied in many papers.

6.3 Photo-Induced Effects

The structure, composition, phase, and many physicochemical properties of AGC can be changed due to exposure by light of proper energy (wavelength) and intensity. Intense illumination can also partly or fully damage (or evaporate) a-chalcogenides. The photo-induced changes can be purely electronic (electrical conductivity, photovoltaics, etc.), or atomic (structure, composition, density, etc.) or a combination of both. The purely electronic PEs (luminescence, photoconductivity, nonlinear effects, etc.) will be discussed separately. In this section only the effects connected with changes of atomic structure will be discussed.

The optically induced changes of atomic structure are not rare in solids and have been found (and in many cases exploited) also in crystalline compounds, for example, in AgX (X=Cl, Br, I), in the so-called photochromic materials, as well as in many molecular organic compounds, dyes. The PEs in AGC are numerous and have been found in elemental chalcogens, binary, ternary, and more complex chalcogenides. The photo-structural changes, frequently observed, are not restricted to AGC. They are often more intensive in AGC than in other systems, probably because their disorder is higher, their density is generally lower than that of crystalline counterparts, and larger free volume is also available. The important feature of AGC is lower energy of chemical bonds between forming elements. The larger free volume and broader composition regions of glasses and thin films are favorable for the formation of compositional and coordination defects and for the stabilization of newly formed structures. In amorphous films or in powdered glasses, the disorder is even larger than in bulk massive glasses; the movement of atoms and changes of atomic structure of thin films can be easier and more pronounced. The largest photo-induced changes of optical properties were found in

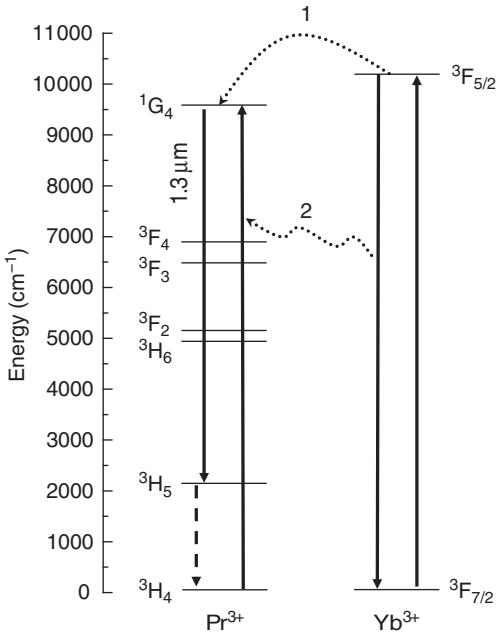

Figure 13 Energy level diagrams of Yb^{3+} and Pr^{3+} ions in GeS_2–Sb_2S_3–PbI_2 glasses (Frumarova *et al.*, 2009). There are two possibilities of transfer of energy from Yb^{3+} to $^1G_4$ level of Pr^{3+}, either the direct transfer of excited electrons from $^3F_{5/2}$ level of Yb^{3+} to $^1G_4$ level of Pr^{3+} (1), or the excitation of electrons of Pr to the $^1G_4$ level by absorption of emission light from $^2F_{5/2}$ to $^2F_{7/2}$ transition of Yb ions (2), since the $^2F_{5/2} \rightarrow {}^2F_{7/2}$ emission band of Yb^{3+} overlaps the $^3H_4 \rightarrow {}^1G_4$ absorption band of Pr^{3+}.

AC systems with the largest free volume. In crystals the changes of atomic structure can take place on the surface only – there is mostly no free volume; thus, the density of larger defects is low inside the bulk crystals.

Chalcogens (S, Se, and to some extent also Te), pnictogens (As, Sb and partly, Bi), and group 14 elements (Si, Ge) can form chemical bonds between like atoms (e.g., S–S, Se–Se, As–As, Sb–Sb, Si–Si, Ge–Ge, generally M–M, where M is for metalloid, metal, or chalcogen). The energies of such bonds are not far from the energies of heteroatomic bonds M–C, where C is for chalcogen. This fact enables the change of coordination of individual atoms so that the energies necessary for the optically induced or optically enhanced chemical reactions are much lower than in oxides:

$$2|\mathrm{M}-\mathrm{C}| \overset{h\nu_i, I_i, T_i}{\longleftrightarrow} |\mathrm{M}-\mathrm{M}| + |\mathrm{C}-\mathrm{C}| \qquad [20]$$

The reaction energy for As–S system (eqn [20]) for example is $\Delta E \approx 40$ kJ mol^{-1}.

Here $h\nu_i$ and I_i are energy and intensity of the incident light, T is the temperature, $i=1$ for the direct reaction, and $i=2$ for the backward reaction. The exposure to light or annealing of the AGC shifts the reaction equilibrium to the right- and left-hand side depending on the system, its temperature, energy, and intensity of light. For $h\nu_1 > h\nu_2$ and for $I_1 > I_2$, the forward reaction is enhanced, while annealing ($T_2 > T_1$), or exposure to light of $I_1 < I_2$ shifts the reaction in the backward direction.

It is motivated by effort to apply the PE in optics, opto-electronics, and in optical data storage. The large effort given to this research was successful, the PEs have been applied in optical memory materials (rewritable CDs, DVDs, and Blue-ray) (Raoux and Wuttig, 2009), holography (Gonzales-Leal, 2003), high-resolution photoresists, IR waveguides, and diffractive optical elements (Richardson, 2003), etc., as we have already mentioned.

The mechanisms of the PEs in AGC can be very different. One photon is usually absorbed at a time by each molecule or structural unit and is responsible for primary photo-chemical or photo-induced processes. This rule is broken when high-intensity lasers are used as source of radiation and the structural units may absorb more than one photon. Such effect is probably behind a large increase of efficiency of PE, when very intense pulses are used for excitation (Lyubin *et al.*, 1997).

The first step of interaction of radiation (UV, VIS, IR light, neutrons, γ- or X-rays) with the AGC is the light absorption, excitation of electrons or atomic vibrations, displacement of atoms, creation or amplification of phonons. Such processes can result in changes of structure, electrical conductivity, and of temperature; they can even melt or evaporate the material. Exposure can lead to chemical bonds redistribution or reorientation, to photo-induced crystallization or amorphization, to photo-chemical reactions, to change of chemical reactivity, surface profile, optical transmittivity and reflectivity, index of refraction, hardness, thickness, fluidity, optical anisotropy, elastic module, etc. Interdiffusion of some elements or compounds within AGC can also be induced or enhanced by exposure to radiations.

Optically excited states can relax to the original state or to new one, either directly or via intermediate steps. The time of relaxation varies from picoseconds to years, depending on the system, its structure, and temperature. The photo-induced changes can be reversible or irreversible.

6.3.1 Reversible PEs

The atomic structure and many physicochemical properties of AGC can be reversibly changed by radiations (tautomeric changes, vectorial effects, changes of optical properties of bulk and well-annealed samples, photodarkening, photobleaching, changes of optical transmittivity and reflectivity, absorption edge shift, changes of index of refraction, of hardness and fluidity, of chemical bonds statistics, of volume and reactivity, opto-mechanical effects, some defects formation, and annihilation). Isotropic reversible PEs can be found in well-annealed films and in bulk glasses after their exposure by nonpolarized light. After exposure of AGC to polarized light, the resulting state of the material can become optically anisotropic with preferential orientation of a part of structural units (nano-volumes) in the amorphous solid (vectorial effects). Changing the orientation of the polarizing plane of the exciting light can change the orientation of these units.

The photodarkening can be seen also in powdered bulk glasses, where the effect is more pronounced than in massive bulk samples (Frumar *et al.*, 2003a,b). The original state before exposure can be restored by interruption of excitation or after proper treatment (exposure of material to light of lower energy or lower intensity), in vectorial PE by changes of plane of light polarization. Annealing of films or glasses near glass-transition temperature, T_g, can turn these changes back again. The isotropic reversible effects are often accompanied by photodarkening or photobleaching, while some vectorial effects are not. The chemically (but not structurally) simplest system with reversible PEs is amorphous selenium, in which nearly no photo-induced changes in coordination number of Se were found. The photo-induced transformation can proceed probably via changes of Se_8 rings to Se_n chains, by change of the polymerization level, or by defect formation. In liquid sulfur, the changes of optical transmission due to exposure are explained also by destruction of S_8 rings (Popescu, 2000). Charged diamagnetic polymeric chains are then created, which are supposedly responsible for the photodarkening.

The explanation of reversible changes of optical properties of AGC is not always unambiguous; partly because some of these effects are not very strong. They were already discussed and reviewed several times (Frumar *et al.*, 2003a, b).

The adiabatic potential has two minima of different energy in the phenomenological configuration–coordination model. Optical excitation transfers the electrons to excited state with higher energy. The electrons may overcome the potential barrier and after relaxation come to the second metastable state with higher energy than the original one. The material in this second state has different physicochemical properties. Such a model does not imply atomic changes of structure. It was suggested (Frumar *et al.*, 2003a,b) that at least in binary and ternary chalcogenides, for example, in As–S, As–Se, Sb–S, As–Ga–S, As–Sb–S, Ge–As–S, Ge–Sb–S, the exposure changes chemical bond distribution (by a sort of photolytic and/or photosynthetic reactions) according to eqn [21], which is a modification of eqn [20] for the As–S system:

$$2|As-S| \overset{h\nu_1 I_1 h\nu_2 I_2, A(T)}{\underset{\rightarrow}{\leftarrow}} [As-As]+[S-S] \qquad [21]$$

The $h\nu_1 I_1$ is for photodarkening ($h\nu_1 I_1 > h\nu_2 I_2$). The $h\nu_2 I_2$, $A(T)$ is for reversible process by lower energy or intensity of light, or for thermal annealing $A(T)$. The backward shift of the reaction equilibrium (eqn [21]) toward left-hand side can be described by an increasing chemical homogenization (the system is shifted toward a chemically ordered amorphous chalcogenide), the shift of equilibrium toward the right-hand side can be ascribed to the increased disorder; the system is shifted toward the random covalent network model. The newly formed bonds between like atoms (e.g., As–As or S–S bonds) remain embedded in glassy matrix without any phase separation. In the As–S system, the excess As–As bonds are apparently behind the shift of absorption edge (photodarkening), because analogous shift of absorption edge can be obtained in bulk glasses of As–S system by increasing of As content without any exposure (**Figure 8**; Frumar *et al.*, 2001a,b). The new As–As bonds are formed with the increasing as content, the E_g^{opt} then decreases. The analogous process proceeds in thin films of As–Se, Sb–S, As–Ga–S, As–Sb–S, Ge–As–S, Ge–Sb–S systems (Frumar *et al.*, 2001a).

The processes described by eqn [21] require the changes of atomic positions and proceed more easily in materials with larger free volume. The largest changes of photo-induced properties were really found in samples with composition corresponding to the largest free volume (Vlcek and Frumar, 1987).

Another type of photo-chemical reaction, namely photo-induced change of coordination of individual atoms, can be also found in AGC (eqn [22]). Such a reaction corresponds to chemical disproportionation:

$$2MX_n \Leftrightarrow MX_{n+\gamma} + MX_{n-\gamma} \qquad [22]$$

where part of atoms change their coordination numbers; the mean value of $\gamma \leq (\sim 0.03\text{–}0.1)$, M stays for metal, X is for chalcogen (Frumar *et al.*, 1988). Here again, the left-hand side represents the state closer to the thermodynamic equilibrium, and $MX_{n+\gamma}$ and $MX_{n-\gamma}$ represent over- and under-coordinated atoms of metal or metalloid, respectively. Over- and under-coordinated atomic defects are common in chalcogenide glasses. Such defects can be negatively or positively charged (e.g., C_3^+ or C_1^-, where C is for chalcogen, subscript for coordination number, and superscript for the charge); they can increase the densities of the localized states

in the band tails and cause the shift of the absorption edge. The changes of coordination numbers due to exposure were found in many chalcogenides (Gladden *et al.*, 1988); their formation was confirmed, for example, in GeS_2 and $GeSe_2$ by EXAFS experiments (Shimakawa and Ganjoo, 2001). The mean coordination number of Ge is increased due to exposure, while the chalcogen decreases its mean coordination number (Sakai *et al.*, 2000).

The chalcogens and pnictogens possess nonbonding orbitals (lone pairs), which form the upper part of valence band states (Fritzsche, 2000). These orbitals can be transformed by exposure into the bonding ones and vice versa, and can be used for the formation of new chemical bonds with changed geometry of local structural units.

Until now, only changes of short-range order have been discussed; however, the light exposure can induce changes also at medium-range order as it may be deduced, for example, from the shift and lowering of the first sharp diffraction peak of As_2S_3 after exposure of annealed samples (Tanaka, 1998a). This peak is typical for glasses and its intensity decrease corresponds to a decrease of medium-range order.

In As_2S_3 bulk glasses, photo-induced changes of hardness were also observed. The films were hardened by annealing and softened by light exposure (Popescu, 2000), which is in agreement with the scheme proposed in eqn [21]. Analogously, the exposure decreased the viscosity (Hisakuni and Tanaka, 1995). In parallel to observed changes of hardness, reversible changes of E_g^{opt} (photodarkening) and of the index of refraction were observed, again in accordance with eqn [21]. The changes of hardness and of viscosity can also be connected with polymerization–depolymerization reactions. Some authors connected it with breaking of van der Waals bonds.

The light exposure of annealed amorphous chalcogenides changes reversibly the index of refraction. The changes are much smaller than in the irreversible process. Part of the changes of the index of refraction can be ascribed to changes of the volume and density of AGC. The changes of index of refraction cause changes of third-order nonlinear susceptibility $\chi^{(3)}$. This question was discussed in Frumar *et al.* (2003a,b).

The photo-induced expansion was found by exposition of AGC to light with $\hbar\omega > E_g$ and even to subband gap light. The effect can be explained also by chemical bonds redistribution.

Tanaka (1998b) observed also the so-called giant photo-expansion. The glassy As_2S_3 illuminated by laser light increased its thickness by $\sim$4%, which is 10 times more than in conventional photo-expansion. The effect is specific to chalcogenide glasses. The value of photo-induced expansion is however higher with subband gap illumination. It is believed that the giant photo-expansion is a combined effect of expansive forces (Kolobov, 2003) and of decreased viscosity. The effect is not fully understood but it can be applied for production of micro-lenses.

Changes of viscosity. The illumination of AGC by the subband gap light can also decrease the viscosity of the glass. In a-Se it was described as a photo-melting; the surface profile of bulk Se was changed due to exposure. The effect was demonstrated to be purely optical (Poborchii *et al.*, 1999). It is supposed that in As_2S_3 (Hisakuni and Tanaka, 1995) the light can break van der Waals bonds and excite the tail states of the valence band. The glass becomes less interconnected and can flow. When the exposure is terminated, the chemical bonds form again and restore the original state and viscosity. Photo-induced fluidity (fluidity is reciprocal value of viscosity) was reviewed as photo-plastic effect in chalcogenide glasses by Yannopoulos (Yannopoulos and Trunov, 2009).

Photo-induced anisotropy in AC. Exposure by polarized light can induce optical anisotropy in illuminated AC. The optical anisotropy can be induced by over-gap ($h\upsilon > E_g$) as well as subgap ($h\upsilon < E_g$) photons (Kolobov, 2003).

The origin of the effect is not fully clear. Tikhomirov and Elliott (1995) explained the effect by photo-induced reorientation of valence alternation pairs, for example, according to the scheme that is again connected with the change of coordination numbers:

$$2C_2^0 + h\nu \rightarrow C_1^- + C_3^+ \qquad [23a]$$

$$C_2^0 + P_3^0 + h\nu \rightarrow C_1^- + P_4^+ \qquad [23b]$$

where C_2^0 is a twice coordinated atom of chalcogen without a charge (e.g., –S– with two chemical bonds), C_1^- is once coordinated negatively charged (e.g., $-S^-$), C_3^+ is a threefold coordinated chalcogen atom with one positive charge (e.g., $=S^+-$), P_3^+ is threefold coordinated atom of pnictogen (e.g., =As–), P_4^+ is a four times coordinated pnictogen atom with one positive charge. Newly formed structural units can be preferably oriented according the light polarization planes. The interaction of the polarized light with anisotropical structural elements of the glass can also be supposed (Fritzsche, 1995).

The polarization of the light transmitted through polarized chalcogenide film is not full (only several %). This is probably the reason why such effect has not been really applied yet.

The opto-mechanical effect is another vectorial PE in AC (Krecmer *et al.*, 1997). The linearly polarized light can displace upward or downward the cantilever of an atomic force microscope, AFM, covered from one side by a thin film of AC. The cantilever displacement depends on the angle between the polarization vector of light and the cantilever axis (**Figure 14**; Stuchlik *et al.*, 2001).

The effect is dynamical; the contraction and expansion of the film takes place only during the illumination. The effect is spectrally selective, and the maximal effect and fastest response can be observed for light with energy close to E_g of a given chalcogenide. The deflection is relatively slow; the speed depends on wavelength and light intensity; the full deflection (maximum displacement) was found in amorphous $As_{50}Se_{50}$. There is also a scalar part of the effect (volume expansion) that is probably

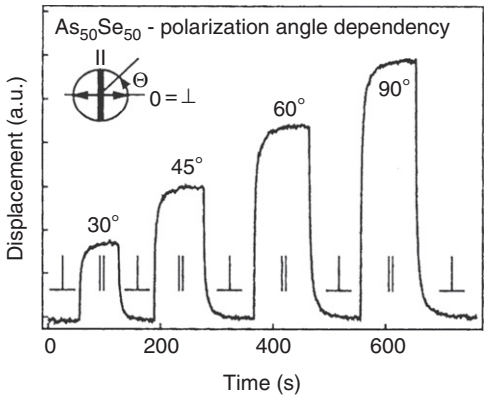

Figure 14 Dependence of the deflection of cantilever coated with a-$As_{50}Se_{50}$ as a function of angle θ between the electric vector of the illuminating linearly polarized light and the normal to the cantilever axes (Stuchlik *et al.*, 2003). With kind permission of Wiley-VCH.

caused by different thermal expansion of chalcogenide film and metallic substrate, because the film is heated by absorbed light. A full understanding of the opto-mechanical effects is however still lacking.

6.3.2 Irreversible photo-induced changes

Some photo-induced changes of structure and properties of AGC cannot be reversed by interruption of excitation or by annealing of the samples nearby T_g. Such changes can result during the light exposure of as-evaporated inhomogeneous films and give rise to some crystallization processes. Further, they accompany some photo-induced changes of reactivity, photo-induced oxidation or hydrolysis, photo-induced dissolution and diffusion of metals in AGC, interdiffusion of AC with another AC of different composition (e.g., Bi_2Se_3–Bi_2Te_3), or with other compounds. They include also photo-decomposition of materials (Frumar *et al.*, 2003a,b). Photolysis of some powders or thin films, photo-induced synthesis of layers from reactive materials (e.g., Sb + Se, Bi + Se), etc., are also irreversible. During the interdiffusion and photo-induced synthesis, homogeneous solid solution or compounds of lower Gibbs energy are formed.

The light irradiation of as-evaporated films can induce synthetic chemical reactions among the fragments, which result in their chemical equations [23a] and [23b] (backward direction) and polymerization. Irreversible photo-structural and photo-chemical effects were found in most as-evaporated systems, for example, in As–S, As–Se (Frumar *et al.*, 2003a,b), As–Ga–S (Frumar *et al.*, 1999), Ge–Sb–S (Vlcek and Frumar, 1987), Sb–S (Frumar *et al.*, 2001a), and many others. The Ge–Sb–S system with relatively broad glass-formation region can serve as a model material with different photo-induced changes. In thin films of this system, prepared by flash evaporation of $Ge_5Sb_{45}S_{50}$, $Ge_5Sb_{40}S_{55}$, $Ge_{10}Sb_{40}S_{50}$, and $Ge_{10}Sb_{50}S_{40}$ glasses, crystallization as well as photobleaching or photodarkening were observed. The dissociation of vapors into fragments analogously to eqn [2] proceeds during evaporation. After the condensation of vapors, local inhomogeneities are formed. The films with overstoichiometry of metallic part (Ge + Sb) are photo-darkened; the films with excess of sulfur are photobleached. The discussion of these effects can be found in Frumar *et al.* (2001a).

In some cases, bubbles can be formed in exposed AC containing volatile components due to rapid local vaporization in consequence of high energy of light pulses (Popescu, 2000). This phenomenon was proposed for optical data storage but the application met serious difficulties. The effect can be partly reversible.

Irreversible changes of optical transmission, photodarkening, and photobleaching. The exposure of freshly evaporated films by light shifts their absorption edge either toward longer wavelengths (red shift, photodarkening) or toward shorter wavelengths (blue shift, photobleaching). In many papers, the photodarkening, or reversible part of it, is assigned phenomenologically to the formation of defects and localized electronics states in the tails of conduction and valence bands, which lower the energy gap (Fritzsche, 2000). The photodarkening is much stronger in a-thin films or in powdered glasses with higher density of defects than in bulk glasses (Frumar *et al.*, 1988). Larger surface of powdered glasses or films also plays a role.

The photodarkening can be induced not only by the light with energy $h\nu \geq E_g$ but also by lower energy light (subgap photo-induced phenomena). The quantum efficiency is however quickly decreasing for decreasing photon energy.

Irreversible photo-induced changes of index of refraction. The changes of index of refraction, Δn, of fresh-evaporated films of As–Se, Ge–S, Ge–Sb–S are larger than those of annealed films. The Δn can be as large as 0.78 for $As_{0.6}Se_{0.4}$ (Lyubin *et al.*, 1997; Frumar *et al.*, 2003a,b; Popescu, 2000). The spectral dependence of index of refraction of a-chalcogenide films can be described by simple Wemple–DiDomenico relationship for a single-oscillator approach. Results for As–S system thin films and discussion of the problem are given in Polák *et al.* (1999).

The index of refraction of fresh-evaporated $As_{38}S_{62}$ and $As_{40}S_{60}$, as well as of $As_{42}S_{58}$ films is increased by illumination. By subsequent annealing the increase is even more pronounced. Such an increase can be connected with the increase of dispersion

energy, E_d, which obeys an empirical Wemple–DiDomenico relation:

$$E_d = \beta N_c Z_a N_e (\text{eV}) \quad [24]$$

where N_c is the coordination number of the cation nearest neighbor to the anion, Z_a is the formal chemical valence of the anion, N_e is the effective number of valence electrons per anion, and β is a constant (~ 0.37 for amorphous materials).

Photo-induced changes of reactivity of AC. The light exposure of a-chalcogenide films changes also their solubility in chemical solvents. The difference in dissolution rates of exposed and unexposed parts can be increased using specific reactants.

The dissolution rates can also be influenced by presence of oxidizing (I_2, $KClO_3$), or reducing agents (e.g., methol; Vlcek *et al.*, 1991) in the solution. The process can be well illustrated by taking the dissolution of As–S films. As we have mentioned above, the fresh-evaporated films of the As–S system contain a large amount of As_4S_4 due to dissociation of vapors during deposition. Dissolution of As_4S_4 in alkaline solutions is relatively slow, partly because of elemental arsenic formed on the surface of the film (eqn [25]) and partly because As_4S_4 is relatively resistant to alkaline solutions:

$$3As_4S_4 + 24OH^- = 4AsS_3^{3-} + 4AsO_3^{3-} + 4As + 12H_2O \quad [25]$$

The dissolution of As_2S_3, that is the prevailing compound in the exposed parts of films, is much faster:

$$As_2S_3 + 6OH^- = AsO_3^{3-} + AsS_3^{3-} + 3H_2O \quad [26]$$

The reducing agents, added to the alkaline etchant, can increase the content of As on the surface of the film and slow down the dissolution. The oxidizing agents speed up the dissolution of the unexposed films by oxidation of As and/or As_4S_4 (eqn [25]; Vlcek *et al.*, 1991). Similar effects were observed when the films were dissolved in dimethylamine.

The dissolution rates of films with excess of As (e.g., $As_{42}S_{58}$) in alkaline solutions are lower than those of stoichiometric films; these films contain larger amount of As and As_4S_4 (Frumar *et al.*, 1997) which are poorly soluble in alkaline solutions.

The solubilities of as-evaporated and illuminated films can be drastically influenced by absorption or chemisorption of some organic compounds, for example, of aryl- or tetra-alkyl-ammonium salts (Frumar *et al.*, 2003a,b), in which at least one alkyl group is long enough (e.g., cetyl–, $C_{16}H_{33}$–). It behaves as a hydrophobic element toward the ionic etchant. These compounds can be selectively chemisorbed on the unexposed parts of films; As-rich parts of the film are apparently preferred. After such a sorption, the dissolution of the unexposed films can be completely blocked. The nitrogen of $[N^+R_4]$, or $-[N^+R_3]$, $=[N^+R_2]$ and of similar groups is positively charged and can be bonded to As–As structural units, which act as Lewiś bases. The long alkyl- (aryl-) chain of alkyl-ammonium salts is hydrophobic; when the compound is chemisorbed, it protects the surface against the attack of the alkaline solution. Both positive and negative etching can be obtained (Vlcek *et al.*, 1994). The etching of As_xS_{100-x} (with $x < 40$) thin films in alkaline solvents is positive (exposed part dissolved more quickly), while the films with excess of As (with $x \geq 40$), which were treated before etching by CS_2, were etched negatively; the unexposed part of film dissolved more quickly. The CS_2 can dissolve free sulfur or sulfur-rich fragments of the film that are present in fresh-evaporated films. The surface area of the unexposed part of film is considerably increased after such etching and the following dissolution in alkaline solvents is quicker (Vlcek *et al.*, 1994).

The $AgAsS_2$ and $AgGeS_2$ glasses are, contrary to As_2S_3 or GeS_2, stable in alkaline nonoxidizing solutions. They can be dissolved in 0.1 M NaOH + 0.9 M $NaNO_3$ solution at higher temperatures. The solubility of Ag^+-doped parts of chalcogenide films in alkaline solvents becomes very low as compared with undoped part (Shkol'nikov, 2001). Very deep etching can then be easily realized and submicron features with sharp edges can be obtained. Such films can be applied as optical waveguides, optical gratings, for production of high-resolution photoresists, in holography, and for data storage (Section 7).

Photo-induced oxidation and hydrolysis of AGC is a part of photo-induced changes of reactivity. The sensitivity of many chalcogenides to oxidation and hydrolysis enhanced by light has been well-known to chemists and mineralogists for a long time. The photo-induced reaction of some AGC films with atmospheric O_2 and with H_2O vapors leads to oxidation and enhanced hydrolysis of AGC. The Ge–O–Ge bonds, embedded in the glass matrix as a solid solution, or some $Ge–O^-$ or Ge–OH bonds are formed on the surface of Ge-containing AGC. Analogous products are formed in other AC. As the optical energy gap E_g^{opt} of oxides and hydroxides is larger than that of sulfides and selenides, the absorption edge is shifted toward shorter wavelengths (photobleaching) due to oxidation or hydrolysis. The $\equiv Ge - O - Ge\equiv$, $Ge–O^-$, or Ge–OH bonds are relatively strong, and, consequently, their formation is irreversible (Tichy *et al.*, 1986).

Photo-induced crystallization of AGC. The amorphous films that are close to, or even outside the borders of regular glass-forming regions are highly metastable; they can easily crystallize. The crystalline state with lower Gibbs energy is closer to thermodynamic equilibrium. There is, however, a barrier between amorphous and crystalline states; many AGCs can be stable for centuries as it can be judged from extrapolated values. This energy barrier can be overcome by increasing the temperatures (heating, annealing), or by electrical or optical pulses. The absorption of light with the photon energy close to E_g^{opt} can result in weakening of chemical bonds (Feinleib, 1971) (lower bonding order due to electrons in anti-bonding orbital (in conducting band) and in possible bond breaking that can facilitate structural changes and start nucleation and crystals growth). In many cases the temperature of AC is also

increased due to light absorption. From the viewpoint of thermodynamics, the light supplies the energy for overcoming the thermodynamic barrier of nucleation and kinetic barrier for crystal growth. Optically induced crystallization was observed in many amorphous systems (Se, S, Se–Te, Sb–S, Sb–Te, Ge–Sb–S–Te, Ge–Se, Ge–Sb–S, Ge–Sb–Te, Ge–In–Te, $Ge_2Sb_2Te_5$, $Ag_{10}In_4Sb_{58}Te_{28}$). Some of them were proposed as active materials for phase-change optical memories, for example, Ge–As–Te, Sn–Se–Te, Ga–Se–Te, Bi–Sb–Se, Ge–Te, Sb–Se, In–Se, GeTe–Sb_2Te_3, In–Sb–Te, Sb_2Te_3–Bi_2Se_3, Ag–Sb–In–Te, and others – all are materials which form unstable glasses.

The time necessary for optically induced irreversible crystallization of thin films can be very short ($\sim^{\circ}10^{-9}$ s). However, only few complex tellurides with high crystallization speed and other suitable properties have been used commercially (e.g., Ag–Sb–In–Te, $Ge_2Sb_2Te_5$, $Ge_8Sb_2Te_{11}$, etc.). The effect has been applied in optical and electrical nonvolatile memories (CD, DVD, Blue-ray disks), because optical and electrical properties of amorphous and crystallized chalcogenides are often different. Very high contrast and storage capacity up to 100 Gb per disk has been achieved commercially, in laboratory much more (Section 7).

From a certain point of view, the process of crystallization can be reversed by melting and quickly cooling and could therefore be defined as reversible processes. Annealing of the crystallized film or interruption of light exposure cannot however reverse the process.

Photo-induced changes of thickness and volume of AGC. Exposure of amorphous chalcogenides can cause irreversible photo-contraction that is mainly observed in obliquely deposited films (during the deposition, the angle between the vapors flux direction and substrate is $<90^{\circ}$; the largest effects were found for angles $\sim 40^{\circ}$). Obliquely deposited films have a column-like structure with a large space around individual columns (Kuzukawa *et al.*, 1999). After the exposure, the columns can interact and collapse; more homogeneous film of higher density and lower thickness is then obtained. If the film with the columnar structure is annealed before exposure, or the vapors are deposited on a heated substrate, the photo-contraction is lowered or even completely vanishes.

Photo-induced amorphization. The light exposure of AC can induce their crystallization as already mentioned. In some cases, a reverse process was observed, namely the exposure-induced amorphization of crystalline chalcogenides below their melting point. The effect was observed in thin films of $As_{50}Se_{50}$ (Kolobov, 2003) as a-thermal process. Its nature is not fully understood. The amorphization of crystalline As_2S_3 proceeded even at low temperatures (36 K; **Figures 15(a)** and **15(b)**; Frumar *et al.*, 1995), which proves that the effect is not of thermal nature. It is well known that the preparation of As_2S_3 crystals from the melt is an extremely difficult task and even several-month annealing of As_2S_3 glass at temperatures close to T_g does not transform the glass into crystal. It can be supposed (Frumar *et al.*, 1995) that the difference between the Gibbs energy (ΔG) of crystals and glasses of As_2S_3 is very small. Furthermore, the As_2S_3 crystals with layered structure are very soft and their powdering creates large amount of defects. The density of defects in powdered crystalline As_2S_3 can be so high that its structure is not far from a-state (Section 4); the value of Gibbs energy becomes even closer to the value of G of amorphous state. The amorphization is then possible.

Presence of some elements such as Cu, Ni, Bi, and Pb in AGC lowers the efficiency of the above-mentioned PE (Lyubin, 1997). All of these elements can form coordination bonds with sulfur or selenium and can be bound with chalcogens forming structural units with higher coordination numbers (e.g., CN$\leq$6). The structural units with higher coordination number are mostly 3D; the glass structure becomes less flexible, and resistant to any structural change.

Photo-doping of AC by Ag was described many years ago (Kostyshin *et al.*, 1966), when Ag contacts on AC were quickly dissolved after their illumination. Not only AC but many AGCs (e.g., As–S, As–Se, Sb_2S_3, Ge–S, Ge–Se, As–Te, Si–S, Se–Te Ge–Se, Ge–S

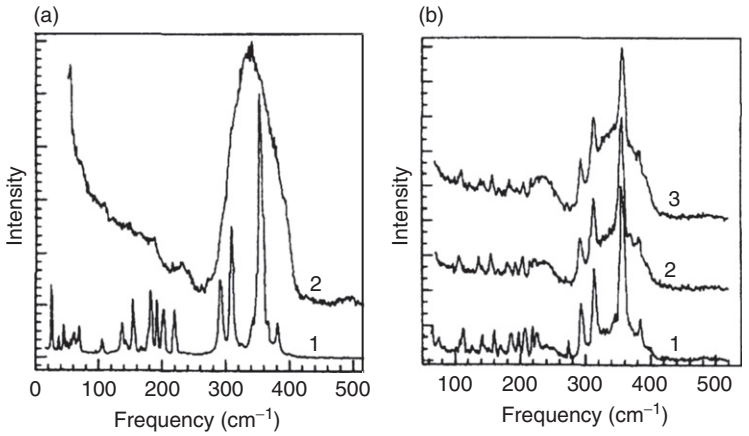

Figure 15 (a) Raman spectra of As_2S_3: 1, orpiment crystals; 2, glass. (T=300 K, λ=530.9 nm (Kr laser), and $I\approx$0.2 W cm^{-2}). (b) Raman spectra for As_2S_3 (orpiment) at T=36 K, illuminated by Kr laser (λ=568.2 nm): 1, I=10 mW ($\approx$1 W cm^{-2}); 2, I=30 mW ($\approx$3 W cm^{-2}); 3, I=80 mW ($I\approx$8 W cm^{-2}). Relatively intensive bands near 340 cm^{-1} and 231 cm^{-1}, corresponding to AsS_3 pyramids' vibrations and As–As vibrations in As_2S_3 glasses, respectively, can be seen (curve 3). The narrow bands from crystalline As_2S_3 are of lower intensity (Frumar *et al.*, 1995).

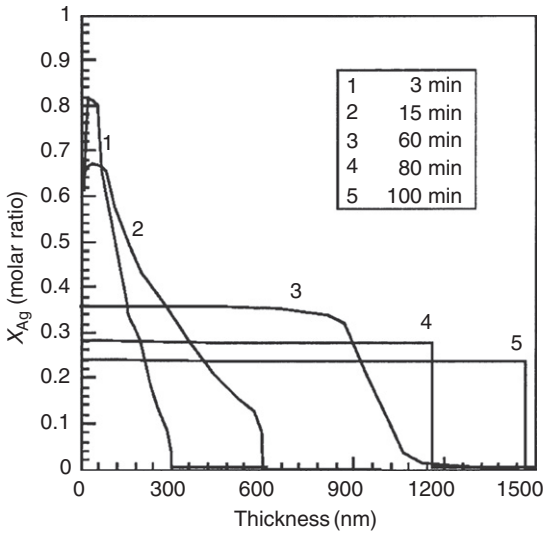

Figure 16 Photo-induced dissolution and diffusion of Ag in a-$As_{30}S_{70}$. The depth profile was obtained from Rutherford backscattering spectra. The diffusion profile has a very sharp edge (Wagner *et al.*, 2003). Illumination 100-W tungsten lamp, T=120 °C.

Ge–Sb–S, $(As_{0.33}Te_{0.67})_{100-x}Te_x$), and others) can behave in this way. The sensitivity of Ag/chalcogenide bilayer to radiation is relatively high but lower than the sensitivity of silver halides in photographic process. The composition of photo-doped layers depends on thickness and composition of chalcogenide, thickness of Ag, temperature, conditions of exposure, etc.

The silver dissolved on the surface of AGC diffuses into its volume and gives relatively thin Ag-doped films. Deeper patterns can be prepared by illumination of multi-layers of alternating Ag-chalcogenide–Ag-chalcogenide layers, etc. (Wágner and Ewen, 2000).

The dissolution and diffusion of Ag and other metals (e.g., Cu) in AGC can proceed even in dark; the reaction rate is however much lower without illumination. The concentration profile of photo-doped metal does not obey Fick's law; it is often of step-like form with a sharp diffusion front (**Figure 16**). The step-like profile of diffusion front can be explained by the formation of a Coulomb potential on the diffusion front due to quick diffusion of mobile Ag^+ ions. This potential stops further diffusion of Ag^+ ions on electrically isolating substrates. Without illumination, the free holes that are majority charge carriers in undoped AC diffuse together with mobile Ag^+ ions into undoped part of chalcogenide. The free electrons are captured more quickly. Due to this process, a Coulomb potential is formed on the interface of doped/undoped part of a-chalcogenide. This potential slows down and eventually stops any further Ag^+ diffusion (Wagner *et al.*, 1991). The exposure of the interface metal/chalcogenide to light of energy close to the band gap of chalcogenide creates electron–hole pairs. Newly created electrons and holes lower the Coulomb potential so that Ag^+ ions can then move (diffuse) further.

The step-like Ag^+ diffusion profile in Ag–As–S and Ag–As–Se systems can also be explained by diffusion in a two-phase system (Wagner and Frumar, 1990), because two glass-forming regions, divided by relatively large immiscibility region, exist in these systems as well as in Ag–Ge–S(Se) system (Wagner *et al.*, 1991).

Due to extremely small diffusion length of free carriers in highly disordered amorphous solids, their lateral diffusion (perpendicular to the direction of light) is extremely small. It is much quicker when the substrate is covered by a conductive film or when the chalcogenide is deposited on an electrically conductive substrate (Wagner *et al.*, 1991). In this case, the electrical Coulomb potential formed at the doped–undoped interface of chalcogenide is lowered by conductivity of the substrate and the diffusion of metal ions can proceed also in lateral direction.

Large amounts of Ag (up to 30–40 at.% in Ge–Se or in As–S sytems; Wagner *et al.*, 1994; Wagner and Frumar, 2003), up to 57 at.% in $GeSe_3$ (Kawasaki *et al.*, 1999), can be dissolved in AC layers. The diffusion of Ag^+ follows the direction of light, and very sharp edges between doped (exposed) and undoped (nonexposed) areas can be obtained. This effect can be applied for the production of optical gratings, waveguides, high-resolution photoresists, and planar optical circuits (see Section 7).

The photo-induced dissolution and diffusion of Ag^+ in AGC proceeds more quickly in the films with excess of sulfur or selenium, which suggests that excess chalcogen plays an important role in the reaction with silver.

The whole process of photo-induced dissolution of metals in a-chalcogenides consists of several steps. At the interface silver/silver-doped chalcogenide ionization of Ag occurs:

$$Ag + S = Ag^+ + S^- \qquad [27]$$

or

$$2Ag + S = 2Ag^{+} + S^{2-} \quad [28]$$

$$Ag + h^{+} = Ag^{+}, \quad \text{or} \quad Ag = Ag^{+} + e^{-} \quad [29]$$

in which the silver atom captures the dominant free carrier (hole) or loses its electron. As a result, very mobile Ag^{+} ions are formed. Ag metal can also react with excess sulfur of the chalcogenide according to the reactions or reduce the chalcogenide, for example,

$$Ag + 2As_2S_3 = As_4S_4 + 4Ag_2S \quad [30]$$

The reduction of As_2S_3 in Ag–As–S system leads to As_4S_4 as it can be inferred from Raman spectra.

Analogous schematic chemical reactions can be used also for selenides:

$$2Ag + Se = Ag_2Se, \quad \Delta G^{0}_{298} = -25.13 \text{ kJ mol}^{-1} \quad [31]$$

$$4Ag + 2As_2Se_3 = 2Ag_2Se + As_4Se_4, \Delta G^{0}_{298} = -12.365 \text{ kJ mol}^{-1} \quad [32]$$

$$6Ag + As_2Se_3 = 3Ag_2Se + 2As; \quad \Delta G^{0}_{298} = -8.155 \text{ kJ mol}^{-1} \quad [33]$$

During the photo-doping process, all resulting products remain dissolved in amorphous matrix. The change of standard Gibbs energy, ΔG^{0}_{298}, of is negative. These reactions can thus proceed spontaneously even without illumination, but very slowly. The ΔG^{0}_{298} change per 1 mol of Ag calculated from the reaction [31] gives –12.5 kJ mol^{-1}, from reaction [32] it is –3.1 kJ mol^{-1}. and finally from reaction [33] it is –1.3 kJ mol^{-1}. Without illumination, the most probable reaction is that shown in eqn [31], if there is an excess of Se. The exposure to light changes the energetics of these reactions, because the light energy can be added to the energies of the above-mentioned reactions. The kinetic reaction barrier can thus be lowered.

The values of ΔG of the above-mentioned system Ag–As–Se, as well as for other chalcogenide systems, are further decreased by considering the mixing entropy part ($-T\Delta S_m$), due to dissolution of products of reactions in glassy matrix.

The absorption edge of AC is shifted by Ag doping toward longer wavelengths.

Silver surface photo-deposition. The Ag-rich chalcogenide glasses, containing more than 30 at.% of Ag formed silver particles on the surface, when illuminated by band-gap light. The phenomenon is referred as photo-induced surface deposition of Ag (Kawaguchi, 2003). In this effect, the illumination induces diffusion of Ag^{+} ions and precipitation of metallic Ag on the AGC surface from Ag-rich Ag–As–S, Ag–Ge–S, Ag–Ge–Se, and Ag–As–Se or other glasses (Kawaguchi *et al.*, 2001) with higher Ag content. In the $(Ge_{0.3}S_{0.7})_{100-x}Ag_x$ or $(Ge_{0.3}Se_{0.7})_{100-y}Ag_y$ glasses, the silver precipitates on the surface, when $x > 45$, and/or when $y > 22$, respectively. The precipitated Ag forms on the surface small clusters, or crystals with a typical dimension of 10 nm in diameter and 1 nm in thickness (**Figure 17**). The segregated Ag particles can be dissolved again in the amorphous chalcogenide substrate after annealing at higher temperatures. The process can be repeated many times (Kawaguchi and Maruno, 1994). The explanation of photo-induced silver deposition can be based on thermodynamic considerations, or on the hole-ion process. The hole-ion process explanation suggests that the optically created electrons are captured in illuminated parts, while the more mobile holes move away from illuminated spot. The illuminated part becomes negatively charged and attracts the Ag^{+} ions, and, eventually, makes them to precipitate as Ag neutral atoms (Kawaguchi *et al.*, 1996).

The process can be also understood, if we suppose that the Ag solution becomes oversaturated at room temperature with the concentration of Ag corresponding to the solubility of Ag at higher temperatures, when the glass was prepared. If illuminated, the oversaturated Ag solid solution overcomes the reaction barrier and the excess silver is released. The reflectivity of the Ag particles is higher than that of the AC; the effect can be applied for data storage and reproduction (**Figure 17(c)**). The effect is however relatively slow and the necessary intensities of band-gap light must be relatively high. Au addition, analogously to conventional photography, increases the photo-sensitivity of the photo-deposition process (Kawaguchi, 1998) at least for two orders of magnitude. The Au can probably form clusters, which behave as nucleation centers for Ag precipitation. The exposure can be done also by laser beam, the contrast obtained can be very high. The sensitivity of photo-induced silver deposition is higher than the sensitivity of other photo-induced effects in amorphous chalcogenides but still lower than the sensitivity of classical silver halide photographic process.

The photo-induced changes of optical properties in AGC can have a deteriorating effect on optical elements and such changes are undesirable. They can lower the performance of fibers or of optical elements as noticed in many materials, for example, in Ge–Ga–S glass (Frumar *et al.*, 2003a,b). Such materials are often used as hosts for rare-earth ions and have a relatively intense luminescence in the near-infrared region. Exposure to UV light causes a red shift of the absorption edge and lowers the

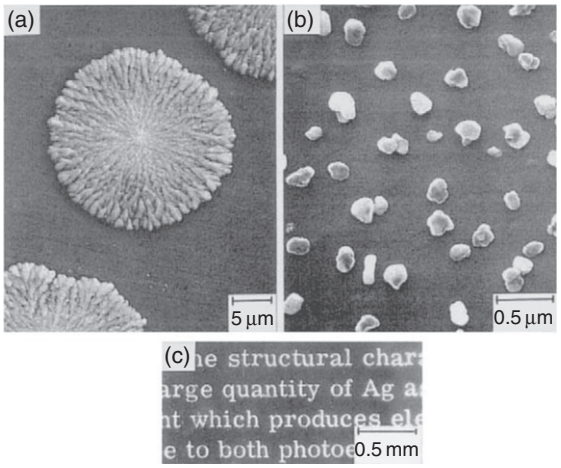

Figure 17 Scanning electron microscope (SEM) photographs of photodeposited Ag particles on a bulk glass (a) and on a-film (b). The intensity of the light and exposure time was higher for (a). The Ag patterns can be used for optical recording (c). The contrast is high (Kawaguchi, 2003). With kind permission of Wiley-VCH.

transmission of the material. The crystallization can also lower the transmittance of optical elements because of scattering effects. In such cases, lower light intensities, longer wavelengths of light, or materials with negligible photo-induced effects have to be used.

6.4 Nonlinear Optical Effects

These effects are large in AGC containing highly polarizable atoms or ions (Frumar *et al.*, 2003a,b; Ticha and Tichy, 2002). The effect is strong also in chalcogenide crystals; the AGC have some advantage over crystals in terms of lower cost, easier processing, and in the possibility to include them into optical fiber systems and planar circuits.

The refractive index, n, can be expressed as $n = n_0 + n_2\langle E^2\rangle$, where $n_0 \gg n_2$. The $\langle E^2\rangle$ is the mean square of electric field of the light. The nonlinear part of index of refraction, n_2, is connected with nonlinear electron polarizability, P_{NL}:

$$P = \chi^{(1)}E + P_{NL} \quad [34]$$

where

$$P_{NL} = \chi^{(2)}E^2 + \chi^{(3)}E^3 \quad [35]$$

where P is the polarizability, $\chi^{(1)}$ is the linear optical susceptibility, $\chi^{(2)}$ and $\chi^{(3)}$ are second- and third-order nonlinear optical susceptibilities that are related to electronic and nuclear structure of the material. For crystals with a center of symmetry and also for optically isotropic glasses, the second-order nonlinear susceptibility $\chi^{(2)}$ is zero (Lines, 1990). The third-order susceptibility $\chi^{(3)}$ is important because its real and imaginary parts give rise to the nonlinear refractive index and nonlinear absorption coefficient. The third-order nonlinearity of most transparent materials results from anharmonic terms of the polarization of bound electrons. The fast component of n_2 and $\chi^{(3)}$ is believed to arise from pure electronic effects. The nonlinear effects are influenced also by nuclear contributions. The nuclear contribution gives only 12–13% of nonlinearities in sulfide glasses as it was evaluated in Kang *et al.* (1996). The response of nuclei is much slower and the two effects can be separated.

The covalency or ionicity of chemical bonds strongly influences the magnitude of nonlinearity. Single crystals of highly covalent Ge reached surprising $\chi^{(3)} = 10^{-9}$ esu, while highly ionic materials such as NaF only 9.4×10^{-14} esu.

The linear optical susceptibility in an isotropic medium can be expressed by (Ticha and Tichy, 2002):

$$\chi^{(1)} = \left(n^2 - 1\right)/4\pi \quad [36]$$

The dependence of $(n^2\text{–}1)^{-1}$ on $(\hbar\omega)^2$ is often linear and this dependence can be described by the single oscillator formula of Wemple and DiDomenico as it was already mentioned:

$$n^2(\omega) - 1 = E_0E_d/\left(E_0^2 - (\hbar\omega)^2\right) \quad [37]$$

From eqns [36] and [37], we obtain

$$\chi^{(1)} = \frac{E_d E_0}{4\pi\left(E_0^2 - (\hbar\omega)^2\right)}$$

For long wavelengths ($\hbar\omega \to 0$), then $\chi^{(1)} = E_d/4\pi E_0$.

The $\chi^{(3)}$ as a dominant nonlinearity in all glassy materials is produced by excitation in the transparent frequency region, well below the band gap E_g^{opt}. The $\chi^{(3)}$ of AGC can be determined experimentally by several methods, for example, by degenerate four-wave mixing method, by Z-scan method, by third-harmonic generation, etc. (Zakery and Elliott, 2007). The $\chi^{(3)}$ can be also roughly evaluated from linear refractive index (n_0), or from optical susceptibility $\chi^{(1)}$ (see e.g., Nasu *et al.*, 1994, and references therein). The use of physically-based Miller's rule is one of the convenient ways for rough evaluation of $\chi^{(3)}$, especially for near-infrared frequencies. In the spectral region far from resonance, the $\chi^{(3)}$ is approximately equal to $\chi^{(3)} = A(\chi^{(1)})^4$; then:

$$\chi^{(3)} = A\left[E_d E_0/4\pi\left(E_0^2 - \hbar\omega\right)^2\right]^4 \quad [38]$$

for $\hbar\,\omega \to 0$, one obtains

$$\chi^{(3)} = \frac{A}{(4\pi)^4}\left(\frac{E_d}{E_0}\right)^4 = \frac{A}{(4\pi)^4}\left(n_0^2 - 1\right)^4 \quad [39]$$

where n_0 is the linear index of refraction for $\hbar\,\omega \to 0$. The mean value of the constant A, as evaluated from 97 experimentally found values, is about 1.7×10^{-10} (for $\chi^{(3)}$ in esu) and $\chi^{(3)} = 6.8 \times 10^{-15}(E_d/E_0)^4$ (esu) (Ticha and Tichy, 2002). The accuracy of Miller's rule is generally better than the order of magnitude for many covalent or ionic compounds. For many halides, oxides, and sulfides values calculated by Miller's rule agree with experimental values within a factor of 2.

The value of $\chi^{(3)}$ for As_2S_3 glass was found to be $\chi^{(3)} = (1.48\text{–}2.2) \times 10^{-12}$ esu (measured by different methods), while for GeS_2 glass $\chi^{(3)} = 1 \times 10^{-12}$ esu, and for SiO_2 glass $\chi^{(3)} = 2.8 \times 10^{-14}$ esu for $\lambda = 1900$ nm (Vogel *et al.*, 1991). The nonlinear susceptibility $\chi^{(3)}$ of chalcogenide glasses was therefore found to be several orders of magnitude higher than those of SiO_2 glass. The AGCs have generally high values of n_0; they are promising candidates for optical switching and other nonlinear applications. The high nonlinear part of the index of refraction of AGC can be used in active parts of optical integrated circuits.

Very prospective nonlinear optical materials are AC containing nanoparticles of Ag, Au, CdS, CdSe, CdTe, PbS, CuCl, etc. Their third-order optical nonlinear susceptibility can be much higher than in pure AGC.

The nonlinear effects in AGC could have, however, a limitation for their application, because high intensities of light should be used for nonlinear effects. High light intensities can induce formation of intrinsic defects that lower the transparency. When the AGCs are used in their high-transparency IR region, the formation of such effects can be negligible.

7 Applications of AGCs

The AGCs, contrary to oxides, are well transparent in the near- and mid-infrared region of the spectrum ($\sim$0.6–20 mm, sulfides 0.6–11 mm, selenides 0.9–15 μm, tellurides 1.3–20 μm), and they have been used for many optical applications in this region. Furthermore, the refractive index of AGC is larger than in silica (typically from 2.2 to 2.9, for tellurides up to 5–6) so that chalcogenides can match with high-refractive-index materials, such as Si, GaAs, ZnSe, InSb, and others. The AGCs possess high optical nonlinearity, large free volume, and large optically and thermally induced changes of structure and properties, which make them attractive for many applications in optics and opto-electronics (e.g., anti-reflection coatings, photoresists, optical circuits and devices, light emission, up-conversion, signal couplers, frequency mixing, light amplifiers, lasers, etc. (Frumar *et al.*, 2003a,b; Jain and Vlcek, 2008). The AGC and elements made from them can also be applied in solid-state batteries and microbatteries, in environmental monitoring, in IR, chemical and ionic sensors, as biomedical, pollution, X-ray and diagnostical sensors, as surgical lasers, eye safe radars, etc.

The melts of many chalcogenides can dissolve larger amounts of their own components, and of other different elements or compounds than the corresponding crystals. They can easily become nonstoichiometric as already mentioned. As a result, glasses with very different composition can be prepared from such melts with structure and properties that change over very broad ranges. Such possibility is very advantageous for many applications.

The GC can be applied also as fibers, for signal and power delivery, for mechanical and chemical sensing, for temperature and remote monitoring, in medicine, *in vivo* spectroscopy, as un-cladded fibers for evanescent wave spectroscopy in fiber light amplifiers and lasers, for optical signal processing.

The rare-earth-doped chalcogenides are materials with intensive luminescence in near-infrared (NIR) and mid-infrared (MID-IR) spectral regions (Section 6). From RE-doped chalcogenide glasses fibers, waveguides and parts of planar optical circuits can be fabricated. When the pumping (excitation) is intense, the spontaneous transition can be observed in RE-doped AGC and they can

be used as light amplifiers or lasers. The advantage of AGC for such a purpose lies in the much lower energy of phonons (typically 300–400 cm^{-1}). The probability of nonradiative transition is therefore much lower (eqn [16]). The emission cross section of RE-doped chalcogenides is due to higher index of refraction also higher. The RE-doped chalcogenides are also good candidates for fiber lasers in the infrared region of spectrum; the intense luminescence of rare-earth-doped chalcogenides in the NIR and MID-IR regions can be applied also in sensors of chemical compounds and pollutants (Zhang and Lucas, 2003).

Numerous photo-structural or photo-induced effects were detected in amorphous chalcogenides. The physico-chemical properties of many AGCs can be changed by exposure to suitable light (usually $h\upsilon \geq E_g^{opt}$) and applied as very-high-resolution photoresists, waveguides, gratings, in holography, as diffractive elements, etc. Planar waveguides are produced by lithography, including lithography-applying photo-induced changes of reactivity. Photoresists of large size (areas) can be prepared by vacuum evaporation, and very high resolution of 5000–10 000 lines mm^{-1} can be obtained after their exposure. The resolution capability of chalcogenide films can be further increased to sub-wavelengths region by near-field optical technique. Nanowriting is then possible. Nanometer dimension lines (patterns) for different applications can be formed by focused laser beam in Ag-doped chalcogenides (Mietzsch and Fitzgerald, 2000). The AGCs have much higher absorption in UV spectral region than most organic photoresists. Due to UV sensitivity, thinner lines and patterns can be produced. The sensitivity of AC photoresists can be further increased by several orders when short intense pulses are used instead of continuous-light exposure (Lyubin *et al.*, 1997). This effect is not fully understood; possibly nonlinear effects or two-photon excitation are behind it.

Using chalcogenide photoresists, optical elements, optical circuits, and diffractive gratings can be produced also by holographic or electron beam lithography technique. They found wide application in various optical and opto-electronic devices and elements. The diffraction efficiency of gratings can be very high.

For some pattern production, for example, for waveguides or IR gratings production, deep etching is necessary. Sharp edges with height up to 5–10 μm were obtained (see, e.g., Wágner and Ewen, 2000). The etching solutions for arsenic chalcogenides are based on alkyl amines or on other alkaline solutions. Surface-active additives to etching solutions are also applied. Solutions containing H_2O_2 are used for Ge–chalcogenide-based photoresists (Frumar *et al.*, 2003a,b). The contrast obtained after etching can be very high (with sharp edges). It can be also very gentle or low, and gray tones or gray scale can be achieved by variation of exposure and etching conditions. Micro-lenses or micro-lens arrays can be fabricated from photoresists of As–Se and As–S systems by exposure through a mask with microholes (**Figure 18**; Wágner and Ewen, 2000). Lenses with focal length of several tens of micrometers and diameter of several micrometers as well as spherical micro-lenses can also be prepared. The optical image of the patterns is often directly visible after exposure. Such micro-lenses can be applied in CCD cameras, imaging machines, optical communication, and in IR technology.

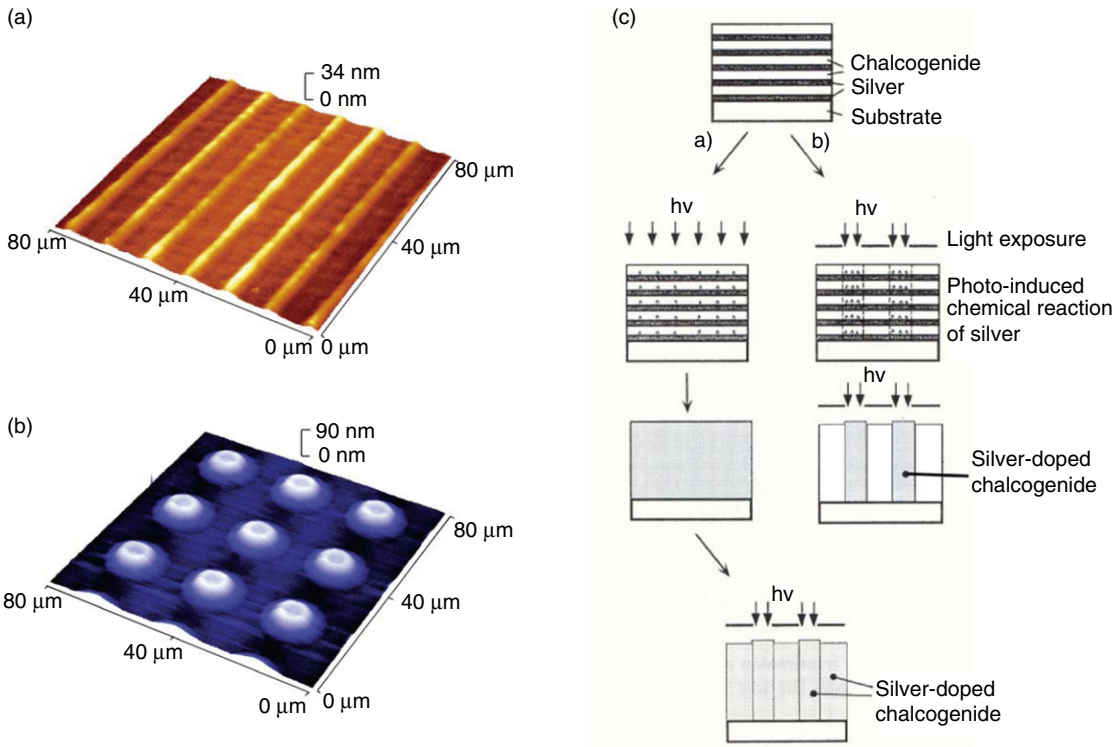

Figure 18 The optical phase diffraction grating (a) and micro-lenses array (b) prepared from Ag-doped amorphous chalcogenide (AC); for deeper relief a multilayer array can be used (c) (Wágner and Ewen, 2000).

Table 1 Chalcogenide glass ion-selective sensors

Determination n(X)	*Membrane composition*	*Sensitivity (mV pX^{-1})*	*Detection limit (10^{-7} mol^{-1})*	*pH*
Ag	Ag–As–S, Ag–As–Se	59	5	Up to 6 mol l^{-1} HNO_3
Cu	Cu–Ag–As–Se	29	1	Up to 1 mol l^{-1} HNO_3
Pb_2	PbI_2–Ag_2S–As_2S_3, PbS–Ag_2S–As_2S_3	29	1	2–6
Cd^{2+}	CdS–Ag_2S–As_2S_3, CdI_2–Ag_2S–As_2S_3	28	1	1–7
Fe^{3+}	$Ge_{28}Sb_{12}Se_{60}$(Fe)	58	500	1–2
Br^-	AgBr– Ag_2S–As_2S_3	59, 5	5	2–10
Tl^+	Tl-chalcogenide glass	59	50	0–5
Hg^{2+}	Hg-chalcogenide glass	28	5	0–6
Cr(IV)	Cr-chalcogenide glass	30–60	1	–
Na	NaCl–Ge_2S_3–GeS_2	58	400	1–2

Diffraction gratings can be prepared from Ag-photo-doped chalcogenide films, such as As_2Se_3–Ag, As_2S_3–Ag (**Figure 18**). Very good diffraction efficiencies were obtained also for chalcohalide glasses from the Ag–Se–I system, particularly for $Ag_{15}Se_{70}I_{15}$ (Wagner and Frumar, 2003).

Photo-dissolved silver in a-chalcogenides can be used in relief images in optical elements, in microlithographic schemes, and for direct imaging. Nanometer dimension lines (patterns) can be formed by focused electron beam. The width and height of Ag-doped lines can be influenced by beam parameters, such as accelerating voltage.

The exposure as well as Ag photo-doping can also change the volume and surface profile. The exposed parts often have larger volume by which gratings and micro-lenses were prepared (**Figure 18**).

The Ag-doped chalcogenide glasses and films have many applications as ionic conductors in solid electrolytes (batteries, thin film batteries), electrochemical sensors, and also as optical waveguides, diffraction elements, Fresnel lenses, optical memories, and other optical and nonlinear optical elements. Amorphous Ag^+ chalcogenides with various compositions were proposed as solid electrolytes for batteries, for example, the systems: Li_2S–B_2S_3, Li_2S–TiS_2, Ag_2S–GeS_2, In–Se, Ag_2Se–$GeSe_2$, Li_2Se–$GeSe_2$, and also for microbatteries, for example, Li–Li_2S–B_2S_3, Li–Li_2S–TiS_2, Ag–Ag_2S–GeS_2, Li–In–Se, Ag–Ag_2Se–$GeSe_2$, Li_2Se–$GeSe_2$ that can be few micrometers thick. Since the electrolyte is solid, batteries can be easily included into different circuit cards. The Ag-doped chalcogenide glasses and thin films, for example, of the composition of $AgAsS_2$ and $AgGeS_2$, can be used as ionic-sensitive electrochemical electrodes or their membranes for sensors for potentiometric determination of Ag^+, Se^{2-}, S^{2-}, Pb^{2+}, Cd^{2+}, and other ions (**Table 1**; Bychkov *et al.*, 2004). The membranes from doped AC have been applied also in ionic-sensitive field-effect transistors (ISFETs) that can be very small and the transistor current is controlled by electrochemical potential of membrane. This allows many chemical and biochemical applications. The ionic-sensitive membranes made from AC have high ionic conductivity and are well resistive to acidic and alkaline nonoxidizing solutions.

Chalcogenides with higher Ag content are ionic or super-ionic electrical conductors.

The optical applications of Ag-doped AC can be in etched gratings and etched waveguides and in optical elements. They are based on a large decrease of etching rates of doped chalcogenides in alkaline solutions as compared with undoped films and bulk samples.

Electronic conductivity of AGC can be applied in p–n junctions, sensors, Xerox processes, and in memory and threshold switches. In particular, the fabrication of p–n rectifying junctions is made possible by the p-and n-type conductivity of different ACs (Tohge *et al.*, 1986). The n-type part was formed by $Ge_{20}Bi_{11}Se_{69}$ glass ($d = 50$ μm); p-type by thin film of $Ge_{20}Se_{80}$ or As_2Se_3 ($d = 0.1$ μm). The electrical conductivity of Bi-doped AC ($c_{Bi} > 10$–13 at.%) is of six to seven orders of magnitude higher than that of undoped p-type chalcogenides (Frumar and Tichy, 1987). The chalcogenide p–n junction cannot however compete with traditional p–n junctions based on crystalline semiconductors and were used for special applications only, for example, in the area of high radiation (astronautics, defense), because the AGCs, contrary to Si circuits, are nearly insensitive to high level of radiation.

Optically induced changes of conductivity of amorphous chalcogenides have been applied in xerography, in photovoltaic and photoconductive elements, in laser printers, light sensitive camera tubes (Harpicon, Saticon, etc.), high-speed optical switches, in X-ray radiography.

Threshold and memory switches. Another important application of some AGCs is in threshold and memory switches (**Figure 19**). Threshold switches can be made from AGC by applying high voltage to the film, to a glassy plate, or even to the thin chalcogenide crystal. The high electrical resistivity of many AGCs is abruptly lowered when the applied electrical field is high enough ($\approx 10^5$–10^6 V cm^{-1}; **Figure 19**). The materials of such systems are stable glasses, and the threshold voltage corresponds to the formation of a very narrow high-conductivity filament between the electrodes. The free carriers are injected from electrodes into the hot filament. The conductive filament has a metallic-like conductivity and its diameter increases with the current, whereas the current density inside the filament is nearly constant (Ovshinsky, 2000). The process resembles the electrical breakthrough of dielectrics; the threshold switching can be reversible if the value of highest current is limited by proper serial resistor (Ovshinsky, 2000).

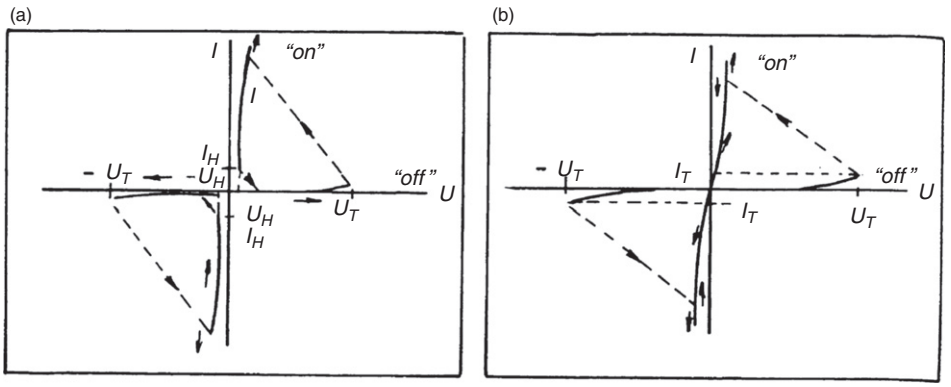

Figure 19 Current–voltage characteristics of threshold switch (a) and memory switch, (b) in thin films of chalcogenide glasses (Popescu, 2000). With kind permission of Springer Science and Business Media.

During the performance of a threshold switch, no crystallization of the filament can be observed. After removing the applied voltage, the material returns to its amorphous state with high resistivity (**Figure 19(a)**). Materials for treshold switches can contain (Ge + Si)–As–Te glasses. The effect can be, however, realized in many materials. Switching time to the low-resistance state is very short. The fast operation of threshold switches allows the construction of elements that can remove short high-voltage pulses superimposed over normal low-voltage signal, etc.

The other type of switch is the so-called memory switch (**Figure 19(b)**). When a high voltage is applied to a AGC thin plate, or film that crystallizes easy, its conductivity increases abruptly. Contrary to the former case, the crystalline filament is formed due to heating of material above its crystallization temperature by the electrical current. In these switches the high conductivity of the filament is preserved even when the voltage is removed. The original high-resistance state of the film can be obtained by passing higher current that melts the crystalline filament. They become amorphous again upon quick cooling. The unstable glasses, similar to those used in phase-change memory (PCM) materials, found application as memory switches. The effect of crystallization and melting is partly thermal, partly electronic. Both threshold and memory AGC-based switches were developed in parallel with silicon planar integrated circuits in the 1960s and early 1970s and at that time they were believed to be an alternative solution. The silicon technology however has much higher repeatability (number of cycles) and the amplitude of voltage necessary for switching is lower. The memory threshold switches offer the advantage of nonvolatility. It is important to notice that nowadays there is an important development in the field of electrical phase-change memories that might replace flash and other nonvolatile memories in the near future.

Optical fibers. Optical fibers can be prepared from GC with good transparency in the IR part of spectrum and with good ability to form glass. Optical fibers can be used for transmission of light or information to remote parts, bodies, and devices. They can also be used as sensors for many chemical and physical parameters. When doped with RE ions, they can work as light amplifiers and light generators, in defense applications, as well as surgical knives in bloodless operations. In the last case, the emission wavelength can be tuned to the absorption of tissue proteins. They are then coagulated and stop the blooding. The process is prospective for brain and other operations. The advantage of GC fibers is in their small thickness, long possible lengths, flexibility, and possibility to change their properties by doping. Fibers were prepared from many glassy systems, for example, from As–S, As–Se, As–(S, Se), As–S–P, As–Sb–S, Ge–Sb–S, Ge–Sb–Se, Ge–As–S, Ge–As–Se, Ga–La–S, and Ga–Na–S.

The GC fibers for all mentioned purposes must have very low optical losses; their optical thickness is equal to their lengths (from several centimeters up to several hundred meters). Transmission losses are caused by sum of absorption (impurities, Urbach tail), Rayleigh scattering (fluctuation of density and refractive index), and in the long-wavelength part of the spectrum by multi-phonon absorption. The multi-phonon absorption edge is shifted toward longer wavelengths by the addition of heavier chalcogens into chalcogenide glass. The Rayleigh scattering is proportional to λ^{-4}, and is relatively low in the IR region.

The purity of fiber glasses must be at least two orders of magnitude better than the purity of the glasses for optical elements of lower thickness, for example, for lenses, plates, and thin films. Generally, the purity of fiber glasses should be on the ppb level. For shorter fibers, a lower purity is allowed, but only for lower intensity of light, because the absorption on impurities can increase the temperature of the fiber, make self-focusing of light, and melt or crystallize the fiber. The concentration of metallic impurities in the fiber glasses can be lowered sufficiently but a problem arises with oxygen and hydrogen that form M–OH, M–H, and M=O bonds that are the main absorbing elements in the given transparency window. The M is chalcogen or some other elements such as Ge, Sb, and As. Even at their smallest concentrations these impurities create absorption bands that are absorbing in the transmission window.

Purification of As–Ch glasses can be done by sublimation of traces of As_2O_3 from pure As, and/or by sublimation of As, by distillation of S and/or Se. The Ge-containing glasses can be purified by heating in H_2 atmosphere (Ge), or by processing under reactive atmosphere (distillation of S, or Se in gas stream of S_2Cl_2 or Se_2Cl_2, etc.). The high-purity glasses for fibers can be prepared also by CVD; the Ge–Se glasses can be prepared from $GeCl_4$, $SeCl_2$, and H_2 streams by heating in electrical furnace.

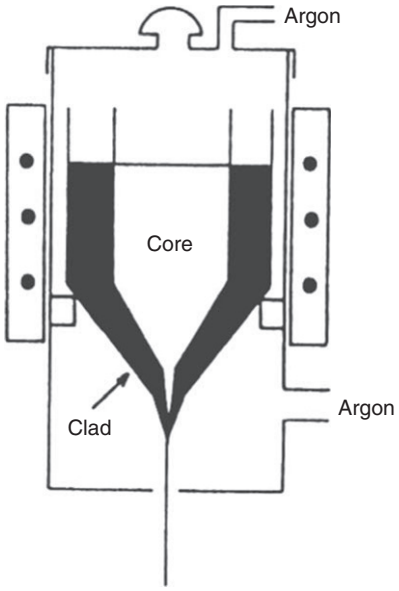

Figure 20 A double crucible used for pulling core–clad fibers directly from two melts (Kanamori *et al.*, 1984).

The chemical reaction:

$$GeCl_4 + xSeCl_2 + (x+2)H_2 \rightarrow GeSe_x + (2x+4)HCI \quad [40]$$

takes place at higher temperatures. The Cl_2 can also be formed when the amount of hydrogen is low. The germanium and selenium halides, as well as other liquid precursors, can be purified by rectification to get extremely low content of metallic impurities. Also, organic or organometallic compounds can be used as precursors for high-purity glasses. These compounds can be easily obtained in high purity without traces of metallic impurities.

Optical transparency of amorphous tellurides is high up to 20 μm, but they are not very good glass formers, and even small crystallization nuclei can decrease fibreś transparency. For that reason only sulfides and selenides, maximally with small addition of tellurides, were applied up to now for fiber production. The amorphous tellurides themselves can be potentially applied in planar circuits. The best and sufficiently stable fibers were made from As–S, As–(S, Se), Ge–As–(S, Se) system glasses. The As–Ge–S and As–Ge–Se glasses have been proposed for CO laser light transmission ($\sim$5.5 μm). The glasses from the system As–Ge–Se–Te were studied and applied as fibers for CO_2 laser light transmission at 10.6 μm.

For fiber production, either two preforms are prepared at first from the very pure glass, or the pulling is made from double crucible (**Figure 20**; Kanamori *et al.*, 1984). Two glasses of different compositions and of different index of refraction are used for outer and inner part of preform. The outer glass (for clad of the inner fiber) has lower index of refraction in order to decrease the losses of light by total reflection in the inner part of the fiber. The whole fibers are protected by a polymer clad from contact with the environment.

The transmission losses in chalcogenide fibers are higher than those in silica fibers not only due to impurity content but also due to lower chemical bond energies and higher content of extrinsic and intrinsic defects in these glasses. The content of intrinsic defects and the fluctuation of chemical composition cannot be lowered to the level of silica fibers (Section 5), so the chalcogenide fiber cannot be used for long-distance transmission of light. The losses of As–S fibers at the level of 1 cm^{-1} were obtained in the spectral region of 0.62–11.5 μm for As_2S_3, in region of 0.8–17.5 μm for As_2Se_3, and in the region of 0.75–12.25 μm for $As_2S_{1.5}Se_{1.5}$. Minimum losses of the level $(6–7) \times 10^{-2}$ dB km^{-1} were found at 4–6 μm. The impurities typical for arsenic chalcogenide fibers and their usual content are given in (Churbanov and Plotnichenko, 2004). Membranes made from AGC were used for determination of many elements (**Table 1**) and also for preparation of a chemical tongue (Bychkov *et al.*, 2004). Chalcogenide lasers can be applied for monitoring absorption bands in atmosphere, vapors, or liquids. The evanescent wave sensing can also be exploited. The thin chalcogenide fiber can be immersed even in biological systems and tissues and chemical sensing can be made even *in vivo*.

Chalcogenide fibers allow also the measurement of temperature in very narrow regions without interference from microwaves or electromagnetic waves. In such a way, the local temperature of material during its grinding could be measured (Sanghera and Aggarwal, 1998). It allows also remote temperature sensing.

Photoconductors. The excellent photoconductivity of amorphous Se is well-known since a long time; amorphous Se has been applied in Se photocells, in many sensors in different parts of spectra, even in X-ray panels (**Figure 21**; Kasap and Rowlands, 2000). The large densities of electron and hole traps in the forbidden gap of AGC near the band edges lower substantially the free path of

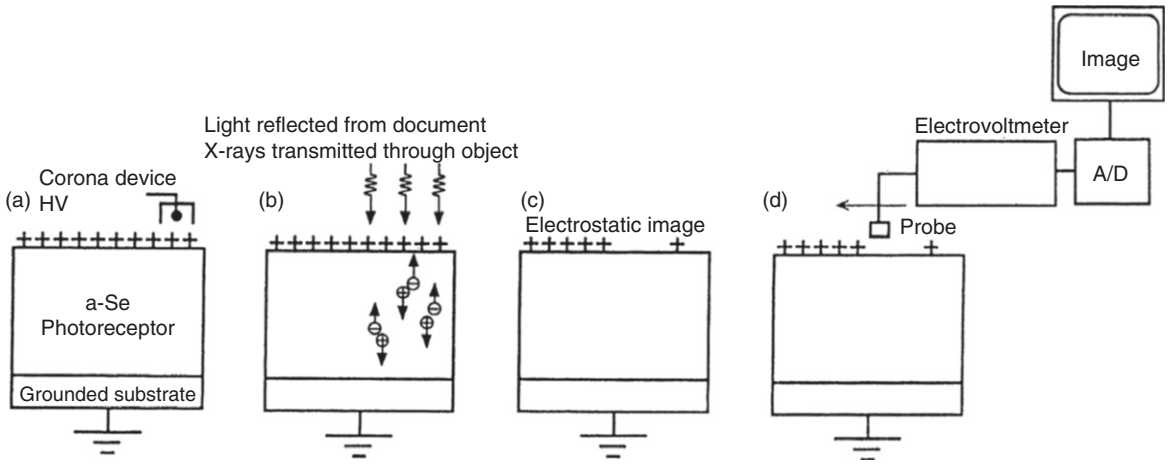

Figure 21 Scheme of xerography and radiography device with active amorphous chalcogenides (AC) film. (a) In xerography and xeroradiography, the a-Se photoreceptor surface is electrostatically charged to positive voltage (e.g., 500 V in xerography and 2000 V in xeroradiography). (b) Light reflected from the white regions of the document or X-rays modulated by absorption in a subject (e.g., human body) becomes absorbed in the active AC film (photoreceptor) and thereby photogenerate electrons and holes that discharge the exposed region of the AC. (c) At the end of exposure, the image is in the form of an electrostatic potential distribution on the surface of the photoreceptor. In xerography, this electrostatic image provides the basis of the toner development method. (d) In radiography, the electrostatic image on the photoreceptor is readout using an array of electrostatic probes scanning the surface of the photoreceptor (Kasap and Rowlands, 2000). With kind permission of World Scientific Publ. Co.

charge carriers and lower their mobilities. The very short free path of free carriers in AC localizes the increased photoconductivity to small illuminated areas and has been applied in early Xerox-type photocopying machines and later in laser printers. Amorphous selenides are still used in some color copying and printing facilities (Kasap and Rowlands, 2000). The a-Se and other AC were replaced recently in classical black and white xerography by amorphous Si (higher hardness for heavy-duty printers), or by organic photoconductors that are cheaper and do not contain any arsenic. For X-ray radiography the organic photoconductors have too low absorption of X-rays and their sensitivity is low, while heavier elements like Se and selenides absorb much more. Amorphous Se is relatively unstable, it crystallizes very easily, and it can be stabilized by small amounts of As and Cl. The so-called stabilized Se contains typically $\sim$0.3–0.5% As and 10–40 ppm Cl. Such Se has high room-temperature resistivity and, therefore, it can be corona charged to high voltage. Due to illumination by light or by X-rays, the conductivity of illuminated parts is increased and their charge is lowered. Due to low mobility of free carriers, the illuminated areas have very sharp edges. The voltage profile of illuminated (exposed) and unexposed surface can be detected by reading by electron probe (**Figure 21**; Kasap and Rowlands, 2000) or by charged fine toner particles that adhere to the sensitive cylinder and can be electrostatically transferred to the paper (transparences, etc.) and fixed by heating, which melts the thermoplastic part of the toner particles. The advantages of Xerox copying and laser printing are in high resolution, speed, and high contrast. The resolution of the X-ray imaging systems is limited by pixel sizes that can be small ($\approx$50 μm), which is fully acceptable for most applications (Kasap and Rowlands, 2000). The contrast of resulting picture can be controlled, so also soft body tissues can be envisaged. The sensitivity of X-ray xeroradiography is higher than in classical photographic process; the image can be seen immediately and computer processed, sent, or stored. Due to higher sensitivity of X-ray radiography based on AC films, the necessary X-ray irradiation (dose) (e.g., for imaging of a human body or its parts) is lower. The xerographic process was rewieved recently in Mort (1989) and the xeroradiography in Kasap and Rowlands (2000).

The electrons in amorphous Se at sufficiently high electrical fields exhibit avalanche multiplication (up to 800x; Kasap and Rowlands, 2000) that can be used for the construction of TV or other pick-up tubes of very high sensitivity (**Figure 22**). The highly sensitive a-chalcogenides have been used, for example, in Hitachi Saticon and Harpicon (NHK Japan) pick-up tubes (**Figure 23**). Commercially available Saticon uses Se–As–Te alloys (**Figure 23**; Kasap and Rowlands, 2000). Due to the Te content, the sensitivity is increased in red region and the tubes are panchromatic. Super-sensitive Harpicon of NHK Japan is used for high-definition television cameras. They are able to capture even star-light images. Their high-gain results from the multiplication effect: one photo-generated hole can result in several hundreds of electron–hole pairs (**Figure 22**). The details of such applications are given in Kasap and Rowlands (2000). The chalcogenide-based camera tubes were used also in former Soviet lunar vehicle (Lunochod).

Nonlinear optical effects in AGC have been the focus of many laboratories because of their potential application in ultrafast optical switching devices (switching time $\approx 10^{-15}$ s), frequency converters, couplers, electro-optic modulators and devices, all-optical circuits. We have reported on the nonlinear properties of AGC in Section 6.4.

High $\chi^{(3)}$ value was obtained also in nonchalcogenide (oxide) glasses containing heavy cations, such as Ti, Bi, Tl, Pb, and Nb, in which the oxygen has small polarizability. The chalcogenide glasses formed by heavier elements (including S, Se, and Te) have

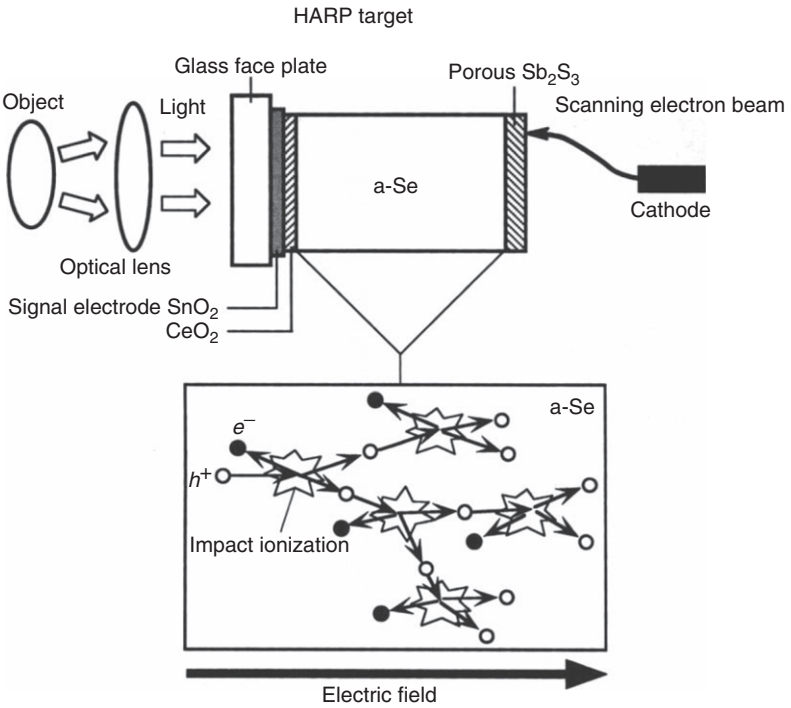

Figure 22 A schematic illustration of a high-spatial-resolution medical-imaging system (HARPICON). Avalanche breakdown by impact ionization in the a-Se layer is also illustrated. One photo-generated hole results in many electron–hole pairs to be generated by impact ionization (avalanche breakdown) in the a-Se layer where the electric field is very large (Kasap and Rowlands, 2000). With kind permission of World Scientific Publ. Co.

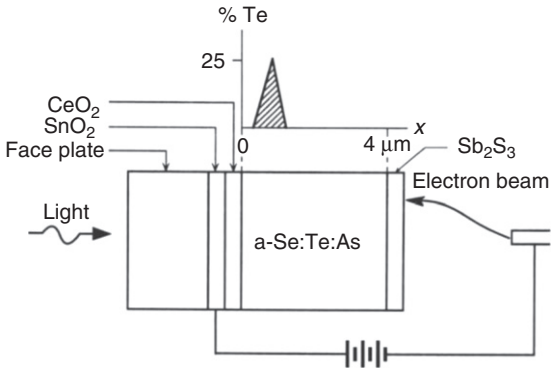

Figure 23 Schematic diagram of a Saticon TV image pick-up tube utilizing an a-Se:Te:As alloy. The Te composition is concentrated in a narrow region, whereas the bulk is mainly a-Se:As (Kasap and Rowlands, 2000). With kind permission of World Scientific Publ. Co.

much larger nonresonant third-order nonlinear susceptibility $\chi^{(3)}$ (Zakery and Elliott, 2007; Frumar *et al.*, 2003a,b). While the $\chi^{(3)}$ of silica is 2.8×10^{-14} esu, the nonlinear $\chi^{(3)}$ of As–S–Se is 1.4×10^{-11} esu (Frumar *et al.*, 2003a,b).

The nonlinear response time of AC is also short, between several ps and 100 fs. The switching time of all-optical switches using chalcogenides was also low <15 ps (Yamane and Asahara, 2000).

Analogously as in oxides, nanosize crystals can be formed in chalcogenide glasses by doping and following controlled crystallization at higher temperatures. Such materials are serious candidates for resonant nonlinear devices. The same holds for Ag-doped chalcogenides, which can form separated nanoparticles of silver. The optical resonant nonlinearity in such a case can be of several orders of magnitude larger than in the nonresonant case. In CdS, Cd(S, Se), CdTe, CuCl, and CuBr, Cu_2S-doped oxide glasses, containing semiconducting particles of size from 1.5 to 16 nm, $\chi^{(3)}$ values up to $\sim \times 10^{-7}$ esu were obtained, that means seven orders of magnitude higher than in pure silica. Similar results were obtained for metal (Ag or Cu)-doped oxide glasses. It can be expected that these values will be even higher in chalcogenide glasses due to higher polarizability of sulfur, selenium, and tellurium.

Phase-change memories based on AC. A very important application of AC films is connected with their crystallization and amorphization, (see, e.g., Raoux and Wuttig, 2009, and references therein). As the index of refraction n of amorphous and crystalline materials is often different ($n_{cryst} > n_{amorf}$), the crystallization and amorphization of chalcogenide films is connected with changes of optical reflectivity (eqn [15]). This feature has been applied for optical data storage and it was commercialized in CD, DVD, and Blue-ray disks (Section 6.3).

The optically induced crystallization was observed in many binary, ternary, and quaternary tellurides and selenides, among them in the materials from the systems: Ge–Sn–Te embedded in a TeO_2 matrix, Ge–Sb–Te, Si–Sb–Te, Ge–As–Te, Ge–Sn–Te, Ge–Sb–Bi–Te, Ge–Te, Sb–Te, Ge–Sn–Au–Te, Ge–Sn–Pd–Te, Sn–Ge–Sb–Te, Bi–Sb–Se, Ga–Se–Te, In–Se, Sn_2Se_3, In–Sb–Te, Ge–Sb–Te–Se, Ag–In–Sb–Te, TeO_x, Ge–Sb, Ga–Sb, In–Sb, Al–Te, Sb–Se, and in many others. Some of these materials were proposed for optical recording, in the sense that the information is recorded, read, or erased by focused laser light pulses. Some materials can be used in data-storage devices controlled by electrical pulses that can locally heat the thin film of AC to temperatures above its crystallization or above its melting points (Raoux and Wuttig, 2009). The following fast cooling results in crystalline or amorphous phases that have different electrical resistivity. Compounds formed on the line between GeTe and Sb_2Te_3 ($GeSb_4Te_7$, $GeSb_2Te_4$, $Ge_2Sb_2Te_5$, and $Ge_8Sb_2Te_{11}$), as well as their nonstoichiometric alloys containing excess of Sb and/or Ge, and/or Te (e.g., $(GeTe)_x(Sb_2Te_3)_{1-x}Sb_y$, $(GeTe)_x(Sb_2Te_3)_{1-x}Ge_t$; y, z, $t \geq 0$) can be used for data storage. Their properties are changing smoothly with change of composition without any abrupt changes nearby the composition of stable compounds formed in the system, which suggests the formation of nonstoichiometric compounds in broad composition regions (Frumar, 2007). The crystallization of these thin films is very fast, between 30 and 100 ns; the crystallization time increases with increasing content of GeTe. The shortest crystallization time, τ_c, was obtained for compositions near (Sb_2Te_3), but unfortunately the crystallization temperature T_c of such samples is much too low for practical applications.

Only few complex tellurides with high crystallization speed and other suitable properties have been used commercially (e.g., materials around Ag–Sb–In–Te system, $Ge_2Sb_2Te_5$, $Ge_8Sb_2Te_{11}$, all pure and doped (see Section 6.3; Raoux and Wuttig, 2009, and references therein). For recording, the material is usually heated to temperatures above its melting point, and then cooled very quickly, in order to obtain the wanted amorphous state. For erasing, the material is heated again, but to lower temperatures (above the crystallization temperature, T_c) and consequently crystallized (**Figure 24**; Breitwish, 2009).

The important rewritable materials for phase-change optical storage are Ag-doped binary and ternary tellurides, for example, the $Ag_8In_{14}Sb_{55}Te_{23}$ from the system Ag–In–Sb–Te (Yamada, 2009). The erasing mechanism in rewritable CD disk based on Ag–In–Sb–Te depends on the power of the erasing laser beam. Under low laser power, crystal nucleation is induced, while under higher laser power the controlling process in Ag–In–Sb–Te films is growth-driven crystallization. New information can be written directly on previously used location without need of an intermediate erase step. The speed of transformation of active material should be high, so poor glass formers are applied as phase-change rewritable materials. The chalcogenide materials for phase-change memories are usually in the form of very thin films. The melting pulse should be abrupt so that the thin material is then quickly cooled (cooling rate is estimated to be up to 10^9–10^{11} K s^{-1}) and original amorphous state is obtained. It can be supposed that the melting takes place below the normal melting point. The pulses do not increase only the temperature; they also excite free carriers. If the number of excited carriers is high (the pulses are of high intensity), the chemical bonds are weakened (conductive band corresponds to anti-bonding orbital) and the crystalline solids may become very disordered even below the normal melting

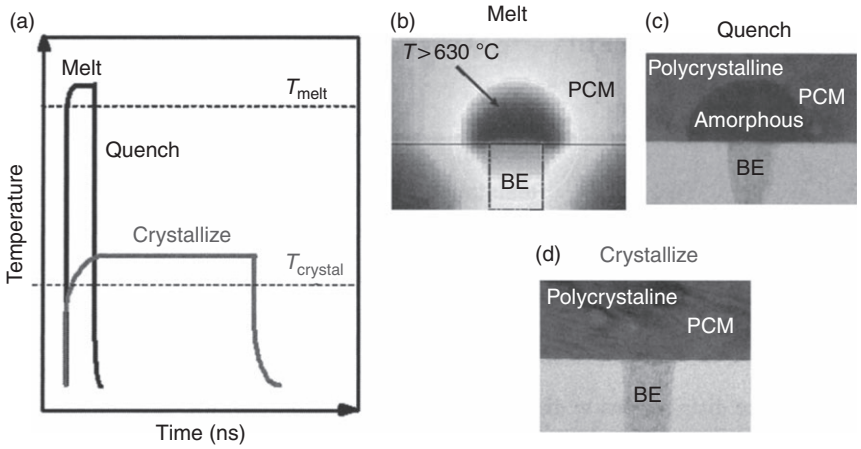

Figure 24 Programming the phase-change memory cell. (a) Temperature vs. time obtained within the cell during RESET (melt, then quench) and SET (crystallize) current pulses. T_{melt} and $T_{crystal}$ are the melting and the crystallization temperatures of the phase-change material, respectively. (b) Temperature profile within the cell during the melt part of the RESET programming. BE, bottom electrode; PCM, phase-change material. (c) Transmission electron microscope (TEM) image of cell in the high-resistance RESET state. (d) Transmission electron microscope (TEM) image of cell in the low-resistance SET state (Breitwish, 2009). With kind permission of Springer Science and Business Media.

point of active phase-change material. The experimental confirmation of this idea is still missing as the measurement of temperature of very thin film (several nanometers up to several tens of nanometers) during the short pulses (several nanoseconds up to several tens of nanoseconds) is extremely difficult. Furthermore, in real cells, the active phase-change material (PCM) is sandwiched between isolation, reflective and other layers, and the conditions in a model cell without these extra layers are different. The PCM after melting is highly disordered as it is inferred from X-ray diffraction data and from abrupt change of electrical conductivity and optical reflection. It can be considered as amorphous.

The erasing of data is initiated by short laser pulses or by short electrical pulses, which increase the temperature of the material above crystallization temperature T_c, and also excite electrons to higher energies. Consequently, some chemical bonds result weakened. The energy barrier between metastable amorphous and more stable crystalline state is then lowered by both effects. This barrier is mainly connected with the processes of breaking some chemical bonds and with re-arrangement of the atoms into a new structure. The existence of crystallization barrier of proper height is necessary for long time stability of the data. Whereas low barriers may lead to spontaneous crystallization and loss of the data, especially above room temperatures, higher barrier can slow down the crystallization and data erasing. The process of crystallization in data-storage materials must be very quick ($\tau \leq 100$ ns, better $\tau \leq 10$ ns). It is generally accepted that the crystallization has to be a diffusion-less process in order to be quick enough. It should include only re-arrangements of atomic structure of amorphous state into the crystalline one without inducing slow diffusion processes. This is probably the reason, why the crystallization of isotropic amorphous phases of the Ge–Sb–Te system results in a metastable cubic (fcc, isotropic) crystalline modification, while the slow crystallization from the melt gives a more stable hexagonal modification that is an anisotropic layer crystal. The small changes between the structure of amorphous and crystalline phases are discussed in many papers. The detailed picture of very fast crystallization process is still a subject of much research.

The demand for long retention time of stored data is very desirable; however, it is difficult to be realized in practice. The active films, used for data storage, are very thin (usually of the order of 10 nm, for Blue-ray disk even less). For optical recording, the active film is sandwiched between thermal isolation layers, often of amorphous $ZnS + SiO_2$ layers (**Figure 25**). The phase-change optical disk consists of a stack of four or more different layers on a polymeric substrate. For electrical recording, the PCM layer is sandwiched between at least two electrodes. The electrodes or isolation films can work as crystallization centers and initiate the heterogeneous crystallization. The composition and state of isolation and contact layers is thus very important and can fundamentally influence the properties of active phase-change materials or of a memory cells and also influence the retention time. The chemical interaction between the active PCM layer and electrodes or active and isolation layers should also be as low as possible. In most cases, the number of write–erase cycles is expected to be large ($\geq 10^4$–10^{12} or more). Nevertheless, the chemical interaction between different layers can change the parameters of the device and eventually damage the disk (**Figure 26**).

The melting and following amorphization of thin PCM films is a quick process while the crystallization of the melt or of the glass is usually much slower. If the crystallization is driven by homogeneous nucleation, the nuclei have first to form which means that the nucleation barrier has been overcome (Section 4.2). The nucleation itself is a stochastic process. The slow homogeneous nucleation process can be changed to the much quicker heterogeneous one by addition of either insoluble, or partly soluble, particles (nitrides, carbides, oxides) to the active film, for example, by their co-sputtering, or by sputtering of active material in a reactive atmosphere containing, for example, N_2, O_2. The crystallization nuclei are preserved in the active material also when melting (reset) pulses of lower intensity are applied and not all microcrystals in the active film are melted. Part of them is left to act as crystallization center for the next crystallization (erasig process). The presence of crystals that work as nucleation centers can

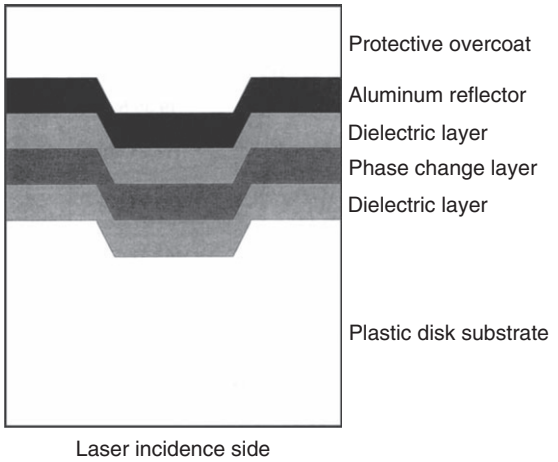

Figure 25 Multilayer device structure in rewritable optical memory digital versatile disks (DVDs) (4.7 GB) (Ovshinsky, 2000). With kind permission of World Scientific Publ. Co.

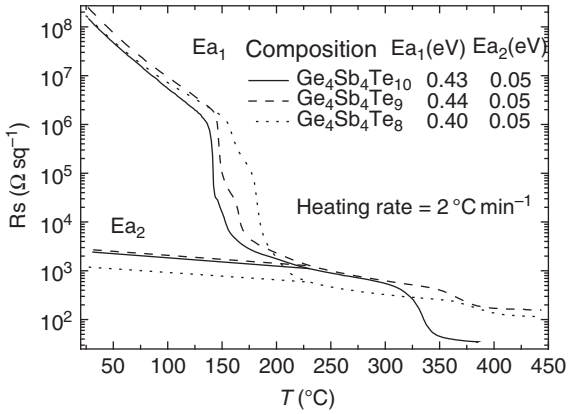

Figure 26 Temperature dependence of resistivity of three different films with composition near to $Ge_2Sb_2Te_5$. The crystallization temperature is slightly increased in films with sub-stoichiometry of Te. Above 150 °C, it can be seen that the crystallization of $Ge_2Sb_2Te_5$, above 300 °C proceeds the change to hexagonal (hcp) modification (Prikryl, 2009).

cause slow spontaneous crystallization and thus lower the lifetime of data storage. If the crystallization barrier is higher, the retention time can be long enough.

The spontaneous crystallization of amorphous material (data points) that would lower the data retention time can start close to the glass-transition temperature, T_g, or at the temperature between $(T_m/3)$ and $(2T_m/3)$ when the atoms become more mobile. The glass-transition temperature of PCM should be high enough, at least $T_g \approx 150$ °C for the material to be stable at temperatures $T \leq 90$ °C, which is set as the practical temperature for such devices. The storage time for consumer data (DVD movies) can be from $t_r \geq A \times 10$ years, at 90 °C, up to $t_r \approx A \times 10^3$ years, where $A \in \langle 1, 9 \rangle$. The problems of retention time were recently discussed by Bez (2009).

The idea of multi-level recording, based on PCM, proposes increased storage density by recording several data levels in one memory spot. In a single-level (classical) recording only two states of phase-change materials (on and off, higher or lower optical reflectivity, or electrical resistivity) are used. In multi-level recording, there are several (e.g., four) states and the record will not correspond only to 0 and 1, but, for example, to 0, 1, 2 (Ohta, 2003). Such an approach implies that the amorphous PCM will be crystallized only partly in several steps, or the crystalline material will be amorphized only partly again in several steps (**Figure 24**). The changes of reflectivity or changes of electrical conductivity must be anyway different enough to distinguish among individual crystallization steps. Recording and erasing can be done either by laser pulses or by electrical pulses. As the changes of electrical resistivity are higher (several orders of ρ between amorphous and crystalline state of PCM), it seems that this idea can be realized at first with cells for electrical recording. There are however still many problems to be solved, for example, the drift of electrical resistivity of individual levels (states) of PCM with time, and also with repeatability and with outer temperature changes that can result in overlapping of individual levels.

The multi-level recording, if fully successful, can not only increase the data-storage density, but also change the philosophy of data storage and computing, which have been up to now based on the binary system. The multi-level recording (increase of number of recording levels in one spot) can be considered as a shift toward analog-to-digital type of recording. It is probably closer to the functioning of animals and humans brains, which are not working digitally but more probably analogously. A large research effort is hence devoted to searching practical solutions both in area of new materials, technology, processes, geometry, stability, and reproducibility. Several strategies to multi-level recording are discussed at the annual European Symposium on Phase Change and Ovonic Science (EPCOS) and other meetings.

Further increase of the resolution and disks capacities can come from Super-Resolution Near-field Structure (Super-RENS) in which the data marks can be smaller than the light diffraction limit (Tominaga, 2003). To this extent, a thin Sb layer is evaporated on the top of recording layers. During recording the Sb is heated, and nonlinear optical properties of Sb cause the opening of small transparent spot on the top of Gaussian distribution of the laser intensity. Through this opening, the intense light in the center of beam may record data spots of smaller size (**Figure 27**; Tominaga, 2003).

New types of electrical memories based on electrolysis of Ag-doped chalcogenides have also been proposed (Soni, 2009). They are based on a thin electrochemical cell which serves as nanoionic switching device or atomic switch (Hasegawa, 2009). The anode is made of Ag, whereas the cathode is formed by an inert conductor (e.g., Pt). Thin film of solid electrolyte prepared from amorphous Ag-doped chalcogenide is placed between them. When a negative voltage is applied to the cathode, the Ag^+ ions are reduced and deposited on the cathode forming a whisker that extends from cathode to anode and eventually short-cuts the electrical circuit. The electrical resistance drops then by many orders of magnitude because of metallic conductivity of the Ag filament. A reverse bias could cause the dissolution of Ag link, and the original high-resistance state is obtained. The write–erase cycle may be repeated tens of million times. As the film between electrodes is very thin, the switching time is short ($1–10^{-7}$ s).

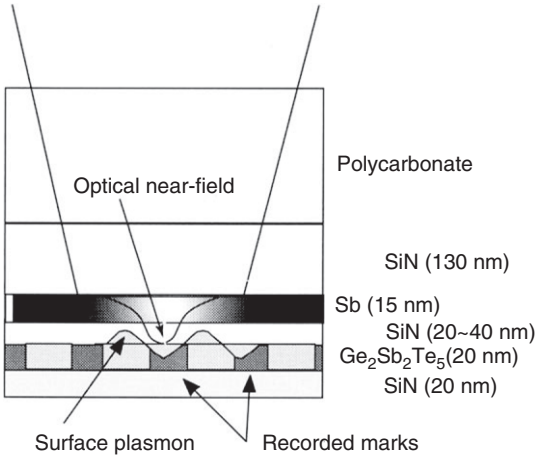

Figure 27 Super-resolution near-field structure using Sb and Ge–Sb–Te layers. The size of the light spot illuminated phase-change material (PCM) film is much lower than the light spot striking the layer (Tominaga, 2003). With kind permission of Springer Science and Business Media.

It depends on switching bias; it is shorter for higher voltage. The recording cells are working at room temperatures, which is an advantage with respect to PCM. The memory is nonvolatile and can be easily scaled down. The multi-level recording is also possible (Hasegawa, 2009). The reading and writing voltages are low: the reading one being lower than the writing–erasing one. There could be a problem with long time stability of very thin Ag whiskers that can spontaneously dissolve in the chalcogenide electrolyte. This type of memory can work also with crystalline chalcogenides such as Ag_2S (Hasegawa, 2009).

8 Conclusion

Chalcogenide glasses and amorphous films possess many interesting physical and chemical properties connected with their unique structure and composition. Properties of AGC are applicable in electronics, optics, opto-electronics, biomedical areas, in physico-chemical sensing, and in data storage. These applications are essentially based on good transparency and intense luminescence, and on infrared region and unique electrical properties. The photo-induced phenomena, high and localized change of photo-conductivity, sensing possibilities, and data-storage abilities also find a wide application.

The understanding of physics and chemistry of AGC, of their structure, and of their preparation technology is reasonably developed. Many basic problems have been solved but many are still open. For example, the nano-separated chalcogenide glasses, which form a new, nearly unknown chalcogenides area, need additional work for the understanding of their properties. This further development is driven by the many promising applications in nonlinear optics and ionics.

Much research has also been devoted to phase-change (DVD, Blue-ray) and holographic memories, to infrared luminescence, to light amplification and generation, to preparation of sensors, fibers, and to search and study of the suitable materials. The multi-level memories from chalcogenide films are now more suitable for use. They will bring a new approach to the computing and to the understanding of animal (human) brain processes and, eventually, they can push ahead many areas of science and technology. Problems of planar optical circuits, of fully optical signals processing, in terms of both processes and materials, are actively studied. The full optical signal processing and, eventually, full optical computing are nowadays a promising dream that can increase the present computing speeds by several orders of magnitude. Memories with increased capacity are also being developed. All these new advances can in turn help our understanding of many problems and support many new technological applications. AGCs, with their unique structure and properties, can play an important role in all these frontier fields.

References

Adam, J.-L., 2002. Lanthanides in non-oxide glasses. Chemical Reviews 102 (6), 2461–2476.
Adler, D., Schwartz, B.B., Steele, M.C., 1985. Physical Properties of Amorphous Materials. New York, NY: Plenum Press.
Aitken, B.G., Quimby, R.S., 1997. Rare-earth-doped multicomponent Ge-based sulphide glasses. Journal of Non-Crystalline Solids 213, 281–287.
Bez, R., 2009. Phase change memory cell concepts and designs. In: Raoux, S., Wuttig, M. (Eds.), Phase Change Materials, Science and Application. New York, NY: Springer, p. 355.
Boetger, H., 1985. Hopping Conduction in Solids. Berlin: Akademie-Verlag.
Borisova, Z.U., 1981. Glassy Semiconductors. New York, NY: Plenum Press.
Breitwish, M.J., 2009. Phase change random access memory integration. In: Raoux, S., Wuttig, M. (Eds.), Phase Change Materials, Science and Application. New York, NY: Springer.

Brocklesby, W.S., Pearson, A., 1994. A spectroscopic study of praseodymium-doped gallium–lanthanum–sulfide glass. Journal of Luminescence 59, 333.

Bychkov, E., Price, D.L., 2000. Neutron diffraction studies of Ag_2S–As_2S_3 glasses in the percolation and modifier-controlled domains. Solid State Ionics 136, 1041–1048.

Bychkov, E., Tveryanovichb, Y., Vlasov, Y., 2004. Ion conductivity and sensors. In: Fairman, R., Ushkov, B. (Eds.), Semiconducting Chalcogenide Glass III: Applications of Chalcogenide Glasses. Amsterdam: Elsevier, pp. 103–168.

Cernoskova, E., Cernosek, Z., Henry, A., Swiatek, K., Frumar, M., 1995. Photoluminescence and optically detected magnetic-resonance in Ge_xS_{1-x} system glasses. Materials Letters 25, 21–25.

Cerny, V., Frumar, M., 1979. ESR study and model of paramagnetic defects in Ge–S glasses. Journal of Non-Crystalline Solids 16, 110–116.

Churbanov, M.F., Plotnichenko, V.G., 2004. Optical fibres from high-purity arsenic chalcogenide glasses. In: Fairman, R., Ushkov, B. (Eds.), Semiconducting Chalcogenide Glass III: Applications of Chalcogenide Glasses. Amsterdam: Elsevier, pp. 209–230.

Elliott, S.R., 1995. Physics of Amorphous Materials. Harlow: Longman.

Feinleib, J., 1971. Rapid reversible light-induced crystallization of amorphous semiconductors. Applied Physics Letters 18, 254.

Fritzsche, H., 1973. Physics of switching and memory devices. In: Le Comber, P.G., Mort, J. (Eds.), Electronic and Structural Properties of Amorphous Semiconductors. London: Academic Press, pp. 557–588.

Fritzsche, H., 1974. Electronic properties of amorphous semiconductors. In: Tauc, J. (Ed.), Amorphous and Liquid Semiconductors. London: Plenum Press, pp. 221–312.

Fritzsche, H., 1995. Optical anisotropies in chalcogenide glasses induced by band-gap light. Physical Review B 52, 15854–15861.

Fritzsche, H., 2000. Light induced structural changes in glasses. In: Boolchand, P. (Ed.), Insulating and Semiconducting Glasses. Singapore: World Scientific, p. 653.

Frumar, M., 2005. Pulsed laser ablation and deposition of chalcogenide thin films. In: Popescu, M. (Ed.), Pulsed Laser Depositions of Optoelectronic Films. Bucharest: INOE, pp. 81–120.

Frumar, M., 2007. Phase change memory materials-composition, structure and properties. Journal of Materials Science: Materials in Electronics 18, 169–174.

Frumar, M., Cernosek, Z., Jedelsky, J., Frumarova, B., Wagner, T., 2001a. Photoinduced changes of structure and properties of amorphous binary and ternary chalcogenides. Journal of Optoelectronics and Advanced Materials 3, 177–188.

Frumar, M., Firth, A.P., Owen, A.E., 1995. Optically induced crystal-to-amorphous-state transition in As_2S_3. Journal of Non-Crystalline Solids 193, 447–450.

Frumar, M., Frumarova, B., Nemec, P., *et al.*, 2006. Thin chalcogenide films prepared by pulsed laser deposition – New amorphous materials applicable in optoelectronics and chemical sensors. Journal of Non-Crystalline Solids 352, 544–561.

Frumar, M., Frumarova, B., Wagner, T., Nemec, P., 2003a. Photoinduced phenomena in amorphous and glassy chalcogenides. In: Kolobov, A. (Ed.), Photoinduced Metastability in Amorphous Semiconductors. Weinheim: Wiley-VCH, p. 2314.

Frumar, M., Jedelsky, J., Frumarova, B., Wagner, T., Hrdlicka, M., 2003b. Optically and thermally induced changes of structure, linear and non-linear optical properties of chalcogenides thin films. Journal of Non-Crystalline Solids 326, 399–404.

Frumar, M., Jedelsky, J., Polak, Z., Cernosek, Z., 1999. Thermally and photoinduced changes of structure and optical properties of As–Ga–S amorphous films and glasses. Thin Solid Films 344, 488–491.

Frumar, M., Polak, Z., Cernosek, Z., Vlcek, M., Frumarova, B., 1997. Photoinduced effects in amorphous chalcogenides. Physics and Applications of Non-Crystalline Semiconductors in Optoelectronics 36, 123–139.

Frumar, M., Polak, Z., Jedelsky, J., Cernosek, Z., Frumarova, B., 2001b. Structure and optically induced changes of reactivity and optical properties of amorphous chalcogenides. In: Thorpe, M.F., Tichy, L. (Eds.), Properties and Application of Amorphous Materials. Dordrecht: Kluwer, pp. 321–328.

Frumar, M., Tichy, L., 1987. N-type conductivity in chalcogenide glasses and layers. Journal of Non-Crystalline Solids 97–98, 1139–1146.

Frumar, M., Vlcek, M., Klilorka, J., 1988. Photoinduced changes of structure and properties of amorphous chalcogenides. Reactivity of Solids 5, 341–349.

Frumar, M., Wagner, T., 2003. Ag doped chalcogenide glasses and their applications. Current Opinion in Solid State and Materials Science 7, 117–126.

Frumarova, B., Bilkova, M., Frumar, M., Repka, M., Jedelsky, J., 2003. Thin films of Sb_2S_3 doped by Sm^{3+} ions. Journal of Non-Crystalline Solids 326–327, 348–352.

Frumarova, B., Frumar, M., Oswald, J., Kincl, M., Vlcek, M., 2009. Structure and optical properties of chalcohalide glasses doped with Pr^{3+} and Yb^{3+} ions. Journal of Non-Crystalline Solids 355, 1865.

Gladden, L.F., Elliott, S.R., Greaves, G.N., 1988. Photostructural changes in bulk chalcogenide glasses – An EXAFS study. Journal of Non-Crystalline Solids 106, 189–192.

Golovchak, R., Shpotyuk, Y., Thomas, C., *et al.*, 2015. Peculiarities of Ga and Te incorporation in glassy arsenic selenides. Journal of Non-Crystalline Solids 429, 104–111.

Gonzales-Leal, J.M., 2003. Evaluation of multiplexing in high-density holographic memories. In: Kolobov, A. (Ed.), Photoinduced Metastability of Amorphous Semiconductors. Weinheim: Wiley-VCH, pp. 338–356.

Grigorovici, R., 1974. The structure of amorphous semiconductors. In: Tauc, J. (Ed.), Amorphous and Liquid Semiconductors. London: Plenum, pp. 45–99.

Gutzow, I., Schmelzer, J., 1995. The Vitreous State, Thermodynamics, Structure, Phenomenology and Crystallization. Berlin: Springer.

Hamakawa, Y., 1982. Amorphous Semiconductor Technologies and Devices. Tokyo: OHN.

Hasegawa, T., 2009. Nanoionic switching devices: "Atomic switches". Material Research Bulletin 34, 929–934.

Hassanien, A.S., Akl, A.A., 2015. Estimation of some physical characteristics of chalcogenide bulk $Cd_{50}S_{50-x}Se_x$ glassy systems. Journal of Non-Crystalline Solids 428, 112–120.

Hisakuni, H., Tanaka, K., 1995. Optical microfabrication of chalcogenide glasses. Science 270, 974–975.

Hruby, A., 1972. Evaluation of glass-forming tendency by means of DTA. Czechoslovak Journal of Physics B22, 1187–1188.

Jain, H., Vlcek, M., 2008. Glasses for lithography. Journal of Non-Crystalline Solids 354, 1401.

Jellison, G.E., Modine, F.A., 1996. Parametrization of the optical functions of amorphous materials in the interband region. Applied Physics Letters 69, 371–373.

Kanamori, I., Terunuma, Y., Takahashi, S., Miyashita, T., 1984. Chalcogenide glass fibres for mid-infrared transmission. Journal of Lightwave Technology LT-2 4, 607–613.

Kang, I., Smolorz, S., Krauss, T.D., *et al.*, 1996. Time-domain observation of nuclear contributions to the optical nonlinearities of glasses. Physical Review B – Condensed Matter 54, 12641–12644.

Kasap, S.O., Rowlands, J.A., 2000. Amorphous chalcogenide photoconductors and imaging technologies. In: Boolchand, P. (Ed.), Insulating and Semiconducting Glasses. Singapore: World Scientific, p. 781.

Kastner, M., Adler, D., Fritzsche, H., 1976. Valence-alternation model for localized gap states in lone-pair semiconductors. Physical Review Letters 37, 1504.

Kawaguchi, T., 1998. Photoinduced surface deposition of Ag–Ge–S films: Its enhancement by addition of small amount of Au. Japanese Journal of Applied Physics Part 1 – Regular Papers Short Notes and Review Papers 37, 6318–6321.

Kawaguchi, T., 2003. Photoinduced deposition of Ag particles on amorphous semiconductors. In: Kolobov, A. (Ed.), Photoinduced Metastability of Amorphous Semiconductors. Weinheim: Wiley-VCH, pp. 182–198.

Kawaguchi, T., Maruno, S., 1994. Photoinduced surface deposition of metallic silver: Basic research for its application to optical recording devices. Japanese Journal of Applied Physics Part 1 – Regular Papers Short Notes and Review Papers 33, 4521–4525.

Kawaguchi, T., Maruno, S., Elliott, S.R., 1996. Photoelectro-ionic processes in photoinduced surface deposition of metallic silver on a chalcogenide glass. Journal of Non-Crystalline Solids 202, 107–112.

Kawaguchi, T., Tanaka, K., Elliott, S.R., 2001. Photoinduced and electron-beam phenomena in Ag-rich amorphous chalcogenide semiconductors. In: Nalva, H.S. (Ed.), Handbook of Advanced Electronic and Photonic Materials and Devices, vol. 5. San Diego, CA: Academic Press, pp. 91–117.

Kawasaki, M., Kawamura, J., Nakamura, Y., Aniya, M., 1999. Ionic conductivity of $Ag_x(GeSe_3)_{(1-x)}$ ($0<=x<=0.571$) glasses. Solid State Ionics 123, 259–269.

Kohoutek, T., Orava, J., Prikryl, J., *et al.*, 2009. Near Infrared quazi-omnidirectional reflector in chalcogenide glasses. Optical Materials 32, 154–158.

Kohoutek, T., Wagner, T., Orava, J., *et al.*, 2007. Surface morphology of spin-coated As–S–Se chalcogenide thin films. Journal of Non-Crystalline Solids 353, 1437–1440.

Kolobov, A.V., 2003. Photoinduced Metastability of Amorphous Semiconductors. Weinheim: Wiley-VCH.
Kostyshin, M.T., Mikhailovskaia, E.V., Romanenko, P.F., 1966. Photographic sensitivity effect in thin semiconducting films on metall substrates. Soviet Physics – Solid State 8, 451.
Krecmer, P., Moulin, A.M., Dtephenson, R.J., *et al*., 1997. Reversible nanocontraction and dilatation in a solid induced by polarized light. Science 277, 1799–1802.
Kuzukawa, Y., Ganjoo, A., Shimakawa, K., Ikeda, Y., 1999. Photo-induced structural changes in obliquely deposited arsenic-based amorphous chalcogenides: A model for photostructural changes. Philosophical Magazine B Physics of Condensed Matter Statistical Mechanics Electronic Optical and Magnetic Properties 79, 249–256.
Lines, M.E., 1990. Bond-orbital theory of linear and nonlinear electronic response in ionic-crystals 2. Nonlinear response. Physical Review B 41, 3383–3390.
Lyubin, V., Klebanov, M., Bar, I., *et al*., 1997. Novel effects in inorganic $As_{50}Se_{50}$ photoresists and their application in micro-optics. Journal of Vacuum Science and Technology B 15, 823–827.
Marsillac, S., Bernede, J.C., Conan, A., 1996. Change in the type of majority carriers in disordered In_xSe_{100-x} thin-film alloys. Journal of Materials Science 31, 581–587.
Mietzsch, K., Fitzgerald, A.G., 2000. Electron-beam-induced patterning of thin film arsenic-based chalcogenides. Applied Surface Science 162–163, 464–468.
Mort, J., 1989. The Anatomy of Xerography. London: McFairland.
Mott, N.F., Davis, E.A., 1991. Electron Processes in Non-Crystalline Materials. Oxford: Oxford University Press.
Nasu, H., Matsyoka, J., Kamiya, K., 1994. Second-order and third-order optical nonlinearity of homogeneous glasses. Journal of Non-Crystalline Solids 178, 23–30.
Nemec, P., Jedelsky, J., Frumar, M., Cernosek, Z., Vlcek, M., 2005. Structure of pulsed-laser deposited arsenic-rich As–S amorphous thin films, and effect of light and temperature. Journal of Non-Crystalline Solids 351, 3497–3502.
Nemec, P., Oswald, J., Frumar, M., Frumarova, B., 1999. Optical properties of germanium–gallium–selenide glasses doped by Samarium. Journal of Optoelectronics and Advanced Materials 1, 33–41.
Ohta, T., 2003. Phase-change optical storage media. In: Kolobov, A. (Ed.), Photoinduced Metastability of Amorphous Semiconductors. Weinheim: Wiley-VCH, pp. 310–326.
Ovshinsky, S.R., 2000. Application of glasses, amorphous and disordered materials. In: Boolchand, P. (Ed.), Insulating and Semiconducting Glasses. Singapore: World Scientific.
Paje, S.E., Garcia, M.A., Villegas, M.A., Llopis, J., 2000. Optical properties of silver ion-exchanged antimony doped glass. Journal of Non-Crystalline Solids 278, 128–136.
Poborchii, V.V., Kolobov, A.V., Tanaka, K., 1999. Photomelting of selenium at low temperature. Applied Physics Letters 74, 215–217.
Polák, Z., Fruman, M., Frunarova, B., 1999. Photoinduced changes of the structure and index of refraction of amorphous As–S films. Thin Solid Films 343–344, 484–487.
Popescu, M.A., 2000. Non-Crystalline Chalcogenides. Dordrecht: Kluwer.
Prikryl, J., 2009. Structure, electrical, optical and thermal properties of $Ge_4Sb_4Te_x$. Journal of Non-Crystalline Solids 355, 1998–2002.
Raoux, S., Wuttig, M., 2009. Phase Change Materials, Science and Application. New York, NY: Springer.
Ribes, M., Bychkov, E., Pradel, A., 2001. Ion transport in chalcogenide glasses: Dynamics and structural studies. Journal of Optoelectronics and Advanced Materials 3, 665–674.
Richardson, K., 2003. Engineering glassy chalcogenide materials for integrated optics application. In: Kolobov, A. (Ed.), Photoinduced Metastability of Amorphous Semiconductors. Weinheim: Wiley-VCH, pp. 383–405.
Sakai, K., Uemoto, T., Yokoyama, H., *et al*., 2000. Annealing time and temperature dependence for photo-induced crystallization in amorphous $GeSe_2$. Journal of Non-Crystalline Solids 266–269, 933–937.
Sanghera, J.S., Aggarwal, I.D., 1998. Infrared Fiber Optics. New York, NY: CRC Press.
Sharma, A., Kumar, A., Mehta, N., 2015. Determination of density of defect states in glassy $Se_{98}M_2$ (M = Ag, Cd and Sn) alloys using ac conductivity measurements. Measurement 75, 69–75.
Shimakawa, K., Ganjoo, A., 2001. Current understanding of photoinduced volume and bandgap changes in amorphous chalcogenides. Optoelectronics and Advanced Materials 3, 167–176.
Shkol'nikov, E.V., 2001. Kinetics of etching of $AgAsS_2$ and $AgGeS_2$ glasses in alkaline solutions. Glass Physics and Chemistry 27, 279–281.
Soni, R., 2009. Reliability analysis of the low resistance state stability of $Ge_{0.3}Se_{0.7}$ based solid electrolyte nonvolatile memory cells. Applied Physics Letters 94, 123503.
Sourkova, P., Frumarova, B., Frumar, M., *et al*., 2009. Spectroscopy of infrared transition of Pr^{3+} ions in Ga–Ge–Sb–Se glasses. Journal of Luminescence 129, 1148–1153.
Srivastava, A., Mehta, N., 2016. Investigation of some thermo-mechanical and dielectric properties in multi-component chalcogenide glasses of Se–Te–Sn–Ag quaternary system. Journal of Alloys and Compounds 658, 533–542.
Stuchlik, M., Krecmer, P., Elliott, S.R., 2001. Opto-mechanical effect in chalcogenide glasses. Journal of Optoelectronics and Advanced Materials 3, 361–366.
Stuchlik, M., Krecmer, P., Elliott, S.R., 2003. The optomechanical effect in amorphous chalcogenide films. In: Kolobov, A. (Ed.), Photoinduced Metastability in Amorphous Semiconductors 112. Weinheim: Wiley-VCH, pp. 109–118.
Tanaka, K., 1998a. Medium-range structure in chalcogenide glasses. Journal of Applied Physics 37, 1747–1753.
Tanaka, K., 1998b. Photoexpansion in As_2S_3 glass. Physical Review B: Condensed Matter 57, 5163–5167.
Tauc, J., 1974. Amorphous and Liquid Semiconductors. London: Plenum Press.
Ticha, H., Frumar, M., 1974. Optical absorption of glassy semiconductors of Ge–Sb–S. Journal of Non-Crystalline Solids 16, 110–116.
Ticha, H., Tichy, L., 2002. Semiempirical relation between non-linear susceptibility (refractive index), linear refractive index and optical gap and its application to amorphous chalcogenides. Journal of Optoelectronics and Advanced Materials 4, 381–386.
Tichy, L., Triska, A., Ticha, H., Frumar, M., 1986. On the nature of bleaching of amorphous $Ge_{30}S_{70}$ films. Philosophical Magazine B – Physics of Condensed Matter Statistical Mechanics Electronic Optical and Magnetic Properties 54, 219–230.
Tikhomirov, V.K., Elliott, S.R., 1995. Model for photoinduced anisotropy and its dark relaxation in chalcogenide glasses. Physical Review B 51 (8), 5538–5541.
Tohge, N., Kanda, K., Minami, T., 1986. Formation of chalcogenide glass p–n junctions. Applied Physics Letters 48, 1739.
Tominaga, J., 2003. Application of Ge–Sb–Te glasses for ultrahigh-density optical storage. In: Kolobov, A. (Ed.), Photoinduced Metastability of Amorphous Semiconductors. Weinheim: Wiley-VCH, pp. 327–337.
Tompkins, H.G., McGahan, W.A., 1999. Spectroscopic Ellipsometry and Reflectometry. New York, NY: Wiley.
Tsiulyanu, D., Ciobanu, M., 2016. Room temperature ac operating gas sensors based on quaternary chalcogenides. Sensors and Actuators B: Chemical 223, 95–100.
Tveryanovich, Y.S., 2004. Rare-earth doped chalcogenide glass. In: Fairman, R., Ushkov, B. (Eds.), Semiconducting Chalcogenide Glass III: Applications of Chalcogenide Glasses. Amsterdam: Elsevier, pp. 160–207.
Usuki, T., Uemura, O., Konno, S., Kameda, Y., Sakurai, M., 2001. Structural and physical properties of Ag–As–Te glasses. Journal of Non-Crystalline Solids 293, 799–805.
Vlcek, M., Frumar, M., 1987. Model of photoinduced changes of optical-properties in amorphous layers and glasses of Ge–Sb–S, Ge–S, As–S and As–Se systems. Journal of Non-Crystalline Solids 97 (8), 1223–1226.
Vlcek, M., Frumar, M., Kubovy, M., Nevsimalova, V., 1991. The influence of the composition of the layers and of the inorganic solvents on photoinduced dissolution of As–S amorphous thin-films. Journal of Non-Crystalline Solids 137, 1035–1038.
Vlcek, M., Prokop, J., Frumar, M., 1994. Positive and negative etching of As–S thin-layers. International Journal of Electronics 77, 969–973.
Vogel, E.M., Weber, M.J., Krol, D.M., 1991. Nonlinear optical phenomena in glass. Physics and Chemistry of Glasses 32, 231.
Vogel, W., 1979. Glass Chemie fuer Grundstoffindustrie (in German). VEB Deutscher Verl: Leipzig.
Wágner, T., Ewen, P.J.S., 2000. Photo-induced dissolution effect in $Ag/As_{33}S_{67}$ multilayer structures and its potential application. Journal of Non-Crystalline Solids 266–269, 979–984.
Wagner, T., Frumar, M., 1990. Photoenhanced dissolution and diffusion of Ag in As–S layers. Journal of Non-Crystalline Solids 116, 269–276.

Wagner, T., Frumar, M., 2003. Optically induced diffusion and dissolution of metals in amorphous chalcogenides. In: Kolobov, A. (Ed.), Photoinduced Metastability in Amorphous Semiconductors. Berlin: Wiley-VCH, pp. 160–181.
Wagner, T., Frumar, M., Suskova, V., 1991. Photoenhanced dissolution and lateral diffusion of Ag in amorphous As–S layers. Journal of Non-Crystalline Solids 128, 197–207.
Wagner, T., Havel, J., Houska, J., *et al.*, 2007. Thin films of $Ge_2Sb_2Te_5$ prepared by pulsed laser deposition. In: European Phase Change and Ovonics Symposium, EPCOS. OC Oerlikon Balzers AG: Balzers.
Wagner, T., Jilkova, R., Frumar, M., Vlcek, M., 1994. Optically and thermally-induced diffusion of silver and its diffusion profiles in amorphous layers of Ge–Se systems. International Journal of Electronics 77, 185–191.
Wagner, T., Kohoutek, T., Vlcek, M., *et al.*, 2003. Spin-coated $Ag_x(As_{0.33}S_{0.67})_{(100-x)}$ films: Preparation and structure. Journal of Non-Crystalline Solids 326, 165–169.
Wagner, T., Perina, V., Mackova, A., *et al.*, 2001. The tailoring of the composition of Ag–As–S amorphous films using photoinduced solid state reaction between Ag and $As_{30}S_{70}$ films. Solid State Ionics 141–142, 387–395.
Weber, M.J., 1968. Spontaneous emission probabilities and quantum efficiencies for excited states of Pr^{3+} in LaF_3. Journal of Chemical Physics 48, 4774.
Wei, K., Machewirth, D.P., Wenzel, J., Snitzer, E., Sigel, G.H., 1994. Spectroscopy of Dy^{3+} in Ge–Ga–S glass and its suitability for 1.3 μm fiber-optical amplifier applications. Optics Letters 19, 904–906.
Wells, A.F., 1975. Structural Inorganic Chemistry. Oxford: Clarendon.
Yamada, N., 2009. Development of materials of material for third generation optical storage media. In: Raoux, S., Wuttig, M. (Eds.), Phase Change Materials, Science and Application. New York, NY: Springer.
Yamane, M., Asahara, Y., 2000. Glasses for Photonics. Cambridge: Cambridge University Press.
Yannopoulos, S.N., Trunov, M.L., 2009. Photoplastic effects in chalcogenide glasses: A review. Physica Status Solidi (b) – Basic Solid State Physics 246, 1773–1785.
Zakery, A., Elliott, S.R., 2007. Optical Non-Linearities in Chalcogenide Glasses and Their Applications. Berlin: Springer.
Zallen, R., 1983. The Physics of Amorphous Solids. New York, NY: Wiley.
Zhang, X.H.M., Lucas, J., 2003. Applications of chalcogenide glass bulks and fibres. Journal of Optoelectronics and Advanced Materials 5, 1327–1333.

Further Reading

Frumar, M., 1979. Semiconducting Chalcogenides of the Elements of 4th and 5th Groups of Periodic Table. DSc Thesis, Charles University.
Frumar, M., Wagner, T., Vicek, M., 1991b. Photoenhanced dissolution and lateral diffusion of Ag in amorphous As_2Se_3 layers. European Journal of Solid State and Inorganic Chemistry 28, 1193.
Kolobov, A.V., 1991. Lateral diffusion of silver in vitreous chalcogenide films. Journal of Non-Crystalline Solids 137, 1027–1030.
Kudryavcev, A.K., 1961. Chimia i Technologia Selena and Tellura *(in Russian)*. Moscow: Vysschaya Skola.